

The Automatic Eye Alignment of an Infrared Optometer

David G Taylor

**A thesis submitted to AUT University in fulfilment of the requirements
for the degree of
Master of Philosophy (MPhil)**

2009

**School of Engineering AUT University
Primary Supervisor: Professor Adnan Al Anabuky**

Table of Contents

1	Introduction	1
1.1	General	1
1.2	The design of optometers in relation to their use	4
1.3	Principles of operation of objective optometers.....	7
1.3.1	Introduction	7
1.3.2	The Scheiner principle	8
1.3.3	Eccentric photorefraction	14
1.3.4	Image analysis	17
1.3.5	Wavefront analysis.....	19
1.3.6	Intensity of the reflected retinal image.....	20
1.3.7	Conclusions	21
1.4	Optometer alignment and eye tracking methods.....	22
1.4.1	Introduction	22
1.4.2	Optometers using the Scheiner principle	23
1.4.3	Eye alignment methods used by non-Scheiner principle optometers	27
1.4.4	Conclusions	28
1.5	The objectives of this investigation	29
1.6	Outline of the thesis	30
2	Optical system design	32
2.1	Introduction	32
2.2	The optical system	32
2.3	The removal of the corneal reflection	39
2.4	Conclusions	42
3	Opto-electronic and electro-mechanical design	43
3.1	Introduction	43
3.2	Opto-electronic systems overview	43
3.3	The infrared system electronics	46
3.4	The two dimensional servo mirror system	47
3.4.1	Introduction	47
3.4.2	Optical requirements	49
3.4.3	Electromechanical design	51
3.4.4	LVDT position measurement resolution	53
3.4.5	Kinematic requirements	53
3.4.6	Mirror control systems error constants	55

3.4.7	The current controller.....	56
3.4.8	The mathematical model the mirror system.....	57
3.4.9	System identification.....	59
3.4.10	Control system design and simulation	62
3.4.11	Performance measurements	63
3.4.12	Conclusions	67
4	Outline of the embedded and computer software	68
4.1	Introduction.....	68
4.2	Development tools	69
4.2.1	The files that make up a project.....	70
4.3	The processor library	71
4.4	The real time executive (RTE).....	72
4.5	The system tasks	73
4.6	Data transfer to the host computer	73
4.6.1	Introduction.....	73
4.6.2	Real Time Structure Files	74
4.6.3	The Xmodem-CRC communications protocol	75
4.6.4	Matlab conversion.....	75
4.7	Conclusions.....	76
5	The experimental evaluation of the optical system.....	77
5.1	Introduction.....	77
5.1.1	General.....	77
5.1.2	The optical system reviewed.....	78
5.1.3	Infrared flux measurements.....	80
5.1.4	Pupil plane positioning of the image of the IREDS.....	81
5.1.5	The X-Y scanning program.....	81
5.2	The artificial eye	82
5.2.1	Physical construction	82
5.2.2	Radiant flux transmission.....	83
5.3	Locating the pupil of the artificial eye	85
5.3.1	The use of photodiodes behind the pupil	85
5.4	Removing unwanted reflections.....	86
5.4.1	Sources of unwanted reflection.....	86
5.4.2	Adjustment of the crossed polarizers	87
5.5	Scheiner principle refractive measurement test	89

5.5.1	Introduction	89
5.5.2	Using the photodiode outputs for Scheiner principle refractive measurement	89
5.5.3	Photodiode position ratio difference measurements	93
5.5.4	Discussion and conclusions	96
5.6	Locating the pupil using the retinal reflection	97
5.6.1	Introduction	97
5.6.2	XY Scan of the artificial eye	97
5.6.3	Discussion and conclusions	97
5.7	Conclusions	100
6	Conclusions and future work	103
6.1	Introduction	103
6.2	The optical system	103
6.3	The electronic and electro-mechanical systems	105
6.4	Detection of the pupil	105
6.5	Refractive measurement using the Scheiner principle	106
6.6	Conclusions	107
6.7	Future work	107
7	References	108
8	Appendices	111
8.1	Appendix 1. Calculation of the size of the corneal reflection of the aperture. 111	
8.2	The Real Time Structures File Format Specification	113
8.2.1	The problem	113
8.2.2	The solution	113
8.2.3	RTS file data types	113
8.2.4	The RTS header section	113
8.2.5	The RTS data section	114
8.2.6	The total number of structures variable	115

Table of figures

Figure 1.1.1 The human eye.....	1
Figure 1.2.1 An optometer with a dichroic mirror.....	7
Figure 1.3.1 The Scheiner principle.....	8
Figure 1.3.2 The biprism infrared optometer.....	9
Figure 1.3.3 The telescopic relay lens pair.	11
Figure 1.3.4 An arrangement of an optometer using the Scheiner principle.	11
Figure 1.3.5 Optometer using photo refraction.....	15
Figure 1.3.6 Refractive errors corresponding to distortions of an annular source.....	18
Figure 1.3.7 The wavefront Optometer.....	19
Figure 1.3.8 Device for evaluating the refraction of the eye.	20
Figure 1.3.9 The output versus eye refraction for Yancey's device.....	21
Figure 1.4.1 An outline of an optometer using the Scheiner principle.	23
Figure 1.4.2 1st and 4th Purkinje eyetracker system.	25
Figure 1.4.3 The optometer system of Crane and Steele.	26
Figure 2.2.1 The optical system of the experimental optometer.....	33
Figure 2.2.2 Photodiode arrangement to detect image movement.....	38
Figure 2.3.1 Azimuth angle versus angle of incidence for reflection from a dielectric surface.	40
Figure 3.2.1 Optometer system block diagram.....	44
Figure 3.2.2 Optometer system with electronics.....	45
Figure 3.3.1 The pulsing of the infrared emitting diodes (IREDs).....	46
Figure 3.3.2 The multiplexing of the IREDS.....	47
Figure 3.4.1 Outline view of the two dimensional servo mirror system.....	48
Figure 3.4.2 Mirror motor driving electronics.....	56
Figure 3.4.3 Mirror system model.....	58
Figure 3.4.4 Closed loop identification scheme.....	60
Figure 3.4.5 Identification step response of the horizontal system.....	61
Figure 3.4.6 The horizontal system simulation block diagram.....	63
Figure 3.4.7 Horizontal system actual and simulation outputs.....	64
Figure 3.4.8 Vertical system step response.....	65
Figure 3.4.9 The horizontal system ramp response.....	66
Figure 3.4.10 The vertical system ramp response.....	67
Figure 5.1.1 The optics of the experimental optometer.....	78

Figure 5.1.2 Images of the sources overlapping the pupil of the eye.....	79
Figure 5.2.1 A schematic diagram of the artificial eye	83
Figure 5.3.1 Contour plot of the summed outputs of photodiodes behind a 5 mm pupil.	85
Figure 5.4.1 Mesh plot of the total output for the top IRED with the output polarizer removed.....	87
Figure 5.4.2. Mesh plot of the total output for the top IRED with the output polarizer optimally adjusted.	88
Figure 5.5.1 The arrangement of the photodiodes to detect image movement.	90
Figure 5.5.2 Plots of vertical difference in position ratio for five retina positions.	95
Figure 5.5.3 Plots of the horizontal difference in position ratio for five retina positions.	95
Figure 5.5.4 Plots of the vertical position ratio difference with lens reflections subtracted.	96
Figure 5.6.1 Contour plot of the total photodiode output from the top IRED.	99
Figure 5.6.2 Mesh plot of the total photodiode output from the top IRED.....	99
Figure 5.6.3 Contour plot of the total photodiode output from the bottom IRED.	100
Figure 5.6.4 Mesh plot of the total photodiode output from the bottom IRED.	100

Table of tables

Table 1-1 Range and resolution of Scheiner principle optometers.....	13
Table 3-1 The mirror system transfer functions.....	62
Table 3-2 Mirror system compensators.	62
Table 4-1 Processor specific software modules.....	71
Table 5-1 Retinal distances for a range of refractions of the artificial eye.....	84
Table 5-2 Overall refractions, retinal and corresponding photodiode distances.....	94

Acknowledgements

I wish to acknowledge and thank the following persons for their participation and help in completing this research work.

- The divine inspiration, guidance and provision of my God, Jesus Christ.
- Supervisor and Associate Professor Rob Jacobs of the University of Auckland, School of Optometry who has provided many references and been very helpful. His contributions of time and effort in attending meetings, consultations and reviewing this work have been tremendous.
- Head supervisor Professor Adnan Al Anabuky and supervisor Dr Hamid Gholam Hosseini for their guidance and reviews.
- The AUT Electrical Engineering academic staff Ross Twine and Les Williams for their advice on electronic design. Thanks to technician Brett Holden for his advice and practical help with the electronics of the project. Thanks also to Dr David I Wilson for his assistance with the use of Matlab and control system design.

Abstract

The ability of the human eye to change its overall refractive power so that people can focus on objects both far and near is termed *accommodation*. Research into how the eye automatically changes its accommodation, demands an instrument capable of tracking the accommodation with fine resolution and adequate corner frequency.

An instrument capable of tracking the ocular accommodation is called an *optometer*. Reports of earlier optometers show that optometers using the older Scheiner principle can have the required precision and dynamics required to track the micro fluctuations of accommodation. However optometers using the Scheiner principle require precise alignment to the patient's pupil to be maintained throughout the measurement time.

Previous optometers have used the radiation reflected from the patient's cornea (called the corneal reflection) to initially align the optical axis of the optometer to the centre of the patient's pupil. Since the Scheiner principle optometer uses radiant energy reflected from the patient's retina to make a refractive measurement, the idea of using this same radiant energy for patient alignment is investigated.

Earlier optometers have blocked the corneal reflection from reaching the photodetectors for the retinal reflection using a small fixed light stop. Since it is not possible to use a fixed light stop if the retinal reflection is used for alignment, the feasibility of using crossed linear polarizers is experimentally evaluated. The results showed that about 78% of the radiant energy reflected from the front lens of an artificial eye could be eliminated using crossed linear polarizers.

Whether the Scheiner principle measurement of refraction of an artificial eye could be done with 78% of the front lens (corneal) reflection removed was investigated. The results were not conclusive. There was not a measureable indication of when the refraction of the experimental optometer matched that of the artificial eye.

The experimental optometer system attempts to use a servo controlled mirror system to move the optical axis of the optometer so that it coincides with the optical axis of an artificial eye. The design, development and testing of the mirror system is described.

The mirror system enables the optometer to perform a two dimensional scan over the pupil plane of the patient's eye or an artificial eye. During the scanning, the total radiant power reflected can be measured. For the optometer to be aligned using radiation reflected from the retina, a scan of the pupil plane of should reveal the pupil boundaries. This was experimentally demonstrated to work. Unfortunately time limitations did not permit further development of an automatic eye alignment and tracking system.

Glossary

Word	Meaning
ADC	Analogue to Digital Converter.
Auto refractor	A computer controlled machine used in an eye examination to provide an objective measurement of the overall refractive state of the eye.
Optometer	An instrument used to determine the accommodation or refractive state of the human eye.
Instrument myopia	Accommodation caused by looking into a confined space even though the target viewed is at optical infinity.
Dichroic mirror	Dichroic means dual chromatic. It is a piece of glass that has been optically coated so as to pass radiation of one band of wavelengths yet reflect radiation of another band. In optometers the dichroic mirror usually passes visible light but reflects infrared radiation.
DAC	Digital to Analog Converter.
GDB	The GNU project debugger. The same debugging software has been ported to many different processors and operating systems.
GNU	A recursive acronym for “GNU is Not Unix”. It refers to software that is Unix like, but entirely free.
IDE	Integrated Development Environment. It refers to a software development system that combines editors, compilers, debugger and other software tools with one graphical user interface.
IRED	Infra Red Emitting Diode.
ISP	In System Programmer.
JTAG	Joint Test Action Group is the common name for what was later standardized as the IEEE 1149.1 standard.
LVDT	Linear Variable Differential Transformer.
PRD	Position Ratio Difference.
PSD	Position Sensitive Detector.
RTE	A Real Time Executive is the software that allows pre-

	emptive multitasking on a microcontroller system.
SFP	Spilt field photodetector.
TCP	Transmission Control Protocol. The connection orientated protocol which used for reliable data transmission using the IP (internet Protocol). Can also be used for communication between two programs on the one computer.

Statement of Originality

‘I hereby declare that this submission is my own work and that, to the best of my knowledge and belief, it contains no material previously published or written by another person not material which to a substantial extent has been accepted for the qualification of any other degree of diploma of a University or other institution of higher learning, except where due acknowledgment is made in the acknowledgments.’

Signed:

Date:.....

1 Introduction

1.1 General

This investigation is about the design of optometers and the control principles necessary for optometers to make precise and continuous measurements. An optometer is an instrument used to determine the accommodation or refractive state of the human eye (Smith and Atchison (1997)). This chapter will begin with explanations of the fundamentals of optometer technology and some of the terms used. It is assumed that the reader has some knowledge of optical science.

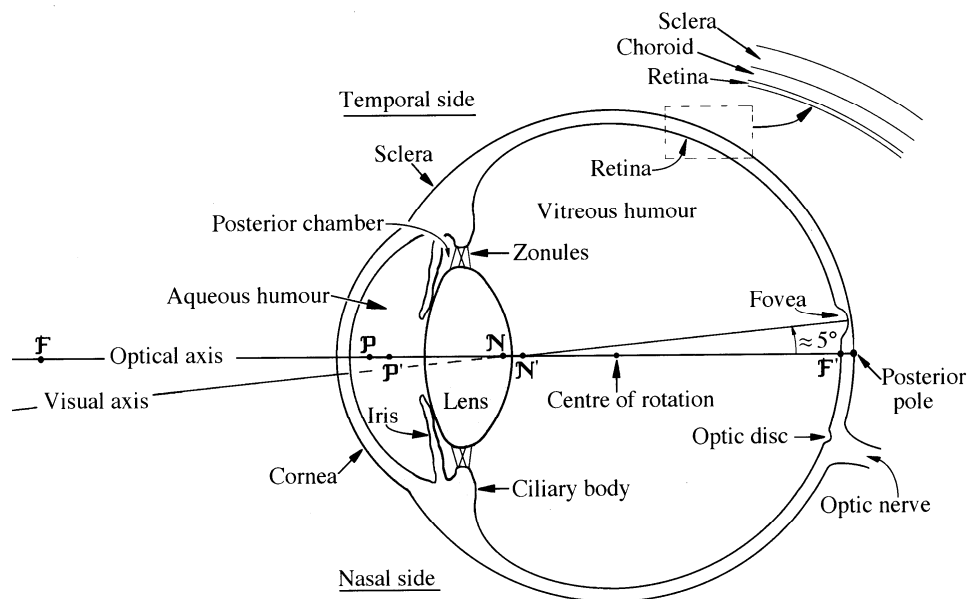


Figure 1.1.1 The human eye.

(Reproduced from Atchison and Smith (2000))

A cross sectional view of the human eye is shown in Figure 1.1.1 for the reader's reference. The refraction of the eye is a measure of its ability to bend (refract) light rays from an object point on a viewed target, so that they arrive at a corresponding image point on the retina. When the eye is perfectly focused on an object point, the object point viewed maps to a single image point on the retina. Such object and image points are referred to as being optically *conjugate*.

Regardless of whether or not the eye has a target to view, or whether or not the eye is correctly focused on the viewed target, there will always be a point in the object space on the optical axis of the eye, that is optically conjugate to an image point on the retina. The point in the object space that is conjugate to the retina is called the *far point*. This object point is used to determine the *end point of refraction*. The end point of refraction is the point in the object space where the target would need to be for its image to be perfectly focused on the retina. The inverse of the distance (in metres) from this end point to the vertex of the cornea of the eye is a measure of the refractive power of the eye in *dioptries*. An optometer measures and/or tracks the *end point of refraction*.

In general the end points of refraction will not be same for all meridians of the cornea. The special case of where the refraction in all meridians is the same is called *spherical* refraction. Where the end points are different for different meridians, the refraction is *astigmatic*. When the type of the refraction is not specified, spherical refraction will be assumed.

The end point measured by an optometer will generally depend on the state of a patient's accommodation. When the accommodation is relaxed the far point will be closest to infinity. The word "accommodation" in this context, refers to the ability of the eye to increase its refractive power so that targets close to the eye can be made optically conjugate to the retina. Physiologically, the eye increases its refractive power by increasing the refractive power of the *lens* shown in

Figure 1.1.1. To distinguish the lens of the eye from lenses that might be worn in spectacles, contact lenses, or be part of an optical instrument, the lens of the eye is often called the "crystalline lens". This convention will be used in this thesis.

Clinical optometrists need to measure the *refractive state* of a patient's eye. The refractive state is a measurement of the end point of refraction when the crystalline lens has its minimum refractive power. When the crystalline lens has its minimum refractive power the accommodation is said to be *relaxed*. The three general refractive states commonly described, following measurements with optometers are *emmetropia*, *myopia* and *hyperopia* (*hypermetropia*).

These states can be defined in terms of the end point of refraction when the accommodation is relaxed. If the patient's end point of refraction is at infinity when the accommodation is relaxed, then the eye is Emmetropic or normal sighted. Myopia is when the end point is at finite distance from the eye that is closer than infinity. In myopia the image of an infinitely distant object will fall "in front of" (anterior to) the retina. In hyperopia the image of an infinitely distant object will fall "behind" (posterior to) the retina when the accommodation is zero. If the eye does not have the same refractive state for all meridians, the eye is *astigmatic*. An optometrist will prescribe corrective lenses for these conditions and therefore the optometer is useful in quickly assessing whether a patient is likely to need corrective lenses. This is the clinical use of an optometer.

A distinction between *subjective* and *objective* measurement needs to be made. A clinical optometrist will usually make a measurement of refractive state *subjectively* by using verbal feedback from the patient about the clarity of distant targets seen with a series of corrective lenses. Some optometers depend on patient feedback and are called subjective optometers.

However it also possible to make an *objective* measurement of the refraction of the human eye. Objective measurements do not depend on the response of the patient to changes in the clarity of vision. An optometer capable of making a refractive measurement without feedback from the patient is called an objective optometer or *autorefractor*. The scope of this investigation will be confined to *objective optometers* or *autorefractors*.

Optometers are also used for research purposes, in particular for measuring the accommodation of the eye. The rapidly changing nature of accommodation requires an objective optometer that can track these changes. Furthermore, such optometers must not interfere with the state of the patient's accommodation. Therefore refractive measurements are made using *infrared radiation* as opposed to visible light. Such optometers are called infrared optometers.

All objective optometers need to be aligned to the patient's eye so that accurate refractive measurements can be made. If more than an instantaneous measurement is required, then the alignment with the eye has to be maintained during measurement.

This accurate alignment might be maintained done by restricting the range of head and eye movement possible by using attaching the patient's skull to the optometer using a bite board. To allow a more comfortable situation the bite board could be replaced with a head rest that allows a limited range of head movements to be made and a system that allows the optometer to track of eye movements can be used. Methods of initial alignment and of tracking eye position are the core themes of this investigation.

1.2 The design of optometers in relation to their use

The requirements for performance and operation of an optometer greatly depend on the intended use of the instrument. General categories of use include the following:

1. Clinical use

- A. Refractive screening.** Used by an optometrist to make a quick assessment of the refractive state of a patient. This is a preliminary test to determine whether a more thorough examination should be done.
- B. An objective prescription.** Used in most eye examinations to provide a non subjective assessment of the visual correction required by a patient. This is usually the starting point for fine tuning by subjective tests.

2. Research use

- A. Population screening.** The rapid assessment of the refractive state of a person is often key to large studies where the development of the human eye or the effects of experimental interventions on the development of refractive errors are being undertaken.
- B. The study of the accommodation and its dynamics.** The study of the micro fluctuations of accommodation is an example.

In category (1) above, the optometer is used for making an assessment of the overall refractive state of a patient, to determine whether corrective lenses are likely to be needed. In this case, it is acceptable that the patient views a target within the optometer itself. The only drawback is the phenomena of *instrument accommodation*, where the patient is unable relax accommodation completely because the target is perceived as being close. The ocular motor control systems in the mid brain automatically set a non zero level of accommodation and a non zero level of convergence of the lines of sight. This unwanted accommodation reduces the validity of refractive measurement.

Optometers where the patient can only view a target within the optometer, are called *closed field*. Conversely, an optometer where the subject can view a target external to the instrument are called *open field*. However in the study of accommodation for research purposes, an open field optometer would certainly be needed.

Another question is, does the optometer only need to make a “snap shot” measurement or continuous recording of the refractive state of the eye? In category (1) a snap shot measurement would be appropriate, but for the study of accommodation, continuous recording would be required. Continuous recording has another implication regarding the alignment of the instrument to the eye.

To allow continuous recording, the optometer must be continually maintained in correct alignment to the eye such that valid measurements can be made. The use of a chin rest and bite bar only provides movement restraint of the head but *not* of the eyes. If the optometer could provide an eye tracking ability sufficient to permit accurate refractive measurements during minor head and eye movements, this would make its use much more convenient and simple

If an optometer is able to track pupil/eye movement, then it should also be possible to automatically align such a system to the eye. Automatic initial alignment could save having a monitor screen and other hardware, such as joy stick to allow the operator to manually align the instrument to the patient.

In designing an optometer, the *resolution*, *absolute* and *relative* accuracy of the refraction measurement should be considered. Firstly these terms will be defined.

The term *resolution* means the smallest change in refraction that the optometer can measure. A resolution of 0.25 dioptre (D) would be adequate for a clinical assessment, since corrective lenses are only made in 0.25 D steps. However, for a research study of accommodation, a much smaller resolution would be required. For example if the micro fluctuations of accommodation are in the order of few tenths of a dioptre in amplitude, then an optometer with resolution of a fraction of this would be required.

The term *absolute* accuracy means how close the refractive measurement of an objective optometer is to the subjective measurement made by an optometrist. An

optometer using infrared radiation can measure changes in accommodation with fine resolution, but the values of end point of refraction measured with an objective optometer can be substantially different from subjective measurements. Cornsweet (1970) measured as much as 1 D difference. Atchison and Smith (2000) on page 77 explain the reasons for the difference between subjective and objective measurements. The optometer for a clinical assessment will want to include algorithms to compensate for these offsets. For a clinical assessment, absolute accuracy is therefore desirable.

The term *relative* accuracy will mean the accuracy of the measurement of refraction *differences*. Refraction differences can be due to accommodation and an optometer can measure in changes accommodation by measuring the differences in the end point of refraction. Although an infrared optometer might be as much as 1 D different in its absolute refractive measurement, it could be more correct in measuring a change in accommodation.

It has been shown that the requirements of an optometer for clinical use are quite different from those used for accommodation research. Optometers used for clinical use are readily commercially available and are made by several manufacturers including Nikon, Canon , Zeiss and Nidek. The requirements of an optometer that meets the research requirements for the study of accommodation include:

1. Open field.
2. Precision resolution preferably less than 0.1 D.
3. Continuous measurement capability.
4. Eye tracking capability sufficient for continuous measurement.
5. Preferably easy or automatic alignment.

The open field requirement is generally made possible by the use of a *dichroic* or *dielectric* mirror. A dichroic mirror is an optically coated piece of glass that allows electromagnetic radiation of visible wavelengths (light) to pass, yet reflects the infrared wavelengths. The mirror is placed directly in front of the patient's eye so that the patient can see a target through it with visible wavelengths. The infrared wavelengths used to make refractive measurements by the optometer are reflected to/from the mirror to the patient's eye. The arrangement is shown in Figure 1.2.1.

An optometer that meets these five requirements for research use will require a method of refraction measurement that satisfies these requirements. A review of the different

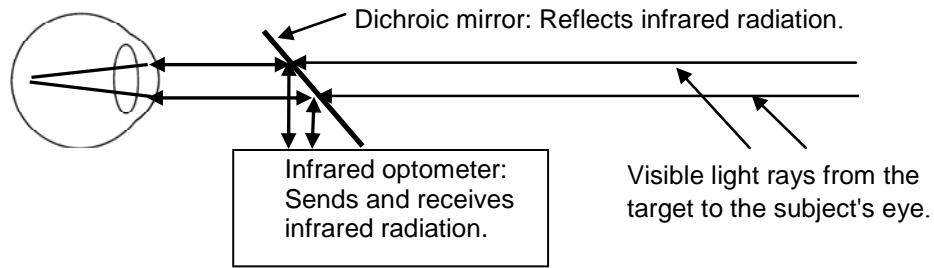


Figure 1.2.1 An optometer with a dichroic mirror.

(Reproduced from Taylor (2003))

methods of objectively measuring refraction will be made so as to identify the methods that offer the most precise relative accuracy. However, the method of refractive measurement also determines how precisely alignment must be made and therefore the need for eye tracking. These two issues will be examined for each method of refraction measurement. The aim is to determine which are best suited for research use.

1.3 Principles of operation of objective optometers

1.3.1 Introduction

Atchison and Smith (2000) in chapter 8 and Smith and Atchison (1997) in chapter 31 give reviews of methods for measuring refraction. For this investigation, the review requires more than just the method of measurement. An assessment must be made of the relative accuracy and the alignment requirements that are needed for the method of measurement of refraction used. This assessment can be obtained from the open literature and from the available specifications of optometers that use a particular method.

In recent years, autorefractors and optometers have become largely commercial products and therefore details of the design principles are considered commercially sensitive. Therefore papers on the detailed design of such optometers do not exist. Instead there are papers describing assessments and comparisons of their performance. In the special case where a commercial autorefractor has been experimentally modified, there have been papers which give some insight into its workings. However, there are reports in open literature on the experimental optometers developed by Universities or research institutions. Such papers describe an optometer's operation in detail and are

therefore the most relevant to this investigation, even though they are not recent in years.

1.3.2 The Scheiner principle

Elkington and Frank (1991) state that in 1619, Scheiner discovered that the end point of refraction could be precisely determined by placing a double pinhole aperture in front of the eye as shown in Figure 1.3.1. A convex lens (positive power, focal point F) is also placed in front of the pinhole aperture, to create a simple subjective optometer, so that the distance of the far point of the eye in relation to the point F would be measurable. The Figure 1.3.1 shows three separate cases. In case (a), the axial object point is further from the eye than the end point. The refraction of the eye causes the two ray bundles from the object point that pass through the two pinholes to cross the optical axis in front of the retina, and two spots appear on the retina. In case (b), the light from an axial point is closer to the eye than the end point. The refraction of the eye is too weak and two spots appear on the retina. Only in case (c) when the object point and the end point coincide is there only one spot on the retina.

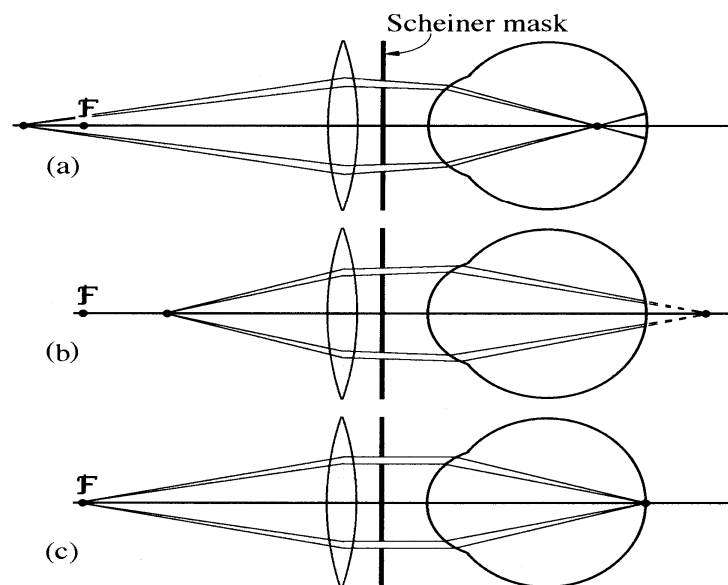


Figure 1.3.1 The Scheiner principle.

(Reproduced from Atchison and Smith (2000))

Once the location of the far point of the eye is known, the distance from the eye to the end point of refraction of the eye without the lens, can be determined by the applying the lens formula. The power of the lens must be known.

Charman and Heron (1975) describe an infrared optometer that use this principle. Instead of a double pinhole aperture, a Biprism is used to produce two bundles of light from the infrared irradiated object. The instrument was further developed by Heron, Winn et al. (1989) into an optometer for measuring the refraction of both eyes concurrently. The optical components and photodetector are shown in Figure 1.3.2 for one channel.

When the eye is focused at infinity a single image of the slit S1 forms on the retina. If the eye accommodates, the single slit image on the retina becomes two separate slits. The retinal image is reflected back and passes through a slit S3 whose width corresponds to the width of a single image of the slit S1 on the retina. The radiation passing through the slit S3 is collected by a photomultiplier tube and amplified electronically to produce an output signal.

The output signal from the photomultiplier does not linearly correspond to the amount of accommodation of the eye. It forms a sharply peaked curve that is shown in the earlier paper by Charman and Heron (1975). Whilst moving parts have been avoided in this design, the non linearity of the measurement is not desirable. The resolution of measurements of accommodation would depend on level of accommodation.

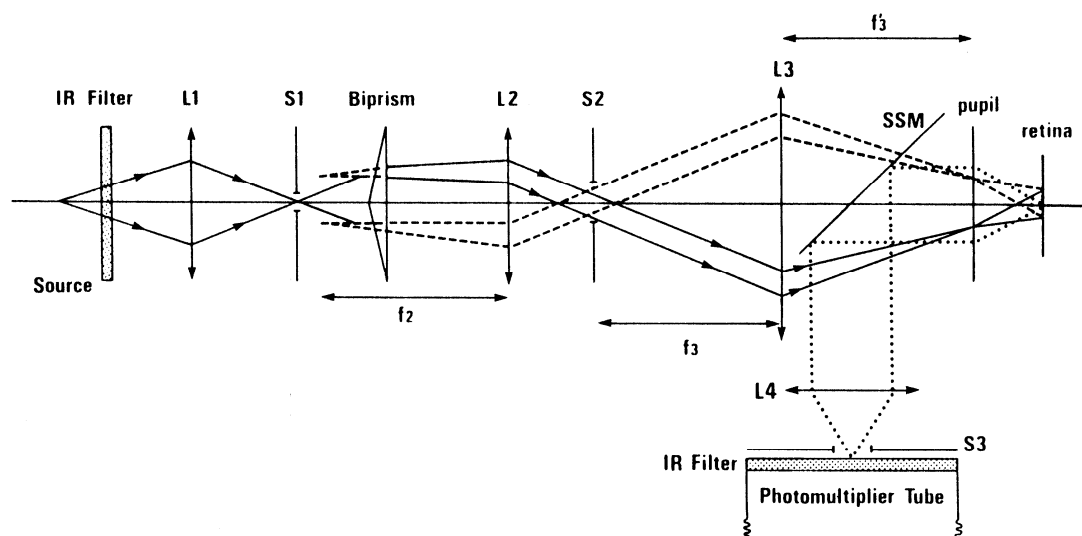


Figure 1.3.2 The biprism infrared optometer.

(Reproduced from Heron, Winn et al. (1989))

Charman and Heron (1975) do not report the resolution of measurements in their paper. It is stated that background lighting is a problem since the infrared source is not chopped and therefore cannot be distinguished from infrared sources outside the optometer. Bite bar and head restraint were required to maintain patient alignment to the instrument.

The output non-linearity of the Charman and Heron (1975) design can be removed by moving the object imaged on the retina until the Scheiner principle indicates that it is conjugate to the retina. Then a measurement of the position of the object conjugate to the retina gives a measure of the refraction of the eye. To do this, the Scheiner principle is applied in a slightly different way.

Suppose in Figure 1.3.1, cases (a) and (b), the pinholes in the plate were alternately blocked. In case (a) the spot on the retina would move to the opposite side of the side that had the blocked pinhole. In case (b) the spot on the retina would move so that it was always on side of the illuminated pinhole. Only in case (c) when the object point is at the same position as the end point would there not be any movement.

This image movement therefore not only indicates a refractive error, but also the sign of the error from the lateral motion of the image relative to the shifting of the apertures. This principle has been used in many optometer designs including those of Okuyama and Tokoro (1989), Takeda, Fukui et al. (1988), Crane and Steele (1978) and Cornsweet (1970). Each of these papers describe an experimental optometer not the implementation of a commercially produced optometer.

Understanding the optics of this type of optometer is particularly relevant to the study reported in this thesis and therefore the optical principles will be further explained. A prerequisite to understanding the optometer optics is the properties of the telescopic lens relay pair shown in Figure 1.3.3. Lenses L1 and L2 are separated by the sum of their focal lengths. In this special case, Crane and Steele (1978) state the relationship between the object distance P and the image distance Q is as shown in equation 1-1.

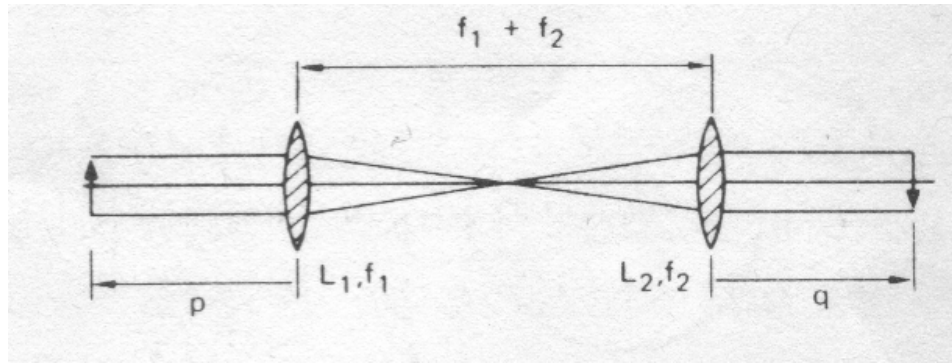


Figure 1.3.3 The telescopic relay lens pair.

(Reproduced from Crane and Steele (1978))

$$Q = f_2 \left(1 + \frac{f_2}{f_1} \right) - P \left(\frac{f_2}{f_1} \right)^2 \quad 1-1$$

Where f_1 and f_2 are the focal lengths of lenses **L1** and **L2** respectively. The important property of the telescopic pair is that the magnification is *independent* of the object and image distances. It is shown in equation 1-1.

$$\text{Magnification} = -\frac{f_2}{f_1} \quad 1-2$$

Now consider a typical arrangement of an optometer using the Scheiner principle as shown in Figure 1.3.4.

Instead of a double pinhole plate in front of eye, two infrared sources (Infra Red Emitting Diodes abbreviated to IREDS) are used shown as **S1** and **S2** in the Figure

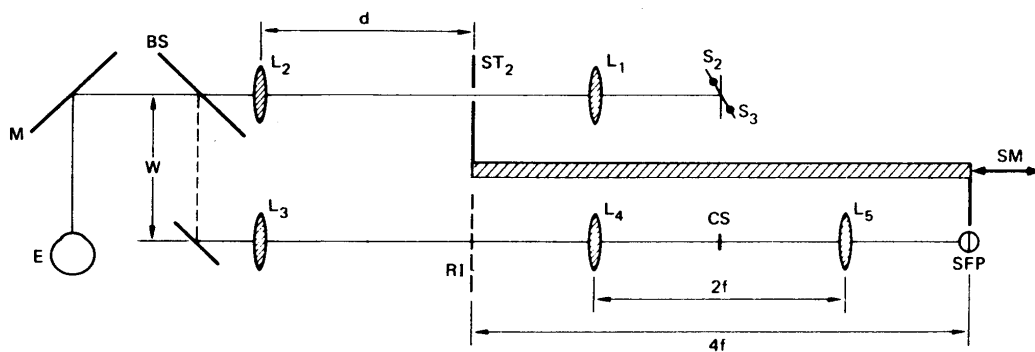


Figure 1.3.4 An arrangement of an optometer using the Scheiner principle.

(Reproduced from Crane and Steele (1978))

1.3.4. The telescopic lens pair **L1** and **L2** relay the image of these sources to the pupil plane of the eye (**E**). When the instrument is aligned to the eye, the image of this pair of sources are centred on the pupil of the eye. This means that any infrared flux entering the eye comes from either one side of the pupil or the other. This creates the same effect as having an aperture that can be moved from one side of the pupil to the other.

The Scheiner principle depends on measuring movement on the retina of an image that is irradiated from two directions. In the case of the optometer shown in Figure 1.3.4, the retinal image is of the aperture stop **ST₂**. The aperture stop **ST₂** is placed a distance d from lens **L2**. The stop **ST₂** is irradiated by the two sources via lens **L1** and an image of it is formed on the retina via the lens **L2**. Lens **L2** is one focal length from the pupil plane of the eye and therefore when d is equal to f_2 , the stop **ST₂** is at optical infinity to the eye.

The optical distance of the aperture stop from the eye can be varied by moving the stop **ST₂** in relation to lens **L2** via a moveable carriage shown as a crossed bar in Figure 1.3.4. The stop **ST₂** can therefore be moved to a distance where there is no lateral motion of the retinal image due to the switching of the infrared sources. At this distance **ST₂** is at the far point of the eye. Crane and Steele (1978) provide an equation that relates the distance d to the overall refraction of the eye (D_E) expressed in dioptres, when there is no lateral motion of the retinal image due to the switching of the infrared sources. This equation reproduced from Crane and Steele (1978) is stated as equation 1-3 and refers to the optometer shown in Figure 1.3.4. The equation 1-3 shows a linear relationship between the measured distance d and the overall refraction of the eye D_E .

$$D_E = \frac{1}{f_2} \left(1 - \frac{d}{f_2} \right) \quad 1-3$$

Now consider output path of the optometer, which is the means by which the retinal image is relayed to the split field photo detector (**SFP**). The infrared radiation from the object on the retina passes back through the optics of the eye towards the optometer. The infrared radiation is then reflected by the dichroic mirror **M** and passes into the beam splitter **BS**. The beam splitter reflects a percentage of the reflected radiation towards lens **L3**. Since the lenses **L2** and **L3** have the same dioptric power, the infrared object on the retina will also appear as an image at a distance d from lens **L3** at a

location labelled **RI** (Retinal Image) in Figure 1.3.4. The telescopic lens pair **L4** and **L5** relay the image at **RI** to a split field photo detector shown as **SFP** in Figure 1.3.4.

The split field photo detector (**SFP**) has two independent photosensitive detectors placed side by side. When an image is centred on the pair, both detectors produce an equal output. This will only occur when **ST₂**, the retina and **RI** are conjugate. Consequently if there is any difference in the image position due to the switching of the sources, it will be detected as changes in the outputs from the detectors of the **SFP**. The carriage can be moved until **ST₂** is conjugate with the retina and there is no motion detected by the **SFP**. When this occurs the distance d corresponds to the end point of refraction of the eye. The carriage movement can be motorised.

The infrared radiation is also reflected from the corneal surface as the infrared beams enter the eye. This will travel back along the same paths to the detectors as has just been described. This radiation must be removed before reaching the photo detectors or it may swamp the infrared radiation reflected by the retina. This is done by the stop labelled **CS** in Figure 1.3.4, between lens **L4** and **L5**.

How well does an optometer of this type perform? The claims of a few authors are stated in Table 1-1.

Table 1-1 Range and resolution of Scheiner principle optometers.

Author	Range (Dioptres)	Resolution (Dioptres)
Crane and Steele (1978)	-4 to +12	About 0.1
Okuyama and Tokoro (1989)	-10 to +10	0.05
Takeda, Fukui et al. (1988)	-12.7 to +26.6	±0.25

It is concluded that an optometer using the Scheiner principle with a motorised carriage is capable of making linear measurements of refraction of adequate accuracy for accommodation research. It has two disadvantages.

1. The infrared radiation must enter and exit the pupil of the eye for all measurements. For small pupil diameters very precise alignment to the patient is required.

2. An electromechanical control system is required to drive the carriage motion to the correct position.

To avoid the non linearity that occurred in the optometer of Heron, Winn et al. (1989), the optometers just described use an annulling principle. The photo detectors and source object are moved to a position conjugate to the retina. When this condition is fulfilled, the position of the detectors is proportional to the end point of refraction of the patient's eye. The Scheiner principle itself is only used to detect the departure from this condition which occurs when the retinal image is out of focus.

Photo refraction is another means of detecting the refractive error of the retinal image and can also be used in with an annulling method to measure the end point of refraction. This will be described next.

1.3.3 Eccentric photorefraction

The term “photorefraction” describes the measurement of refractive error by the analysis of photograph of the eye with a flash placed near the plane of the camera and eccentric to the optical axis of the system. The distribution of light seen in the pupil of the eye gives an indication of how close the eye is focused on the plane of the flash. In eccentric photorefraction the flash light source is just beyond the edge of the camera lens (Smith and Atchison (1997)).

An optometer using photo refraction measures the radiant intensity gradient in the pupil plane of the eye by imaging the pupil plane onto the detector of a CCD camera. This radiant energy distribution is called the *pupil reflex*. It is the result of the double passages of infrared radiation through the optics of the eye. The infrared radiation passing into the eye forms an image on the retina in a particular location depending on the refractive errors of the eye. The infrared image on the retina is then imaged by the optics of the eye. The photorefraction technique does not attempt to measure the image reflected from the retina, but measures the distribution of light within the pupil plane. The refractive measurement is done by analysing the image in the pupil plane received by the CCD camera.

When the position of the camera is conjugate to the retina, the reflex has a uniform intensity. When there is a refractive error, the intensity distribution is sloped. The direction of the slope indicates the sign of the refractive error. A higher intensity on the

side of the infrared source indicates a *myopic* error (Smith and Atchison (1997)). The converse is true for a *hypermetropic* error. The slope of the intensity gradient increases with the refractive error (Roorda, Bobier et al. (1997)). The correlation between the intensity gradient and refractive error is patient dependent and requires a calibration curve (Roorda, Bobier et al. (1997)). However, if an annulling system is used where only a zero slope is located, there is no need for calibration. Such an optometer has been devised by Roorda, Bobier et al. (1997) and is shown in Figure 1.3.5.

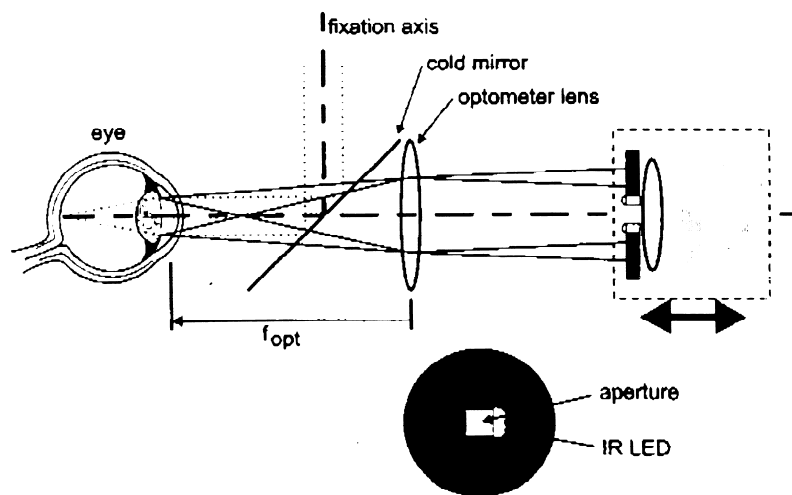


Figure 1.3.5 Optometer using photo refraction.
(Reproduced from Roorda, Bobier et al. (1997))

A lens shown as the optometer lens is placed one focal length from the pupil plane of the eye. The eye is irradiated by infrared emitting diodes on either side of an aperture plate. Behind the aperture is a CCD camera that is used to receive the image formed in the pupil plane of the eye. The detector of the CCD camera is connected to a computer system that calculates the intensity gradient of the pupil reflex. The aperture and camera are manually moved on a rail until the reflex slope is closest to zero. Positions on the rail are calibrated and correspond to end points of refraction of the eye. The calibration depends only on the power of the optometer lens shown in Figure 1.3.5.

The cold mirror shown in Figure 1.3.5 is also a dichroic mirror but optically coated so as to pass infrared radiation but reflect visible light. The cold mirror means that the optometer is an open field instrument.

Computer software is required to detect the edge of the pupil in the received image and calculate the reflex gradient. The rate at which these calculations can be done determines the limiting frequency response of the instrument. Regarding measurements of the dynamics of accommodation Roorda, Bobier et al. (1997) state that moving the camera assembly is not practical. A control system moving the camera would require sampling at 20-40 times the desired corner frequency of the system. It is unlikely that the gradient calculations could be made at the required speeds.

Roorda, Bobier et al. (1997) proposed that the solution to this is to make the dynamic measurements based on the reflex gradient only. However without the use of annulling, the measurements are subject to variations between patients.

It is of interest to ask the question how accurately can the eccentric photorefraction principle detect refractive error? Gekeler, Schaeffel et al. (1997) state the following:

“..there is no doubt that its precision is lower than in autorefractors for the following two reasons: (1) either the height and orientation of reflexes in the pupil must be evaluated subjectively by the experimenter, which limits the reliability of the refraction or, (2) after their objective measurements in digitized video images, slopes of light intensity distributions in the pupil must be converted into refractive error.”

Gekeler, Schaeffel et al. (1997) also state that the variation between subjects is approximately 20%. However, when individual calibration is done, changes in accommodation of 0.25 D can be resolved. It will be seen that this is considerably higher than those obtained with the first two Scheiner principle optometers of Table 1-1. Therefore with regard to accuracy and speed of measurement, the eccentric photorefraction principle is not a good choice for measuring micro fluctuations of accommodation.

The commercial optometer called the Power Refractor that uses this principle has been reviewed by Allen, Radhakrishnan et al. (2003) and by Hunt, Wolffsohn et al. (2003). Hunt, Wolffsohn et al. (2003) comment on the variability due to lack of individual calibration. Allen, Radhakrishnan et al. (2003) state that the Power Refractor is primarily intended as a screening device especially suitable for detecting refractive errors in children. These observations add weight to the assertion that the

photorefraction principle is suited to clinical refractive screening and not precision accommodation measurement.

Instruments using the photorefraction principle are easily aligned to the eye since all that is required is an image of the pupil plane on the camera. Software that analyses the received image detects the boundaries of the pupil (Roorda, Bobier et al. (1997)). The papers reviewed and cited do not mention the effects of eye movements, but it could be predicted that peripheral (off axis) refractive errors would be measured if the fixation of the patient is not close to the optical axis of the photorefracting system. As the camera has limited aperture time, if the eye was moving during the imaging time, then the image of the pupil would be elongated and distorted. This would affect the determination of the gradient of radiant intensity across the pupil, but as the brightness of the eccentric infrared sources can be high, short exposure times (and even video capture) are feasible.

1.3.4 Image analysis

Another method of refraction measurement is by a digital analysis of the retinal image. Instead of photodiodes used with the Scheiner principle optometers, the image on the retina could be relayed to a CCD camera. The image can then be analysed to determine the level of refractive error. A commercial autorefractor that analyses the image on the retina to determine the level of refractive error is the Shin-Nippon SRW 5000 autorefractor. The performance and brief description of internal workings has been described in the open literature by Mallen, Wolffsohn et al. (2001), Wolffsohn, Gilmartin et al. (2001), Roger and Edwards (2001).

The eye receives light from an annular shaped light source. The instrument measures the refraction of the eye by measuring the distortion in the image of a circular annulus reflected from the retina. The distortions of the reflected annulus for different refractive errors are shown diagrammatically in Figure 1.3.6. The distorted shapes are analysed to calculate the refractive error and consequently the refraction of the eye. Wolffsohn, Gilmartin et al. (2001) explain that when used in static mode, an internal lens is moved to bring the image reflected from the retina to an approximate focus on the CCD camera. The image is then analysed digitally to determine the refraction in multiple meridians. The resolution step size offered by the instrument's software is 0.12 D and the results were repeatable. (Davies, Mallen et al. (2003)). The problem with this

method of measurement is the time taken to make a measurement. A measurement time of 0.15 seconds is stated on the instrument's information brochure.

However, with the addition of a computer, a National Instruments Labview card and custom software, Wolffsohn, Gilmartin et al. (2001) explains how a combined instrument can be used to measure the dynamics of accommodation. A resolution of

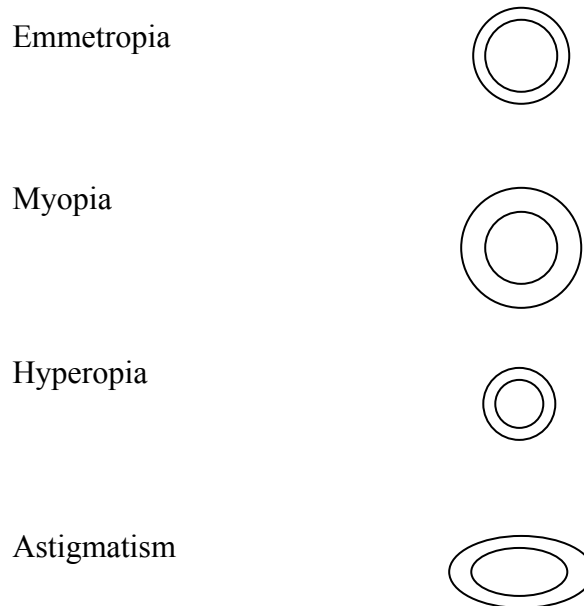


Figure 1.3.6 Refractive errors corresponding to distortions of an annular source.

(Reproduced from Wolffsohn, Gilmartin et al. (2001))

0.0003 D is claimed with 60 measurements per second. These measurements are made by the external Labview software running on a separate computer, not by the SRW5000 as sold commercially. Details of the software involved are not given in the paper by Wolffsohn, Gilmartin et al. (2001). Such a combined system certainly does meet the resolution requirements stated in section 1.2.

The SRW5000 optometer is initially aligned to the eye via the operator's view of the patient's pupil on a monitor screen. A joy stick enables manual alignment of the optometer's optical axis with that of the patient's eye. Regarding eye movement, Wolffsohn, Gilmartin et al. (2001) state that eye movements have little effect on the measurement ring size, since the image analysis program is able to track eye movements. The tracking of eye movements by software analysis of the image also applied to optometers using photorefractometry.

The SRW5000 receives the retinal image via a CCD camera. Instead of analysing the retinal image to determine refraction, it is also possible to measure and analyse the electromagnetic wavefront emanating from the eye. This method is reviewed next.

1.3.5 Wavefront analysis

A wavefront optometer analyses the shape of the wavefront generated by the optics of the eye for a small infrared source projected onto the retina. The optometer uses a Hartmann Shack detector. Schmitzek and Wesemann (2002) describe a handheld optometer using this principle. A diagram of the device is shown in Figure 1.3.7. An infrared laser is projected onto the retina via a beam splitter in front of the patient's eye. The laser is diffusely reflected from a small area of the retina and the reflected infrared radiation passes back through the beam splitter to the Hartmann-Shack detector. This detector consists of a matrix of many lenses. An image is formed by each lenslet on

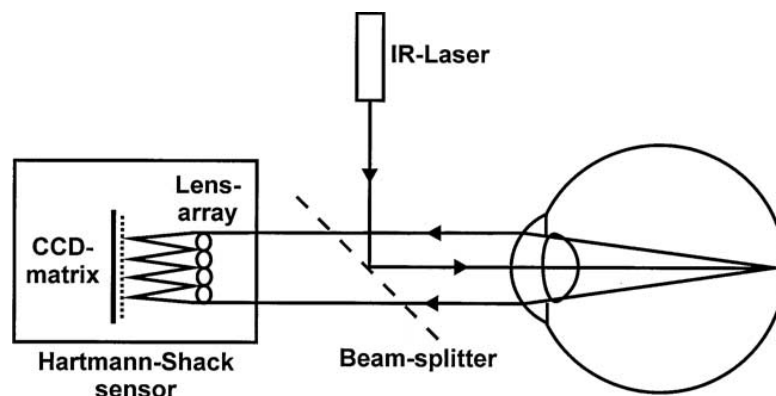


Figure 1.3.7 The wavefront Optometer.

(Reproduced from Schmitzek and Wesemann (2002))

detector of a CCD camera. The positions of the many image spots on the camera can be analysed to determine the shape of the wavefront coming from the eye and from this information about the refraction of the eye is found. The radiant power (flux) of the laser must be safe to shine onto the retina.

Schmitzek and Wesemann (2002) evaluate the commercial SureSight autorefractor that uses this principle. In conclusion, Schmitzek and Wesemann (2002) state that the accuracy is still lower than that of conventional autofractors and that the range of measurement is limited. However a commercial recent wavefront aberrometer called a COAS-HD 2800 produced by Wavefront Sciences (<http://www.wavefrontsciences.com>)

claims a resolution of ± 0.15 D for a refraction range of between -14 to +7 D. No references have been found on devices where the wavefront measurements have been used to measure accommodation dynamics.

1.3.6 Intensity of the reflected retinal image

A patent by Yancey (1997) describes an autorefractor used for measuring the refractive state of the eye. An outline of the device is shown in Figure 1.3.8. The components that are used for refraction measurement will be described here, in order to convey the principle. An infrared source diode labelled 180 is at optical infinity to the eye. Two infrared detectors (diodes) labelled 160 and 150 are at -20 D and +20 D relative to the eye due to the lenses 166 (negative power lens) and 156 (positive power lens). The output received by the diodes depends on the overall refraction of the eye.

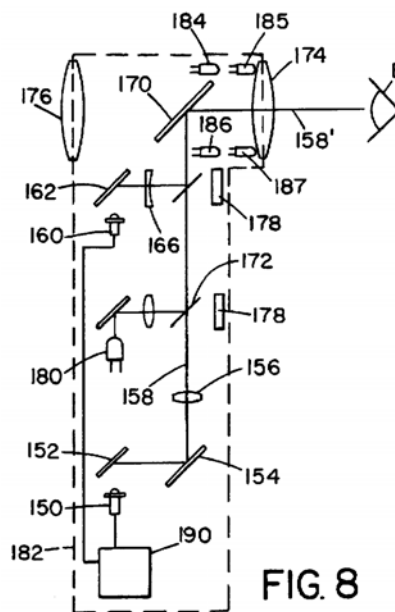


Figure 1.3.8 Device for evaluating the refraction of the eye.

(Reproduced from Yancey (1997))

If S1 and S2 represent the signals received by the photo detectors 150 and 160 respectively, then the quantity $(S1-S2)/(S1+S2)$ is related to the refraction of the eye as shown in Figure 1.3.9. The relationship is not linear but provided the calibration is known then the overall refraction and consequently the end point can be found. The patent describes the principle but not the performance of an actual device. Consequently, this method cannot be legitimately compared with other methods of refraction measurement described.

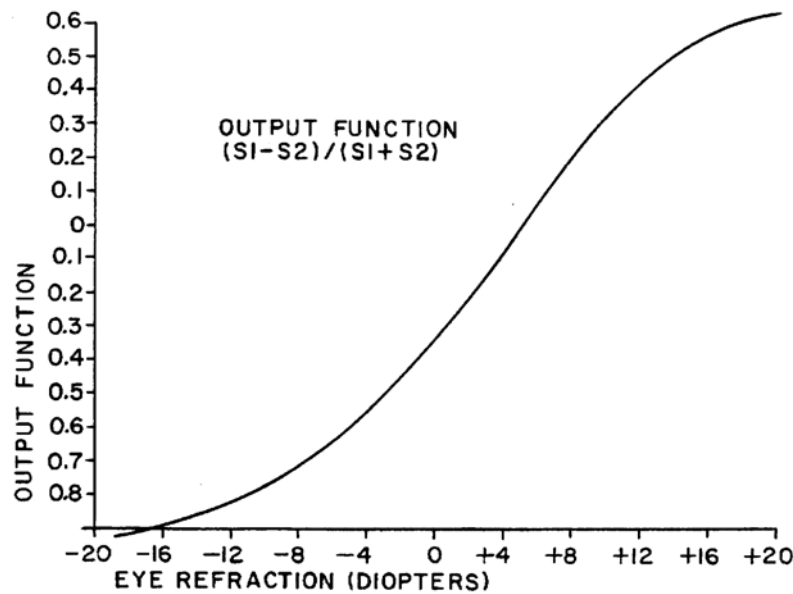


Figure 1.3.9 The output versus eye refraction for Yancey's device.

(Reproduced from Yancey (1997))

1.3.7 Conclusions

Five principles of refraction measurement have been briefly described. These are:

1. The Scheiner principle.
2. The eccentric photorefraction principle.
3. The retinal image analysis principle.
4. The wavefront analysis principle.
5. The principle of measuring the intensity of the reflected retinal image.

In summary, the Scheiner principle is relatively simple, provides adequate resolution and dynamics, but the alignment requirements are very stringent. This means that eye tracking is needed plus some method for initial alignment. The photorefraction principle

analyses the image of the pupil plane. It has limited accuracy, speed of measurement and range. The image analysis principle analyses the retinal image of a known object. With adequate computing power it can resolution and speed of measurement wanted. However, the optometer described is an experimental optometer made from a commercial instrument. The wavefront optometer analyses the wavefront emanating from the retinal image. It is not as accurate as conventional autorefractors and an optometer using it for measuring the dynamics of accommodation is not known of. A measurement of the performance of an optometer using the principle described by Yancey, Schupak et al. (2006) is not known.

If the eye alignment requirements of the Scheiner principle optometer could be met, then an optometer that would meet the requirements of section 1.2 would be a reality. However, this has already been done by Crane and Steele (1978). The optometer of Crane and Steele (1978) will be reviewed in greater detail in section 1.4.2. Unfortunately, the resulting instrument is very complicated with many servo systems. Other developers have achieved similar results for example Takeda, Fukui et al. (1988). Can the same be achieved without such complexity? To investigate this possibility, the methods of optometer alignment and eye tracking will be reviewed.

1.4 Optometer alignment and eye tracking methods

1.4.1 Introduction

The methods of performing and maintaining the alignment of an optometer affect:

1. Ease of use.
2. Additional optics and electronics required for alignment.
3. Whether the optometer can be used for continuous recording or just one shot measurement.

Heron, Winn et al. (1989) point out that there is limit to the time a patient can tolerate when under bite bar and head restraint conditions. The need for such stringent alignment conditions should be avoided in the design of the optometer. This is more important when an optometer is required for continuous rather than one shot measurements.

The technology used to meet the stringent alignment and eye tracking requirements of a Scheiner principle optometers will be described first. Then the alignment methods used by other optometers will be reviewed.

1.4.2 Optometers using the Scheiner principle

Optometer using the Scheiner principle require precision in aligning the optical axis of the optometer to the centre of the patient's pupil. This is because radiant flux entering the pupil from both of the IREDs needs to be equalised. The balance of radiant power input can only occur when the images of both the IREDs equally overlap the area of the pupil of the eye. This stringent requirement is a problem with the Scheiner principle optometer and the methods used to handle it, will be reviewed first.

Early infrared optometers of this type such those of Campbell and Robson (1959) and Cornsweet (1970) required manual alignment. Only Cornsweet (1970) gives an explanation of how this can be done using an infrared viewer.

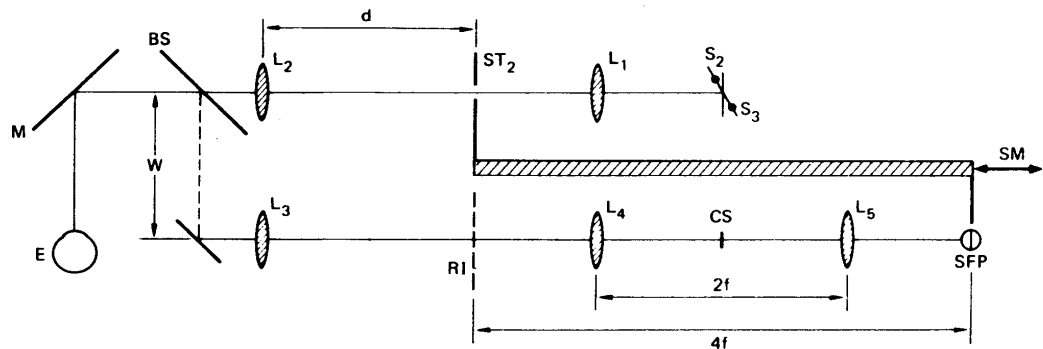


Figure 1.4.1 An outline of an optometer using the Scheiner principle.

(Reproduced from Crane and Steele (1978))

Referring to Figure 1.4.1, an image of the pupil plane appears at the position of the corneal stop labelled **CS** in the diagram. By placing a mirror between **CS** and **L5**, a view of the pupil plane can be seen by an **IR** viewer. This is because the lenses **L3** and **L4** are separated by the sum of their focal lengths and the pupil plane of the eye is one focal length from the lens **L3**. The patient or the optometer can then be moved until the instrument is centred on the pupil. This will be when the infrared reflected from the cornea is blocked by the stop **CS**.

The IR or light reflected from the front (anterior) surface of the cornea is termed the *corneal reflection* or the *first Purkinje image*. Reflections from the other surfaces of the cornea and lens of the eye are also called Purkinje images. In particular, the reflected image from the rear (posterior) surface of the lens is called the 4th Purkinje image. Since

the corneal reflection is used align the optometer to the eye, it could also be used to maintain this alignment.

By measuring the relative positions of both the 1st and 4th Purkinje images, Crane and Steele (1978) have developed a combined optometer and eyetracker. The eyetracker is capable of measuring the rotations of the eye and the position of the corneal image is used to maintain alignment of the instrument to the eye. Combining the eye tracking with the optometer has the huge advantage in that the stringent alignment requirements of a Scheiner principle optometer are met by having an eye tracker automatically align the instrument to the subject. The eyetracker and the optometer share a common input path, so that when the eye tracker is aligned to the eye so is the optometer.

The eye tracking system of Crane and Steele (1978) will be explained, firstly because it explains how the corneal reflection can be used to maintain the alignment of the optometer. Secondly, the idea of using a two dimensional mirror system is relevant to the optical system proposed in this thesis. Finally, the eye tracking system is worth explaining because the method of automatic eye alignment is described.

The optical schematic of the eye tracker is shown in Figure 1.4.2 . At the core of the tracking system is a two dimensional servo mirror system **M1** and **M10** shown more clearly in the inset diagram. The inset diagram shows that the servo mirror system has motor drivers and position detectors. When the first and fourth Purkinje images are centred on their respective quadrant photodiodes **P1** and **P4**, the horizontal and vertical position of their respective mirrors are proportional to the positions of the first and fourth Purkinje images.

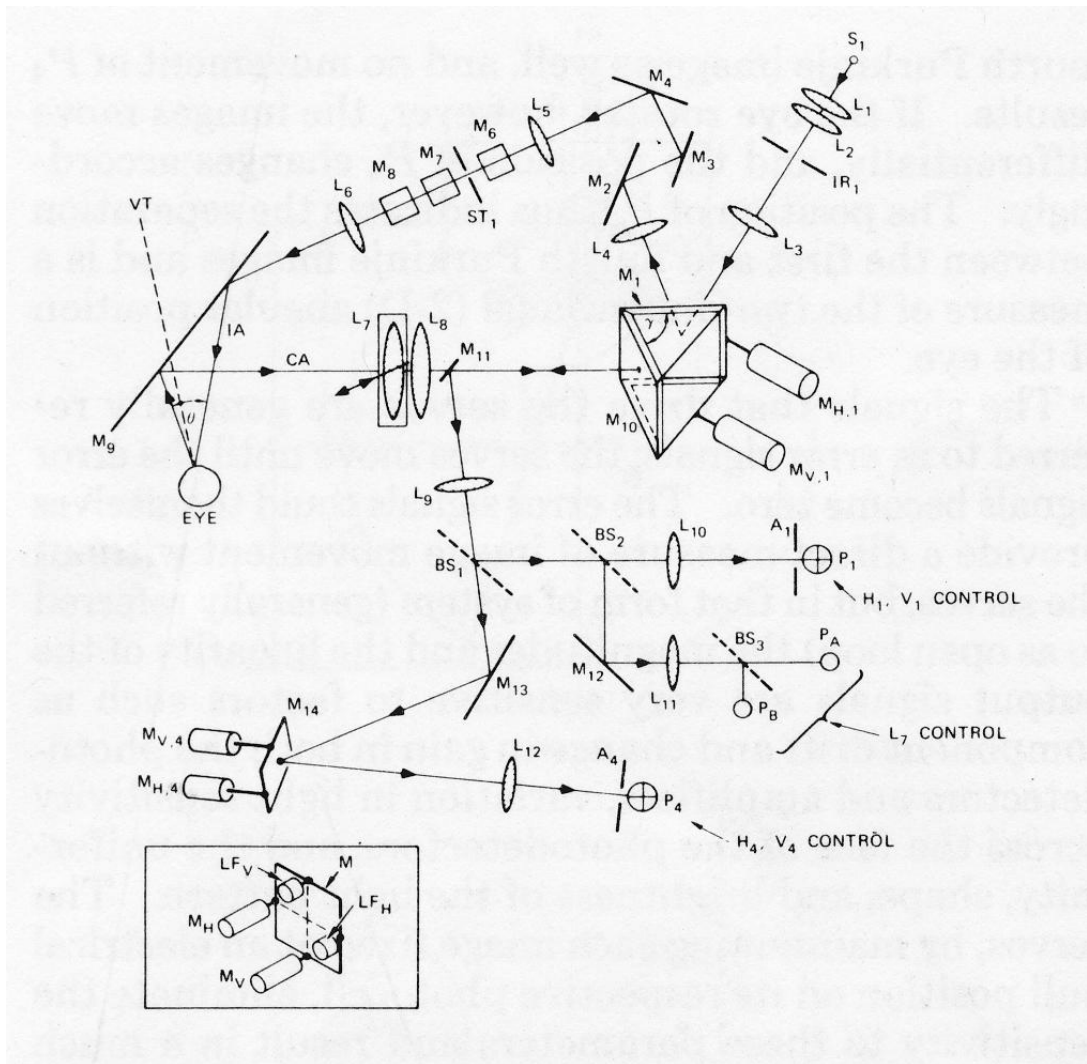


Figure 1.4.2 1st and 4th Purkinje eyetracker system.

(Reproduced from Crane and Steele (1978))

The mirrors **M1** and **M10** are two mirrors that form a prism, driven as one, by horizontal and vertical servo systems. This enables both the input and output light paths to be changed *simultaneously*. The optical/electromechanical control systems are annulling systems so that if the first Purkinje image is not centred on quadrant photodiode **P1**, the mirror system **M1/M10** is driven to centre the image. Similarly, if the fourth Purkinje image is not centred on the quadrant photodiode **P4**, the servo mirror system **Mv4/Mh4** is driven to centre the image on the photodiode **P4**.

The automatic eye alignment is achieved as follows. When the first Purkinje image does not fall on photodiode **P1**, the mirror system **M1/M10** is driven in an outward spiral path from a central position until the first image is found. This initial capture is claimed to occur within $\frac{1}{2}$ a second. Once the first image has been located, a similar spiral path search is made by the fourth Purkinje mirror system **Mv4/Mh4**. The positions of the

first and fourth mirror systems give the positions of the first and fourth Purkinje images respectively and these give accurate translational and rotational position of the patient's eye.

The eye tracker also has an automatic focusing system to allow for a ± 5 mm axial variation in eye position. Without this automatic focusing, intolerable blurring of the Purkinje images would occur. The auto focusing is achieved by moving lens **L7** along the direction indicated by the arrows, which is parallel to the infrared input axis of the eyetracker. The control signal for doing this comes from the difference of signal from photodiodes **Pa** and **Pb**. These photodiodes would be equidistant from the first Purkinje image formed between them.

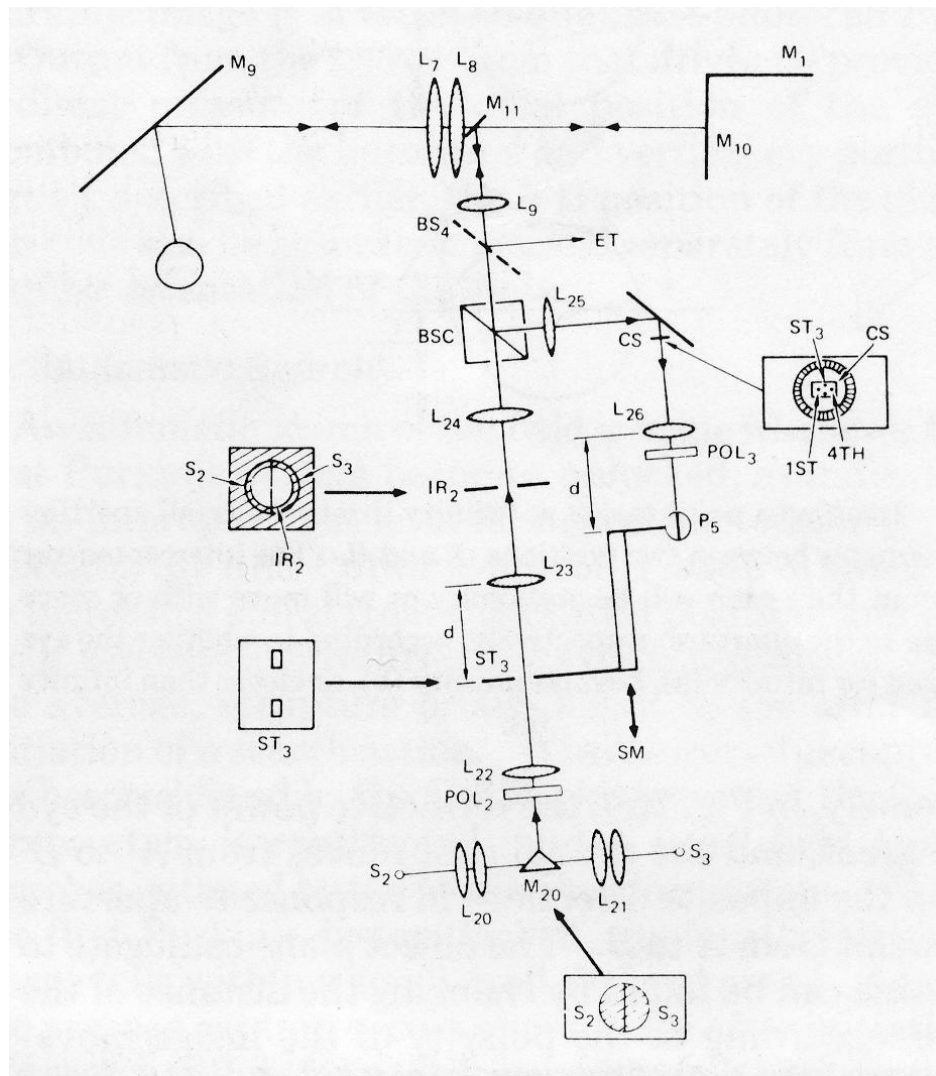


Figure 1.4.3 The optometer system of Crane and Steele.

(Reproduced from Crane and Steele (1978))

Once initial searching is successful, the eyetracker maintains the alignment as it continues to centre the first Purkinje image on the **P1** photodiode. The optometer system is incorporated into the eye tracker as shown in Figure 1.4.3. The input and output axis of the optometer is collinear with the output axis of the eyetracker. The output to the eye tracker comes from the beam splitter **BS4**. *The huge significance of this joining of two instruments is that the optometer will remain centred on the patient's pupil whilst the eyetracker maintains the 1st Purkinje image centred on quadrant photodiodes P1.* The location of the 4th Purkinje image does not appear to have any affect on optometer operation. The eye tracking system enables the optometer system to work over a ± 15 degree angular field.

The Crane and Steele (1978) optometer and eyetracker are automatically aligned to the patient's eye and the system maintains this alignment.

The combined instrument of Crane and Steele (1978) has far more optical components and servo systems than much more recent optometers with monitor screens and manual alignment. The eye tracking optometers of Okuyama and Tokoro (1989) and Takeda, Fukui et al. (1988) are examples of such devices. The extra complexity of the Crane and Steele (1978) instrument enables it to achieve automatic patient alignment and eye tracking without the use of a monitor screen or operator involvement. However all of the extra optics and control systems involved would make the instrument very expensive and perhaps commercially not competitive with those that use simpler optics and fewer control systems.

1.4.3 Eye alignment methods used by non-Scheiner principle optometers

The infrared recording retinoscope of Kruger (1979) for monitoring accommodation inserted in mirror across the optical axis of the optometer. Using a telescope, the operator could see an image reflected from the cornea. The patient's position could then be adjusted to align the patient to the optometer. This is much the same as what was done by Cornsweet (1970).

Many more recent optometers provide a monitor screen where a view of the patient's eye can be seen. The operator can manually move the optical axis of the optometer until the corneal reflections from the patient's eye are aligned to the optometer. A few examples of such optometers are the Shin-Nippon SRW 5000 (Wolffsohn, Gilmartin et al. (2001)), the Canon R1 optometer (Pugh and Winn (1988)), and device described by the patent of Yancey (1997). A more recent patent by Yancey, Schupak et al. (2006) of a closed field autorefractor, describes an instrument that uses monitor screen to show the corneal reflection from the patient's eye. The optical axis of the instrument is moved until alignment is reached. In each of instruments mentioned, the monitor screen provides for initial manual alignment but not for subsequent eye tracking.

It has been seen in section 1.3.3 that optometers using eccentric photorefraction use an image of the entire eye and by image analysis determine the boundaries of the pupil. This eliminates the need for precise operator alignment, although alignment with the visual axis is necessary, if off axis measurement of refraction are to be avoided.

1.4.4 Conclusions

Optometers that use an image reflected from the retina require relatively accurate alignment since the optometer's input light source must pass through the patient's pupil. Conversely an optometer that only looks at the pupil plane or in front of the cornea does not require alignment that is as accurate. The alignment problem is for optometers that use an image reflected from the retina.

The 1st Purkinje image is used in the dominant method of alignment both for manual and automatic use. In optometers using a CCD camera and monitor screen, the visual position of the pupil in relation to the instrument's projected light source is used for manual alignment by an operator. The 1st Purkinje image on the CCD camera can be used to implement an automatic eye tracking system.

Only the eyetracking optometer of Crane and Steele (1978) used an automatic searching system to *initially* align the instrument to the eye. In the other optometers surveyed, the initial alignment was done manually. The optometer of Crane and Steele (1978) needed to track the Purkinje images for its eye tracker but used the retinal reflection for refraction measurement.

However it has been seen that optometers which analyse a digital image such as those using image analysis and photorefractometry can cope with *some* eye movement. This is because the analysing algorithms detect the edges of the image. Nonetheless, the optical axis of the infrared source still needs to be aligned sufficiently with pupil of the eye, in order to get infrared radiation in and out of the pupil. How much eye movements can be tolerated by an optometer analysing a digital image was not reported on.

Apart from optometer using digital image analysis, the radiation reflected from the retina has not been used to align the optometer to the eye, or to maintain alignment. This is the gap in the current technology to be explored in this investigation.

1.5 The objectives of this investigation

The general aim of this study is to improve the technology of optometers used for research with regarding initial alignment and eye tracking for continuous measurement. To align an optometer with the pupil of the eye, the input and output optical axes of the optometer need to be capable of lateral movement relative to the position of the patient's eye.

It is proposed that the degree of alignment can be measured by IR radiant power received from the retina of the patient's eye. The hypothesis is that when the positions of the optical axes of the optometer, maximise the radiate power received from the retina, the optometer aligned to the patient. *Consequently, the first objective of the studies reported in this thesis, is to test whether an optometer system can be developed that can align itself to a patient's eye by maximising the radiant power received from the photo detectors receiving a retinal reflection.*

The eye is in constant movement, hence, to continuously measure refraction, it is expected that a *maintained* or *continuous* alignment of the optometer with the patient, will be required. From this comes the second objective. *This is to test whether an optometer system can maintain its alignment to the patient's eye when the pupil of the eye is moving. The mechanism proposed is that the optometer would adjust its by the alignment to continuously maximize the radiant power received from the retina.*

It could well be possible to build a system that will locate the patient's pupil and track its motion as the eye moves. However the final question remains. Can such a machine

also measure the refraction whilst tracking the pupil movement? From this comes the third objective. *This is to test whether an optometer using the proposed alignment and tracking system is capable of measuring the refraction of the eye in continuous mode.*

A well established method of measuring visual refraction is the Scheiner principle. The Scheiner principle optometer requires that IR radiant energy enter and leave the eye via the pupil, and is therefore a suitable method of refractive measurement on which to test the alignment and tracking system proposed. Optometers of this type surveyed, generally use the Purkinje image reflected from the cornea for alignment to the eye. The proposed system would eliminate the need for separate systems for alignment. The investigation described herein will use Scheiner principle as its method of refractive measurement.

1.6 Outline of the thesis

The optical design of the experimental optometer using the Scheiner principle is presented in chapter 2. This will be the instrument which will be used for the experimental investigation. Removal of the corneal reflection using crossed linear polarizers is discussed and developed.

The ability of the system to have its optical axis aligned to the patient's eye is crucially dependent on the operation of a servo controlled mirror system. The requirements for the mirror control system and the control system design are described in chapter 3. In addition, Chapter 3 also describes the overall electromechanical and outlines the electronics of the optometer system. Most of the optical and electronic hardware was designed and constructed before the time of the current study. The one major exception is the two dimensional servo mirror system developed within this study.

An overview of the embedded software used for performing the measurements and driving the control systems is given in chapter 4. In addition the method of transferring results from the optometer to the host computer system is described.

The experimental tests on the optometer system are described in chapter 5. The artificial eye used in the experimental procedures is described first. Chapter 5 then describes three experimental procedures to test:

1. How well do the crossed linear polarizers remove the unwanted reflection from the front surface of the lens in the artificial eye? (The corneal reflection)
2. Is it possible to make a Scheiner principle measurement of the overall refraction of the artificial eye?
3. Can the boundaries of the pupil of the artificial eye be found by scanning the pupil plane using the servo mirror system?

Finally, chapter 6 summarizes the conclusions reached as a result of this investigation. The deficiencies revealed during the experimental investigation are the basis for future work to be pursued. This proposed future work concludes the thesis.

2 Optical system design

2.1 Introduction

Optometers using the Scheiner principle have been described in many references including Campbell and Robson (1959), Cornsweet (1970), Crane and Steele (1978), Takeda, Fukui et al. (1988), Okuyama and Tokoro (1989) These optometer use a reflection from the retina of the eye to perform refraction measurement and require that infrared radiation enter and exit the eye via the pupil. The entry and exit of infrared radiation via the pupil means that optical alignment of the optometer axis with the eye is crucial. If this alignment could be done using only the infrared reflected from the retina, then there would be a considerable simplification of the optical and electronic systems required, since no additional optical or electronic components would be required for patient alignment. *The research question and hypothesis of this investigation is to test the feasibility of this idea with an optometer system using the Scheiner principle.*

At the commencement of this study, the framework, optics and electronic components of a Scheiner principle infrared optometer had already been built. These systems have undergone considerable modification during the time of the study. This optometer system will be referred to as the “*experimental optometer*” and is the platform on which the hypothesis of this study is to be developed and evaluated. All other systems in an optometer are to support the optical system and therefore the optical principles are described first.

2.2 The optical system

The Scheiner principle and its application to optometers have been described in 1.3.2. The experimental optometer is based around the optical principles of the optometer developed by Crane and Steele (1978) described in 1.3.2 with some differences.

The optometer’s optical system projects an infrared image of a square aperture onto the retina and images the reflection from the retina onto a set of photodiodes capable of detecting lateral motion. The aperture is irradiated from both sides by alternating

infrared sources. The aperture and the photodiodes are fastened together on a moveable carriage so that both move together as shown in Figure 2.2.1. *The optics of the system are designed so that both the photodiodes and aperture have precisely the same optical distance from the eye.*

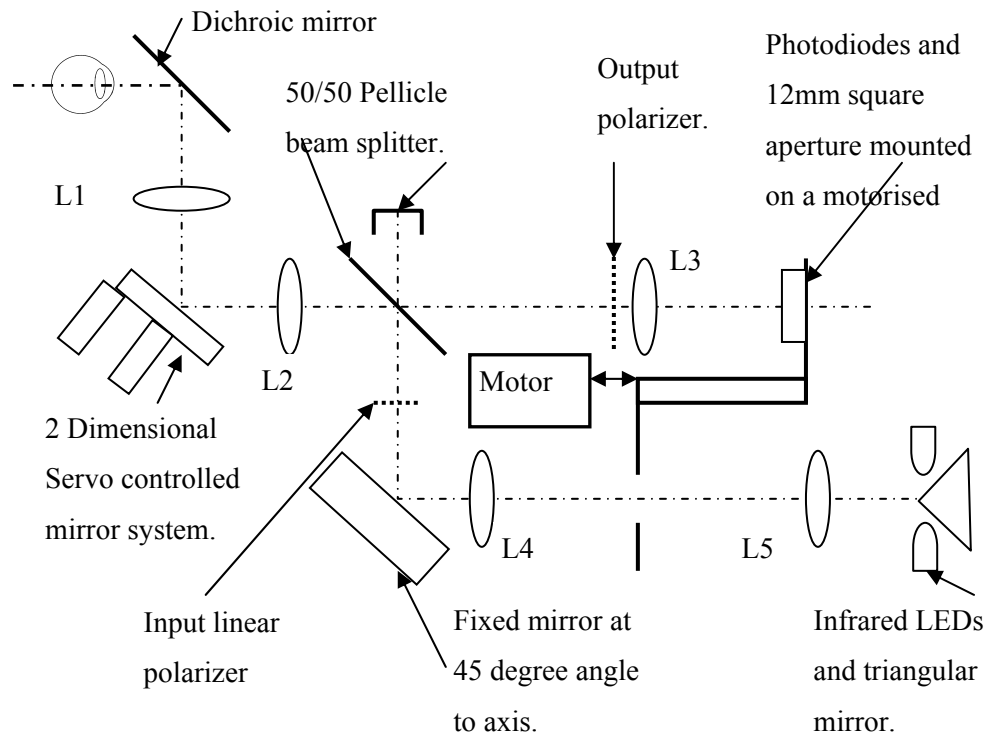


Figure 2.2.1 The optical system of the experimental optometer.

Hence, when the photodiodes are conjugate to the retina of the eye, so is the aperture. To measure the refraction of the eye, the carriage is moved until the photodiodes do not detect any lateral motion of the reflected retinal image as infrared sources are alternately powered. When this condition is satisfied, the aperture and the photodiodes are optically conjugate to the retina. The refraction of the eye can then be calculated from position of the carriage relative to the lenses of the system.

The principles of the optometer's lens layout can be briefly described as follows. Generally speaking these ideas are not new and are already used by optometers of similar type. The patient views a visible target through a *dichroic* mirror that passes visible light but reflects infrared radiation. The optometer measures the overall

refraction of the patient's eye whilst the patient is viewing the target, by finding the plane in space conjugate to the patient's retina.

Let A' be the distance from lens **L2** of the image of the aperture, which is relayed by the lenses **L4** and **L2** and the intervening fixed mirror. Let A be the distance of the real aperture from the lens **L4**. Then since **L4** and **L2** are separated by the sum of their focal lengths, A' can be calculated from the equation for a telescopic lens pair stated in equation 1-1 to give equation 2-1.

$$A' = f_2 \left(1 + \frac{f_2}{f_4} \right) - \left(\frac{f_2}{f_4} \right)^2 A \quad 2-1$$

Where f_4 and f_2 are the focal lengths of lenses **L4** and **L2** respectively. When the image of the aperture at A' is conjugate to the retina, the reflected image of the aperture from the retina will also appear at A' . This is because of the principle of optical reversibility stated by Jenkins and White (1981) on page 14. This reflected image will be relayed to the photodiodes by the lens relay pair **L2** and **L3**. When the image of the aperture at A' is not conjugate to the retina, there will be a blurred reflection of it at A' and this blurred reflection will be relayed to the photodiodes.

The photodiodes should detect the lateral shifting of the blurred image as the infrared sources are alternately powered. The sign of the refractive error at the retina can be determined by whether their movement is in-phase or out-of-phase with alternating infrared sources. If the retinal image moves in the same direction as the powered infrared source, the refractive error is positive. If the retinal image moves in the opposite direction as the powered infrared source, then the refractive error is negative. A positive refractive error requires the carriage be moved further from lens **L3** to reduce the error to zero. A negative error requires the converse.

The input and output paths of the instrument could be separated by having separate lenses **L2** and **L1** for both infrared input and output with the pellicle beam splitter close to the dichroic mirror. Such an arrangement was used by Cornsweet (1970). The separate input and output paths means that infrared reflected by lenses common to the input and output path is not received by the photodiodes. However, by having **L1** and

L2 common to the input and output path, a servo mirror can be placed between them that changes both the input and output paths simultaneously. This should enable the instrument to allow for a range of positions of the patient's eye. The servo mirror system could have been placed between the lens **L1** and the dichroic mirror, but this would be awkward to arrange since **L1** must be close to the patient's eye. It also might have been possible to make the dichroic mirror servo controlled. A known disadvantage of placing the servo mirror between **L1** and **L2** is the vignetting due to the limited diameter of lens **L1**.

Taylor (2003) shows for the system shown in Figure 2.2.1 that when the photodiodes are conjugate to the retina, the spherical refractive power of the eye is given by equation 2-2, where the focal lengths f_1, f_2, f_3 are the focal lengths of lenses **L1**, **L2** and **L3** respectively and X_3 is the distance of the retinal photodiodes from lens **L3**.

$$D_e = \frac{f_2^2}{f_3 f_1^2} \left(1 - \frac{X_3}{f_3} \right) \quad 2-2$$

Since the range of X_3 can be from zero to $2 \cdot f_3$ the range of refractive power measurable by the optometer is as shown in equation 2-3.

$$\text{Optometer range in dioptres} = \pm \frac{f_2^2}{f_3 f_1^2} \quad 2-3$$

Each of the five lenses in the experimental optometer has a focal length of 200 mm at a wavelength of around 930 nm. This results in a maximum refractive range of ± 5 dioptres. Unfortunately this choice of lens power was determined by the availability of lenses at the time the optometer system was originally designed more than design reasoning. The optical components will now be looked at in more detail.

The infrared sources are infrared emitting diodes (IREDs) placed on either side of a prism mirror. The infrared IREDs appear as two half moons when viewed from the position of lens **L5**. This is similar to the optical arrangement of the sources in the optometer of Crane and Steele (1978) as shown in Figure 1.4.3, except that the IREDs here do not have lenses directly in front of them. The lenses **L20** and **L21** shown in

Figure 1.4.3 form a smaller image of the IREDs on the prism mirror so as to obtain a width that will fit within the pupil of the eye. This is a slightly better optical system than the one used here. The optical requirement is that the radiation emitted from the IREDs is collimated by lens **L5**.

Collimation is required so that the aperture will be uniformly irradiated at any position of the carriage. Therefore lens **L5** is placed one focal length from the apex of the prism. Manufacturer's data and experimental measurement shows that infrared diodes have a relatively narrow directional characteristic. The refraction of the encapsulating plastic of the diode means that they do not behave as point sources, so the collimation is approximate. Consequently the positioning of the IREDs and the prism mirror is very sensitive to positioning error. In aligning the system, an infrared photodiode with an amplifier and meter was used to measure the level of radiation around the aperture. The diodes and prism were aligned to obtain the best constancy of radiation level at all carriage positions. This is so that the aperture is uniformly irradiated as it moves between lenses **L4** and **L5**.

The telescopic lens pairs **L4/L5** and **L2/L1** relay the image of IREDs to the pupil plane of the eye. The image at the pupil plane of the eye of the IREDs is called the *image of sources* and will be referred to frequently in subsequent chapters. The focal plane of lens **L2** is at the same position as the focal plane of lens **L4** so the two lens pairs operate as two pairs of telescopic relay lenses in series. The lenses **L5**, **L4**, **L2** and **L1** are on the optical input path to the eye. Infrared flux reflected from the eye returns via the optical output path consisting of lenses **L1**, **L2**, **L3** and the beam splitter to the photodiodes.

As previously explained the beam splitter combines the input and output optical paths of the instrument. The beam splitter is optically coated so as to reflect 50% and pass 50% of the infrared radiation impinging on it. Lenses **L1** and **L2** are common to both the input and output axes of the instrument. Unfortunately the lens surfaces will reflect some of the input radiation back to the output. The lenses **L1** and **L2** have been optically coated to reduce the level of the reflection to approximately 0.5% per lens. The optometer of Okuyama and Tokoro (1989) does not have any lenses common to the input and output optical path thereby avoiding interference due to unwanted reflections. However the optometer system of Crane and Steele (1978) shown in Figure 1.4.3 there are three lenses common to the input and output path of the optometer. Crane and Steele

(1978) explain that reflections from lenses common to the input and output path are removed through using polarization.

In this optometer, polarization is also used for removal of specular reflections. The use of polarization to remove unwanted reflections will be described later in this section. Having the common input and output lenses reduces the total number of lenses in the system.

Between lenses **L2** and **L1** is a servo controlled mirror whose angular position can be controlled about two orthogonal axes. One axis is horizontal and the other is perpendicular to it. The two axes of mirror rotation intersect at the optical axis of lens **L2**. The mirror system is mounted at a 45 degree inclination to the horizontal. This is so that when the mirror is in its central position, the horizontal axis of lens **L2** becomes the vertical axis of lens **L1**. The 45 degree inclination of the dichroic mirror closest to the eye reflects the vertical axis to a horizontal one to match the patient's eye. Rotation of the servo mirror moves the image of the sources at the pupil plane of the eye. The limitations to the available movement are determined by the vignetting of lens **L1**. Experimentally it has been found possible to achieve a ± 10 mm movement of the image of the sources at the pupil plane of the eye. This mirror system forms the basis of the patient alignment system to be investigated in this work.

Rotation of mirror system determines the position image of the sources at the pupil plane. When the instrument is correctly aligned to the patient's eye, the image of the sources will be centred on the patient's pupil allowing equal radiant flux from both infrared IREDs to enter the eye.

Since the lenses all have the same focal length, the image of the sources at the eye has exactly the same size as the actual IREDs although of greatly reduced radiant intensity. The position of the image of the sources is independent of the position of the aperture and therefore of carriage movement. Experimental measurements have shown that there is small drop in radiant power at the eye as the aperture is moved towards lens **L4**. Since the lateral motion of the retinal image is to be measured, a small drop in absolute radiant power should not be a problem.

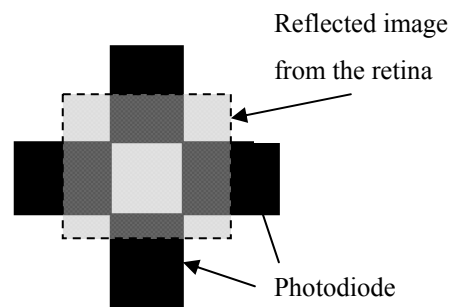


Figure 2.2.2 Photodiode arrangement to detect image movement

The aperture is a 12 mm square aperture. The reason for this choice of size and shape of the aperture is the photodiode arrangement designed to detect lateral movement of the retinal image of the aperture. The photodiode arrangement is shown in Figure 2.2.2. It can be seen that as the reflected image of the sources moves, the area of overlap with the photodiodes changes. The four photodiodes arranged in cross enable both vertical and horizontal movement of the reflected image to be measured.

An image of the 12 mm square aperture will be reflected from the anterior (outer) surface of the patient's cornea. This image is called the *corneal reflection*. It is also known as the 1st Purkinje image. It is important that this reflection and reflections from other refracting surfaces of the eye, do not interfere with the reflection from the retina.

The size of the corneal reflection can be calculated from the lens arrangement and the assumption that the anterior surface of the cornea behaves as a convex mirror with a radius of 7.8 mm (Atchison and Smith (2000)). The details of this calculation are given in Appendix 8.1. The calculation shows that when the aperture is centrally located

between lenses **L4** and **L5** that the size of the corneal reflection approaches zero. When the aperture is either very close the position of lens **L4** or lens **L5** the corneal reflection is approximately 0.23 mm in size and situated 3.8 mm posterior of the corneal apex which is very close to the pupil plane. The relay lens pair **L1** and **L2** produces an image of the corneal reflection in the focal plane of lens **L2**, which is conjugate to the pupil plane of the eye. The radiation from this image must be blocked from reception by the photodiodes. How this is done is discussed next.

2.3 The removal of the corneal reflection

In other optometers of this type the corneal reflection is blocked from reaching the receiving photodiodes by placing an appropriately sized stop in the focal plane of lens **L2**. However, such a system is not possible with the proposed optometer, since when the eye is not aligned to the optical axis of the optometer, *the position of the reflected corneal image in the focal plane of lens L2 will not be centrally located or fixed in position*. The position of the corneal image in the focal plane of lens **L2** will be determined by the position of the cornea relative to the input/output axis of the optometer at the pupil plane of the eye. Consequently, it was decided to try using polarization to remove specularly reflected radiation.

The fundamental principle is that radiation reflected from the cornea and lenses common to the input and output paths is *specular* whereas the radiation reflected from the retina is *diffuse*. When linearly polarized radiation is reflected from a dielectric surface it remains linearly polarized although its azimuth angle will be changed as shown in Figure 2.3.1. The change in azimuth angle depends on the angle of incidence to the reflecting surface. The *azimuth angle* (Ψ) as defined by Jenkins and White (1981) on page 530 is as shown in equation 2-4.

$$\tan(\psi) = \frac{R_p}{R_s} \quad 2-4$$

Where R_p is the component of the electric vector parallel to the plane of incidence and R_s is the component of the electric vector perpendicular to the plane of incidence.

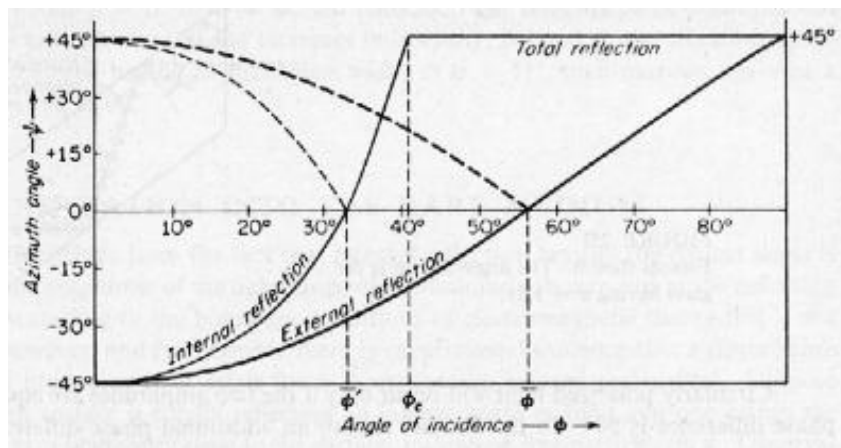


Figure 2.3.1 Azimuth angle versus angle of incidence for reflection from a dielectric surface.

(Reproduced from Jenkins and White (1981))

The cornea of the eye and lenses common to the input and output path are all dielectric surfaces and will change the azimuth angle of linearly polarized radiation reflected from them. Consequently, the reflection can be removed by orientating a crossing linear polarizer at 90 degrees to the polarization plane of reflected radiation. Yet radiation reflected diffusely from the retina will no longer be polarized and a component of it will pass through the crossing polarizer.

The optometer of Crane and Steele (1978) used this principle by using a polarizing beam splitting cube instead of a pellicle beam splitter shown in Figure 2.2.1. A beam splitting cube will reflect S component of radiation (perpendicular to the plane of incidence) whereas will pass the P component of the radiation (parallel to the plane of incidence). Using the cube for beam splitting has the advantage over using a pellicle beam splitter in that the pellicle beam splitter loses 50% of radiation that passes through it. However, the cube passes close to 100% of the P polarized radiation. (Edmund (2008)). The cube has disadvantage that there is some scattered radiation reflected from the diagonal surface. Furthermore it is believed there is another more serious disadvantage the polarizing cube explained next.

Any other mirrors in the path between the beam splitting cube and the eye will rotate the azimuth angle of the polarized radiation going to the cornea and reflected from the

cornea. Consequently, to block the reflected plane polarized radiation, the output polarizer must be at a different angular orientation to the input polarizer. However the polarization angles are fixed with polarizing cube.

Crane and Steele (1978) admits that their polarizing system was not sufficient to remove all the radiation reflected by the corneal image but did remove the reflections from the lenses common to the input and output paths. They attribute this to the scattered radiation reflected by the diagonal surface of the cube, but this might not be the only reason. They do not mention the affects of the *mirrors* on the polarization of the infrared radiation.

In particular, Crane and Steele (1978) do not state whether the servo mirror system shown as mirror **M10** in Figure 1.4.3 is a metallic or dielectric mirror. However, they do state that it is front surfaced mirror. A front surfaced mirror would normally consist of glass coated with aluminium. If it is a metallic mirror it is likely to cause substantial *circular or elliptical polarization* of the incoming plane polarized radiation.

Circular or elliptical polarization occurs when there is a phase difference between the components of the electric field perpendicular to, and parallel to, the reflecting surface. When there is a phase difference between the perpendicular and parallel component of electric field, the resulting electric vector does not have fixed azimuth angle but is continually rotating. Jenkins and White (1981) on page 534 explain that the only exception is when the incoming plane polarized radiation vibrates in the plane of incidence or perpendicular to it. However, since the mirror is moving, such a condition could not be maintained. *The problem with elliptically or circularly radiation is that it will not be removed by a crossed linear polarizer although its amplitude will be reduced.* It is suspected that this is the main reason why the polarizing beam splitting cube of the optometer of Crane and Steele (1978) did not adequately remove the corneal reflection.

To resolve the problem, any mirror system between the input and output polarizer *must* be a dielectric mirror not a metallic mirror. If this is the case, then the mirror will cause changes in the azimuth angle of the plane polarized radiation, but will not cause circular polarization.

Using these principles of polarization, the optometer system shown in Figure 2.2.1 proposes to remove the corneal reflection as follows. A linear polarizer is placed between lens **L4** and the pellicle beam splitter. Reflections by the beam splitter, servo mirror and dichroic mirror will cause the azimuth angle of the input radiation to be changed. The servo mirror will be a dielectric mirror the same as the dichroic mirror in front of the eye. It is proposed to experimentally align the orientation of a crossed linear polarizer placed on the beam splitter side of lens **L3**. The polarizer will be orientated so as to best remove the reflection from the lens surface of an artificial eye. This would be done by adjusting its angular position until the electrical output from the photodiodes is a minimum. Placement next to lens **L3** is most advantageous with regard to removing any other stray radiation.

With the linear polarizers correctly orientated, only diffusely reflected radiation from the retina should be present at the photodiodes. This is what is required for refractive measurement.

2.4 Conclusions

The overall optical design of a Scheiner principle infrared optometer have been described with a modified method of removing the unwanted corneal reflections. It is yet to be established whether the proposed method will work in practice. This will be determined in the experimental work described in chapters 5. Removing the corneal reflection is vital prerequisite for developing the hypothesis of this work. Can the information provided by the radiation reflected by the retina alone, be used to initially align the instrument to the eye? This will also be experimentally examined in chapter 5.

This completes the description of the optometer's optics. The electro-optical and electromechanical systems are vital in making the overall system work. These systems will be described next.

3 Opto-electronic and electro-mechanical design

3.1 Introduction

In the previous chapters the overall design of an infrared optometer based on the Scheiner principle has been described. In this chapter the electronic and electromechanical systems are briefly described so that the reader understands this as the basis for the experiments that follow. Much of the design and construction was done prior to this study. Some of it is referred to in the author's previous thesis for a Post Graduate Diploma (Taylor (2003)). For this reason, much of the design presented is not derived only described.

However, the detail design of the two dimensional mirror system is given, since it was developed during the period of this study and since it is at the core of the operation of the proposed optometer system. The mirror system makes it possible to scan the image of the sources across the pupil plane of the eye to detect the pupil. The details of the carriage motor system for positioning the carriage have been omitted, since this system was not used in the current investigation. Any positioning of the carriage was done manually.

3.2 Opto-electronic systems overview

A block diagram of the optometer systems is shown in Figure 3.2.1. The reader requires an understanding of the overall optometer system before the details can be discussed. The functionality of the blocks in the diagram and their relationship will be described. The optical system has already been described in chapter 2.

The optical system focuses and directs the output of infrared radiation emitting diodes, shown as the IREDS block. The infrared reflected from the retina, focused by the optics of the eye and the optical system of the optometer, is measured by the photodiodes. The photodiodes are shown as the PHOTODIODES block. Using measurements derived from the outputs of the photodiodes, an error signal is generated that is proportional to

the refractive error of the image of the aperture on the retina. This measurement is where the Scheiner principle is applied and this is described in section 5.5.2 .

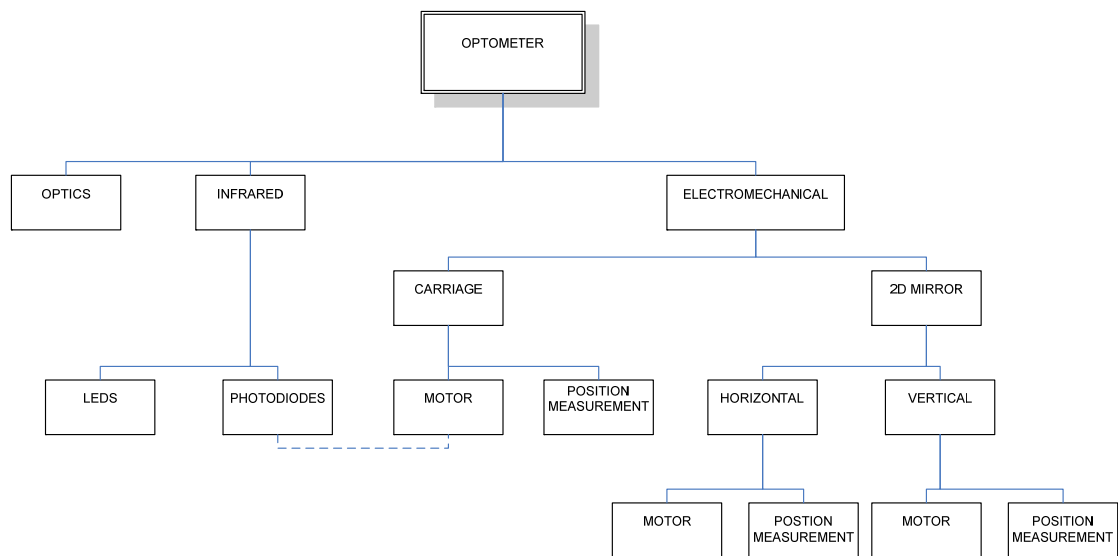


Figure 3.2.1 Optometer system block diagram

The computer control system driving the carriage motor uses this error signal to move the carriage to a position which annuls the error. This is why there is a link shown between the blocks named PHOTODIODES and MOTOR in Figure 3.2.1. The position of the carriage is then proportional to the overall refractive power of the eye. The moveable carriage on which the photodiodes and aperture are mounted, is belt driven by a servo motor (MOTOR) over a range of approximately 347 mm. The POSITION MEASUREMENT blocks refer to a shaft encoder system which provides the electronic signals from which the carriage position can be determined. The carriage control system will not be further described since the carriage was manually positioned in the all of the experiments described in this thesis.

The photodiodes must receive radiation reflected from the retina from both IREDS. This requires that the *image of the sources* are centred on the pupil of the eye, so that equal amounts of infrared are transmitted to the retina and received by the photodiodes from each IRED. Consequently, there needs to be a method of moving the *image of the sources* at the pupil plane of the eye.

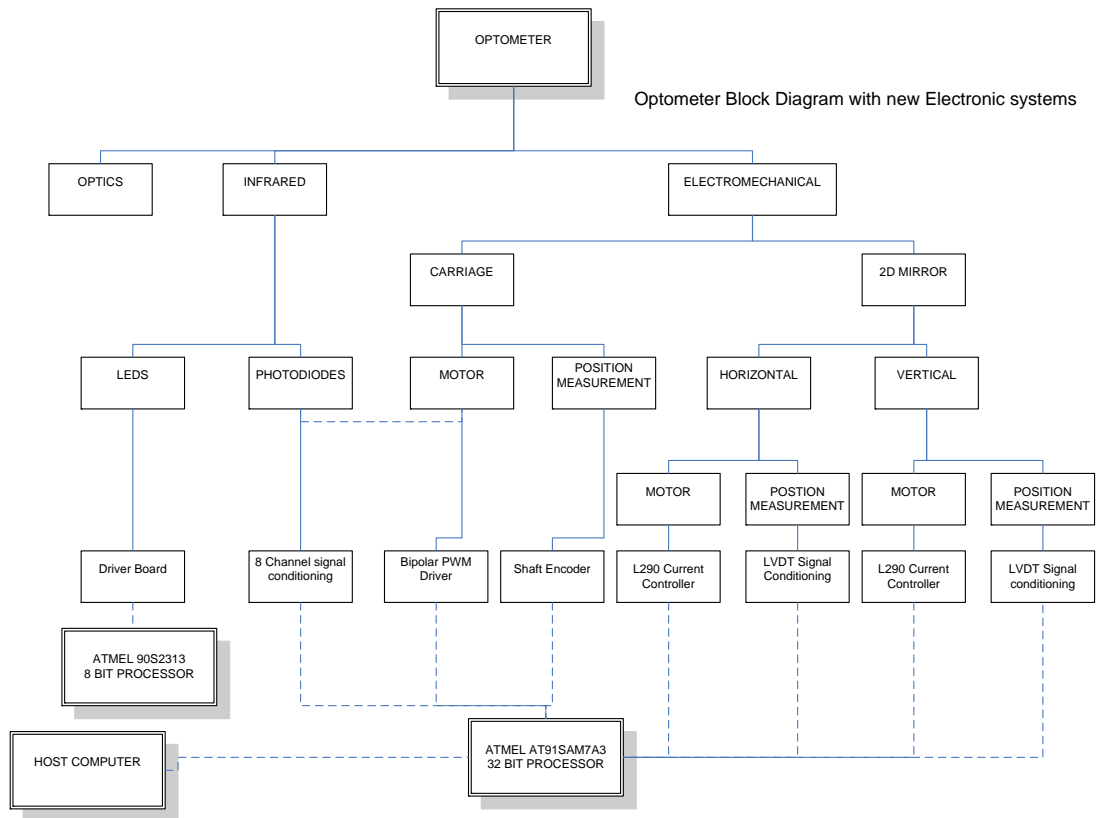


Figure 3.2.2 Optometer system with electronics

This has been implemented using an electromechanical system capable of rotating a mirror surface in two dimensions, placed between lenses **L1** and **L2**. The electromechanical mirror system will be referred to as the *servo* mirror in this thesis. It is shown in Figure 2.2.1 and enables the image of the sources to be moved at the pupil plane of the eye. The servo mirror is mounted at 45 degrees to the horizontal and has separate position control systems for the two orthogonal axes which will be termed the *horizontal* and *vertical* axes. The horizontal mirror control system moves the image of the sources at the pupil in the horizontal direction. The vertical mirror control system moves the image of the sources vertically at the pupil plane of the eye. *The control systems required to initially locate the pupil and then maintain the centring of the image of the sources on the pupil are the core topic and challenge of this research work.*

The radiant flux and position measurements are performed electronically and the information processed by an embedded microcontroller. The microcontroller performs the control system calculations and interfaces with a host computer. Blocks showing the measurement, actuation and electronic interfaces are shown in Figure 3.2.2. The blocks

of this diagram will be referred to in subsequent sections.

3.3 The infrared system electronics

The infrared sources are two Telefunken TSHA520 infrared emitting diodes. These diodes have been termed IREDS in the earlier discussion and diagrams. These diodes were chosen for two reasons, firstly according to the manufacturer's data sheet they are designed as high efficiency infrared emitters suitable for high current short pulse use. The use of short pulses of high current maximises the peak amount of infrared transmitted by the diodes. Secondly, they have a peak infrared output at a wavelength of 875 nm. Other infrared diodes have peak output around 950 nm. The lower wavelength is advantageous since the optical media of the eye have a lower transmittance in the range from 900 to 1000 nm. Atchison and Smith (2000) on pages 108 and 109 show curves for the spectral transmission of the optical components of the eye.

The infrared detectors must be able to distinguish between background light and infrared emitted by the diodes. This is achieved by pulsing the diodes output at 50 KHz so that frequency selective electronic amplification can be used. However, the diodes could not be continually driven at 50 KHz and also be used with maximum current. Therefore, they are driven in bursts of 6 pulses of 9 microseconds every 675 microseconds. This pulsing allows a high pulse current of 0.8 Amp whilst still keeping within the power limits of the diode. To obtain separate photodiode outputs for each of the top and bottom IREDS a time multiplexing interleaving scheme is used. The pulsing of the diodes is shown in Figure 3.3.1.

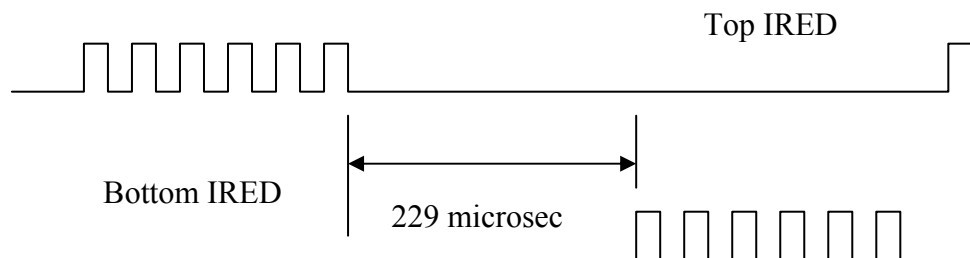


Figure 3.3.1 The pulsing of the infrared emitting diodes (IREDS)

In order to generate these relatively complex signals, the IREDS are driven from timing signals generated by an Atmel 90S2313 microcontroller. Separate outputs from the microcontroller switch the receiving amplifiers so that the outputs of the four

photodiodes as shown in Figure 3.3.2 are split into eight signals. Four signals are for measuring the signal received from each infrared IRED as shown in Figure 3.3.2. The eight outputs of the photodiode amplifiers are connected to separate analogue to digital channels on the system microcontroller. These signals enable the position of retinal image to be calculated for each infrared IRED.

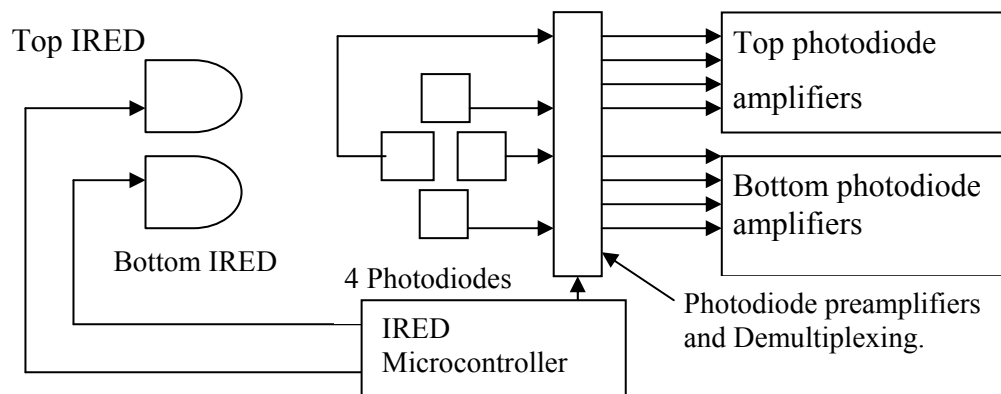


Figure 3.3.2 The multiplexing of the IREDs

3.4 The two dimensional servo mirror system

3.4.1 Introduction

The two dimensional servo mirror system is the essential component that is intended to provide the optometer with the ability to move its optical axis at the pupil plane of the eye. It thereby provides the means for the alignment and tracking of the eye. The feasibility of the method of patient alignment proposed in this investigation strongly depends on whether a suitable two dimensional mirror system can be engineered. The synthesis of the mechanical design has been omitted apart from the geometrical issue of independent rotation about two perpendicular axes. The requirements and design will refer to the system shown in Figure 3.4.1. It will be seen that the optical system places very stringent requirements on the control system performance of the mirror. The control system design and performance measurements will then be described.

A diagram of the parts of the designed system is shown in Figure 3.4.1. The system shown is the end result of the testing a few different arrangements of a two dimensional servo mirror. The fundamental requirement is for a system that can rotate a mirror about two perpendicular axes independently. The system was initially designed for a front

surfaced aluminium mirror. Later the mirror was changed to a dielectric mirror, which weighs considerably less. The range of rotation required is relatively small as will be seen in the following discussion.

The system shown in Figure 3.4.1 contains a mirror that is centrally pivoted. The power for rotation about each axis is provided by separate DC motors driving spiral threaded shafts. The shaft rotates in a threaded PVC block with whose rotational motion is prevented. Consequently motor rotation can move the PVC block both towards and away from the motor. A ball joint at the end of the block fastens the block to the mounting plate of the mirror. The position of the mirror plate is measured by a Linear Variable Differential Transformers (LVDTs) mounted on the opposite side of the pivot

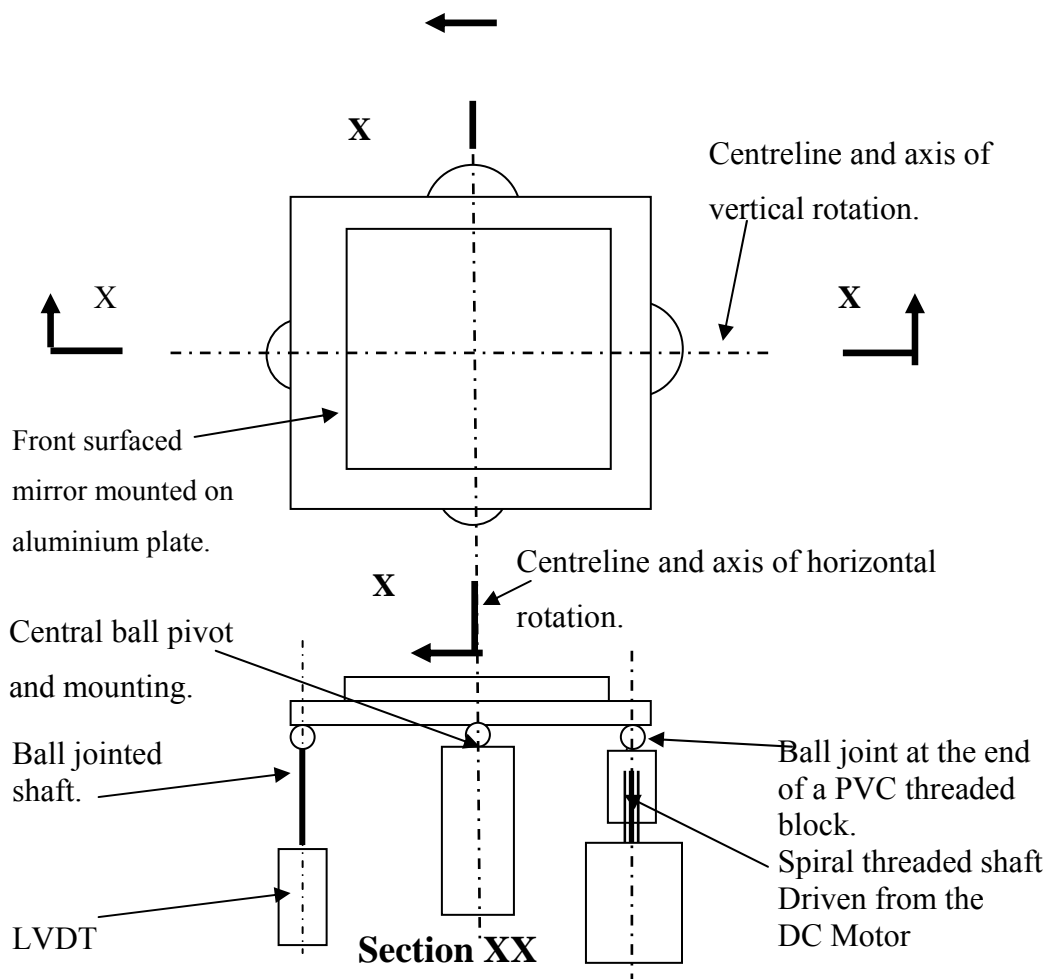


Figure 3.4.1 Outline view of the two dimensional servo mirror system

to the motors. The shaft of each LVDT is fixed via a ball joint to the mounting plate of the mirror.

Rotation about one axis must not affect rotation about the other axis. This is only possible if the following condition applied. For both the horizontal and vertical axes, *the ball joint for the motor, the ball joint for the LVDT and the centre pivot must be collinear and define the axis of rotation.* This condition has been satisfied in the construction of the mirror system. Consequently, rotation about one axis is independent of rotation about the other. This independence has been seen in practice.

3.4.2 Optical requirements

Referring to Figure 2.2.1 the servo mirror is placed between lenses **L1** and **L2**. It reflects input radiation from lens **L2** to lens **L1**. The mirror rotates the axis of the incoming IR beam to lens **L1** and consequently the image formed by lens **L1** at the pupil plane is laterally moved. If the angle of mirror rotation is θ and the focal length of lens **L1** is f_1 , then it can be shown that the image formed by **L1** at distance f_1 will be moved by the amount shown in equation 3-1. (Taylor (2003)).

$$D = 2 * \theta * f_1 \quad \text{3-1}$$

Only the focal length of lens **L1** is relevant in this calculation and the distance between the mirror system and the lens **L1** is not. This relationship between mirror rotation and displacement of the image of the sources at the pupil plane has been validated by actual measurement. The distance between the mirror system and lens **L1** does result in vignetting of the image by the boundaries of lens **L1** with large mirror rotations. This vignetting limits the range of available movement in the pupil plane of the eye.

It is assumed that with the use of a chin and forehead rest, the patient's eye could be positioned within a 20 mm square area. Suppose it is required to move the image of the sources at the pupil plane of the eye by ± 10 mm. Since the focal length of lens **L1** is 200 mm, then the angle θ is required to be ± 0.025 radians or ± 1.43 degrees. The radii from the centre pivot of the mirror system to the axes of the LVDTs are 43 mm and 58 mm for the horizontal and vertical systems respectively. The amount of linear movement at the LVDTs required to produce this angular displacement is then only ± 1.075 mm and ± 1.45 mm for the horizontal and vertical systems respectively.

It is desirable that the instrument operate with a small patient pupil diameter. Assume a minimum pupil diameter of 3 mm, which is a typical size for a room with artificial

lights on. The image of the IR sources needs to be positioned accurately enough within the pupil so that the amount of radiation entering the eye from each IRED is balanced. Suppose that a position resolution of 1% of the pupil diameter with a 3 mm pupil is required. A rotation of θ radians of the mirror produces a displacement of X_L mm at the LVDTs as shown in equation 3-2. A substitution for the value of θ has been made from equation 3-1.

$$X_L = \theta * R_l = D * \left(\frac{R_l}{2 * f_1} \right) \quad 3-2$$

Where R_l is the radius from the centre pivot of the mirror to the axis of the LVDTs and D is the image displacement at the pupil plane as shown in equation 3-1. The values of R_l have been specified in the previous paragraph. This equation relates displacements of the image in the pupil plane, to measurement of the LVDTs and is fundamentally important to the design. Consequently a displacement in the pupil plane of 0.03 mm corresponds to LVDT displacements of 3.2 micrometres and 4.35 micrometres of the horizontal and vertical systems respectively.

This extreme sensitivity to mirror position is a major problem with the current design and is due to the relatively large focal length of lens **L1**. There are three reasons why it is such a problem. These are:

1. Any flexibility in the mounting or mechanical system will mean that precision is lost.
2. The limited position resolution of the LVDTs and the digital resolution of the processor's analogue to digital conversion. This issue will be considered further in section 3.4.4.
3. The control system will have some steady state error, particularly when static friction is present. This will make almost impossible to achieve such precision in practice.

Perhaps a better approach could be to laterally move the IR beam by passing it through a thick plate rather than rotating it by a mirror. When a thick plate is rotated, the output beam will be moved laterally relative to the input.

3.4.3 Electromechanical design

The extreme precision required of the two dimensional servo mirror system makes it very difficult, if not impossible to engineer. Figure 3.4.1 at the start of the chapter shows the arrangement used for the mirror system. This section will explain why such a system was chosen. The problems of developing such a mirror system became a major part of the work of this investigation and have proven to be the most difficult.

Firstly consider the method of position measurement. A commercially available device that will accurately measure such small displacements is an LVDT (Linear Variable Differential Transformer). The ones chosen have a ± 3 mm stroke. The position resolution is dependent on the electronics and A/D conversion used. Using a 10 bit A/D conversion over 6 mm gives a possible resolution of 0.006 mm per digital unit over the full scale range of the LVDT. It will be seen in section 3.4.4 that this not quite adequate. Now look at the device providing the driving force.

Secondly consider the method of moving the mirror. The simplest option would have been to use a linear stepper for positioning but the backlash and slow operation speed rule them out. A previous mirror design attempted to use complete servo systems from model aircraft but the position resolution at the pupil plane was approximately 1 mm which is grossly inadequate. The model aircraft servos use a DC motor and gearing. The backlash in the gearing and limited position resolution of the shaft encoder and motor make these systems inadequate for such precision control. Three more options existed.

Another possibility was to use a switching solenoid and design a control system to handle its non linearity. Switching solenoids have been used successfully this way for linear positioning by Renn and Chou (2004) and Lim, Cheung et al. (1994). The difficulty with this approach is the complexity of the control system involved, since it involves a three level approach. A solenoid system was constructed and tried but it was not possible to produce a working control system using it. The main reason was the magnetic reluctance of the steel used for the solenoid bodies. This prevents the magnetic flux dropping quickly when the current falls, which inhibits the plunger from moving back. Secondly is the huge nonlinearity of the force as the plunger moves. Another disadvantage of the solenoid systems is they require return springs.

Cornsweet and Crane (1973) reports on the servo mirror systems used for a two dimensional eye tracker and state that the servo motors used for the servo mirrors were Pye-Ling vibration generators. Unfortunately, at the time of developing the mirror system, the author was unaware that such devices existed and could be used in this way. Future work could include further investigation into the use vibration generators.

Another possibility would be to use a loudspeaker magnet and voice coil arrangement. Unfortunately, the loudspeaker magnets are large and it would not have been possible to fit them in. Furthermore the stray magnetic fields could well have interfered with the LVDTs.

The final option was to use DC motors and convert the rotating motion of the shaft into a linear motion via a spiral drive screw. Computer floppy disk drives use a spiral screw to position the read/write head. Two old broken floppy drives were dismantled and the spiral screw shafts were used to provide the drive mechanism in the mirror system here. A few windings of a copper wire around the spiral shaft were embedded in a PVC block. The PVC block was fastened to the aluminium plate of the mirror via a ball joint. The rotational motion of the PVC block was restrained by having a 3mm wide channel cut in it. The channel runs along 3mm thick aluminium plate fixed along the linear axis. This system provides a backlash free method of converting the motor shaft's rotation to a linear motion. However, the disadvantage is that there is considerable friction.

Commercially available mirror positioning systems use a moving magnet arrangement for rotation about a single axis. With considerable time it might have been possible to develop a two dimensional moving magnet positioning system. However, it was considered easier to use commercially available actuators such as motors or solenoids rather than design and build custom actuators.

The inertia requiring movement is a major design factor. The mirror is an aluminium front surfaced glass plate 6 mm thick and 80 mm square. Although the mirror system was designed for this aluminium mirror, it was later changed to a lighter dielectric mirror. The mirror itself is by far the heaviest component of the moving system. When the other moving components of the mechanical parts are included, the second moment of inertia for the motion about the horizontal and vertical axes calculated to be $1.1 \cdot 10^{-4}$ kgm^2 and $1.6 \cdot 10^{-4}$ kgm^2 respectively.

3.4.4 LVDT position measurement resolution

The construction of the mirror system allows a maximum LVDT plunger movement of between 4 to 5 mm which is within the limit of 6 mm allowed by the LVDT construction. The extra movement allows some flexibility in the mounting of the entire mirror system. The LVDT signal conditioning amplifiers have been designed to convert the limits of LVDT displacement into a voltage from 0 to nearly 3 volts. These voltage limits are required by the microcontroller hardware. The resulting conversions between LVDT displacement and voltage output to the microcontroller have been measured as 1.763 mm/volt and 1.544 mm/volt for the horizontal and vertical systems respectively. The vertical system has a lower sensitivity since it needs greater displacement for the same angle due to a larger radius to the central pivot.

The microcontroller's Analogue to Digital Conversion (ADC) circuits provides 10 bit resolution with voltage reference of 3 volts. Consequently one bit of digital reading corresponds to a voltage of 2.929×10^{-3} volts. Multiplying this value by the previous values of mm per volt gives the minimum resolvable LVDT displacements of 5.17 micrometres and 4.52 micrometres for the horizontal and vertical systems respectively. These values correspond to rotations of 1.20×10^{-4} radians and 7.78×10^{-5} radians about the horizontal and vertical axes respectively.

Equation 3-2 can be rearranged and used to determine the position resolutions at the pupil plane corresponding to these angular resolutions of the mirror system. These are 0.048 mm and 0.031 mm respectively. The greater radius to pivot of the vertical system allows better resolution but also greater inertia. The greater inertia is a disadvantage for control system dynamic performance. It is concluded that a 4.8 mm pupil larger pupil diameter would enable a 1% diameter of the pupil resolution for the horizontal system.

Concluding, the position resolutions of the LVDT and electronics are barely adequate if a 1% resolution is required at the pupil plane of the eye. Ideally, the position resolutions of LVDTs will be the allowed position errors for the mirror's control system design. In practice, it is very unlikely that precise resolutions will be obtainable.

3.4.5 Kinematic requirements

The above determines static positioning range and resolution, but what about the dynamics? The pupil tracking system need to function well enough to:

1. Initially locate the pupil of the eye.
2. Maintain the operation of the optometer whilst the patient views a target over limited visual angle.

The mirror system is required to implement a pupil tracking system that tracks the lateral pupil motion not the rotation of the eye. These issues have been previously reviewed by Taylor (2003). Both Crane and Steele (1978) and Scerra (2001) and conclude that to track significant eye movements a tracker with a 100 Hz bandwidth is required. Pflibsen and Millbocker (1989) describes a system for tracking movements of the fundus (retina) but does not state the bandwidth requirements of the two single dimensional servo mirror systems used. However, it is stated that the sampling rate is 1000 samples/sec. Since digital control requires a sampling frequency from 20-40 times higher than the corner frequency, it is unlikely that the corner frequencies of the mirror systems would be greater than 50 Hz.

Using the information available on the dynamics of saccadic eye movements some valuable design information can be gained. Straube and Deubel (1995) plot graphs of saccade acceleration versus saccade amplitude. From these graphs it can be seen that the amplitude of the maximum saccadic acceleration is dependent on amplitude. The maximum saccade acceleration for a saccade of 15 degree (0.26 rad) amplitude is about 20000 deg/sec² (349 rad/sec²) } This acceleration is the angular acceleration of the visual axis. Straube and Deubel (1995) also measures saccadic velocity and the maximum graphed is about 430 degree/sec (7.50 rad/sec). Comparable figures for saccade acceleration and velocity have been obtained by Behrens and Weiss (1991). The mirror system's actuators should be able to produce at least the same acceleration and velocity of the image of the IRED sources at the pupil plane of the eye, in order to track these pupil movements.

To convert the angular acceleration and velocity of the saccades into lateral movement of the pupil, the radius of rotation the eye is needed. The radius from the centre of rotation to the corneal vertex is taken as 15 mm from Smith and Atchison (1997) on page 731. Take the average distance from the corneal vertex to the pupil plane at 3.6mm from Atchison and Smith (2000) on page 22. Consequently, the radius from the centre of curvature to the pupil plane is taken as 11.4 mm. Hence the previous figures for angular acceleration and velocity of the eye can be converted into linear acceleration

and velocity of the pupil which are 3.97 m/s^2 over 0.26 radians and 0.085 m/s respectively.

Using equation 3-1 these values can be converted into angular acceleration and velocity of the mirror, which is obtained by dividing the figures for the pupil plane by $(2 \cdot f_1)$. The results are 9.92 rad/sec^2 and 0.212 rad/sec . This angular acceleration and velocity are only required over a very small angular range of 0.025 radian as previously discussed.

3.4.6 Mirror control systems error constants

A starting point for control system design is the velocity error constant K_v , which is defined as the ratio of the velocity of the target divided by the steady state error. Typically the velocity input is taken a unit ramp, but the ratio will still apply to a larger velocity divided by the error the control system produces in tracking it. The angular velocity and position errors at the mirror will be used. The maximum angular velocity for mirror rotation was found to be 0.212 rad/sec in section 3.4.5. Dividing this angular velocity by the angular resolution of the LVDTs found previously results in impossibly high K_v values of 1763 sec^{-1} and 2725 sec^{-1} for the horizontal and vertical systems respectively. A control system must have an error input to produce an angular speed output and these K_v values are calculated for the minimum measureable error input value. A K_v value of 372 sec^{-1} was used for control system design calculations, which allows for an error input of $5.69 \cdot 10^{-4}$ radians for maximum velocity output. This angular error of either axis in the mirror system is equivalent to a pupil plane position error of 0.22 mm. The practical value of K_v is limited the amount of phase lead that can be provided by the control system compensator and the amount of torque available from the motor.

The acceleration constant (K_a) is the acceleration divided by the steady state error tracking it. Using the LVDT resolutions determined in section 3.4.4, and the angular acceleration required for tracking saccadic eye movements, the calculated acceleration constants are $8.26 \cdot 10^4 \text{ sec}^{-2}$ and $1.27 \cdot 10^5 \text{ sec}^{-2}$. These are for the horizontal and vertical system respectively.

Once the closed loop systems have been designed, the actual velocity and acceleration constants can be calculated and measured.

3.4.7 The current controller

A previous attempt at using solenoids to implement the mirror system required the use of hardware current controllers. A current controller is a device that produces an output current proportional to a voltage input. The SGS Thomson L292 was used. This device is rated to provide currents of 2 A (2.5 Max) and Pulse Width Modulation (PWM) up to 30 KHz. Control schemes for DC motors can also use current controllers and it was decided to see if the L292 controllers could be adapted to the purpose.

The presence of a current controller greatly simplifies the system model, since motor electrical characteristics and back EMF are no longer required to be part of the model. The very low inductance and armature resistance of the motors meant that the current controller could be designed for a corner frequency of 151 KHz with a damping factor of 0.83. The details of the design have been omitted from the thesis since it is done with formulae provided with the data sheet of the L292.

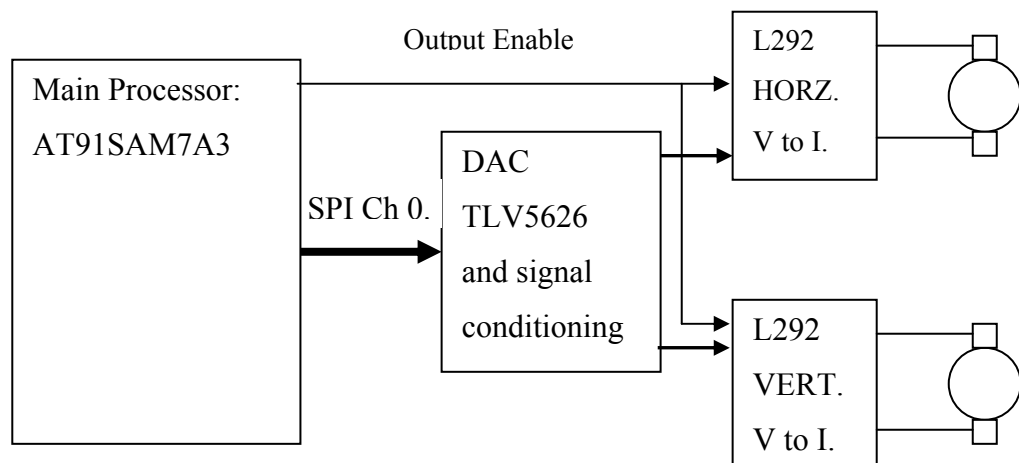


Figure 3.4.2 Mirror motor driving electronics

The voltage inputs to the current controllers come from a two channel Digital to Analogue Converter (DAC) device connected via the Serial Peripheral Interface (SPI) to the main processor. The DAC outputs are amplified and offset by operational

amplifiers so that positive and negative voltages can be applied to the inputs of the current controllers. The current controllers require dual polarity inputs in order to provide bidirectional currents through the motors. The arrangement is as shown in Figure 3.4.2.

The control system model for each motor control of each axis of the mirror system can now be developed.

3.4.8 The mathematical model the mirror system

A precise model based design requires a mathematical model of the system. The model is derived as follows and refers Figure 3.4.3. Define the following symbols:

Symbol	Meaning	Unit
x	LVDT displacement	metres (m)
θ	Mirror rotation angle	radians
R_l	Radius from pivot to LVDT axis	metres
R_m	Radius from pivot to motor axis	metres
J	Second moment of inertia	$\text{Kg}\cdot\text{m}^2$
F_m	Linear force from motor screw	Newton (N)
T_m	Motor torque	$\text{N}\cdot\text{m}$
α	Screw constant	$\text{N}/(\text{N}\cdot\text{m})$
C	Viscous friction constant	$\text{N}/(\text{m}/\text{s})$
K_{mt}	Motor current torque constant	Nm/A

For small rotations:

$$X = R_l * \theta \quad \text{therefore} \quad \dot{X} = R_l * \dot{\theta} \quad \text{3-3}$$

Time derivatives of variables will be denoted by placing a dot above the variable name.

The viscous friction force is proportional to the velocity \dot{X} , and therefore the friction force which acts against the motion is as shown in equation 3-4.

$$\text{Friction force} = -CR_l \dot{\theta} \quad \text{3-4}$$

The force applied by the screw block generated from motor torque, acts against this friction force. The resultant torque acting on the mirror platter causes an angular acceleration $\ddot{\theta}$. The equation of motion of the system is shown in equation 3-5.

$$\left(F_m R_m - C R_l \dot{\theta} \right) = J \ddot{\theta} \quad 3-5$$

The motor torque T_m is related to the linear force F_m by the screw constant α as shown in equation 3-6. The screw constant α depends on the pitch of the spiral screw attached to the motor drive shaft.

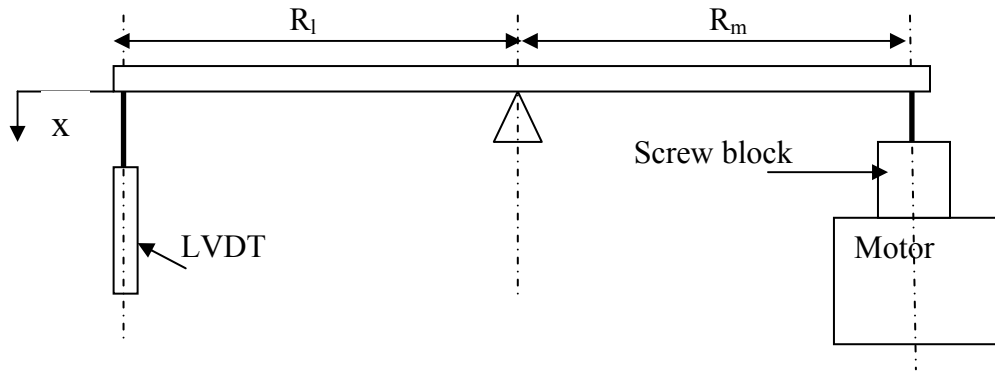


Figure 3.4.3 Mirror system model

$$F_m = \frac{T_m}{\alpha} \quad 3-6$$

The torque of a DC motor is linearly dependent on the motor current as specified by equation 3-7.

$$T_m = K_{mt} I_m \quad 3-7$$

Combining equations 3-5, 3-6 and 3-7 and rearranging results in the time domain equation 3-8.

$$\ddot{\theta} + \left(\frac{C R_m^2}{J} \right) \dot{\theta} = \left(\frac{K_{mt} R_m}{J \alpha} \right) I_m \quad 3-8$$

The coefficient of $\dot{\theta}$ has the dimensions of (1/seconds), and therefore its inverse is a time constant, which will be denoted τ . The coefficient of motor current I_m has the dimensions of (1/Amp*seconds²) and is a gain converting current to angular acceleration. It will be denoted as G_0 . Making these substitutions in equation 3-8 results in equation 3-9.

$$\ddot{\theta} + \left(\frac{1}{\tau} \right) \dot{\theta} = G_0 I_m \quad 3-9$$

Where:

$$\tau = \frac{J}{CR_m^2} \qquad G_0 = \frac{K_{mt}R_m}{J\alpha} \qquad \text{3-10}$$

Taking the Laplace transform of equation 3-9, ignoring initial values and rearranging yields equation 3-11. This equation is the system transfer function between motor current and mirror angular rotation, which applies to both axes. The constants for both axes will be different.

$$\frac{\theta(s)}{\text{Im}(s)} = \frac{G_0}{s\left(s + \frac{1}{\tau}\right)} \qquad \text{3-11}$$

The above analysis is linear and does not include static Coulomb friction. The problems caused by this Coulomb friction will be looked at again later. The present question is how to determine the constants G_0 and τ , which will be looked at next.

3.4.9 System identification

System identification is the process of determining the system model for a control system design by experimental measurement. When the experimental measurements are done without any feedback, the identification is called *open loop*.

If open loop identification was used here, a current input containing a range of frequencies would be applied to the motors. The angular positions of the mirror would be measured. System identification algorithm can then be used to determine an appropriate system mathematical model.

Open loop identification was tried but did not work for the following reason. The range of movement of the mirror system is around 4 mm at the LVDTs. It was found that when *chirp* (a signal whose frequency continuously varies from low to high) signal was applied, that the position quickly reached one of the limit positions at the end of travel. Consequently it was not possible to get sufficient results over a range of frequencies for the identification algorithms to work correctly. The MathWorks Matlab System Identification Toolbox was used.

In order to limit the range of movement, a *closed loop* methodology was used. This method requires that the system be setup in a unity feedback arrangement with a known gain inserted. The arrangement is shown in Figure 3.4.4. The closed loop gain of this system can be calculated by substituting the transfer function and gain into the general

close loop gain formula shown in equation 3-12. Using equation 3-11 as the transfer function (G) and K and the controller gain, the resulting closed loop gain of this system is shown in equation 3-13.

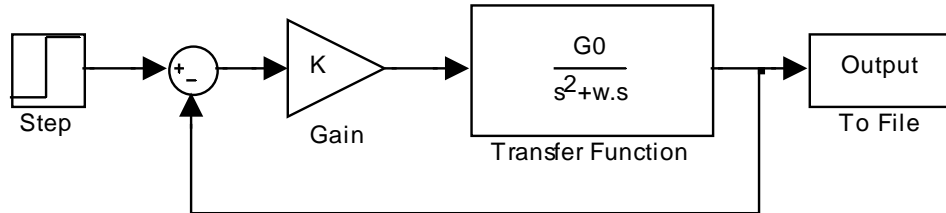


Figure 3.4.4 Closed loop identification scheme

$$G_{cl} = \frac{G}{1 + KG} \quad 3-12$$

$$\frac{\theta_{out}(s)}{\theta_{in}(s)} = \frac{1}{\left(\left(\frac{1}{KG_0} \right) s^2 + \left(\frac{1}{\tau KG_0} \right) s + 1 \right)} \quad 3-13$$

The transfer function for the standard second order system is shown in equation 3-14.

$$\frac{\theta_{out}(s)}{\theta_{in}(s)} = \frac{1}{\left(\left(\frac{1}{\omega_n^2} \right) s^2 + \left(\frac{2\xi}{\omega_n} \right) s + 1 \right)} \quad 3-14$$

By comparison, the constants G_0 and the τ can be expressed in terms of the natural frequency ω_n and the damping ratio ξ . These are shown in equations 3-15.

$$\tau = \frac{1}{2\xi\omega_n} \quad G_0 = \frac{\omega_n^2}{k} \quad 3-15$$

The natural frequency and the damping ratio are related to the damped natural frequency ω_d and the decay ratio D_r by the equations 3-16 (Golten and Verwer (1991)).

$$\omega_d = \omega\sqrt{1-\xi^2} \quad D_r = e^{\left(-2\pi \left(\frac{\xi}{\sqrt{1-\xi^2}} \right) \right)} \quad 3-16$$

The damped natural frequency and the decay ratio can be easily read of a graph of the step response. The gain K must be adjusted high enough to give an under damped response. By experimentation it was found that a gain K of 120 Amp/radian gave such a response.

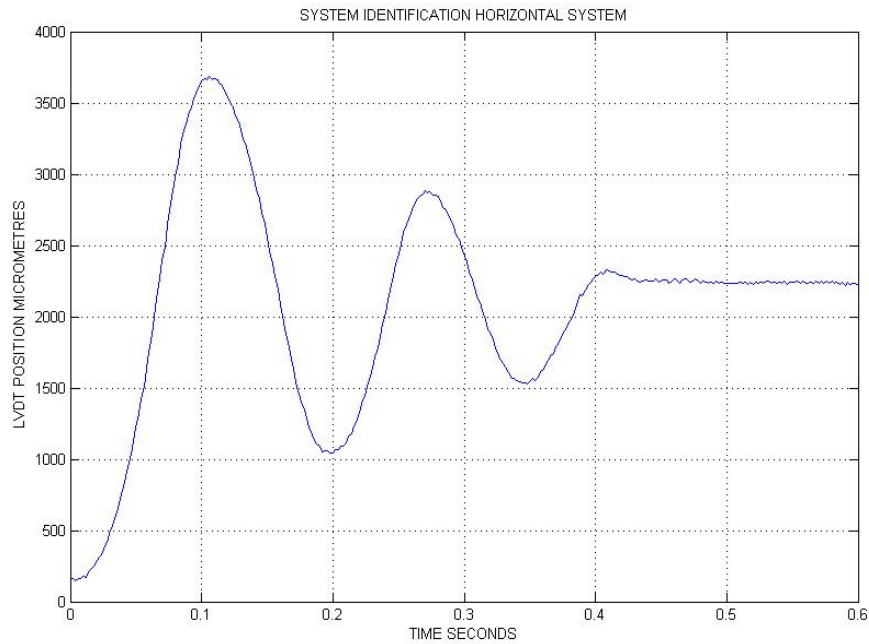


Figure 3.4.5 Identification step response of the horizontal system

The continuous time equations and systems can be converted to discrete time for taking advantage of digital signal processing techniques. This is done by using a sampling period 20-40 times smaller than the periods of the natural frequencies of the system. A sampling period of 2 milliseconds (ms) was used for the mirror control system design. The software for implementing the control systems and measurements is briefly overviewed in chapter 4. It is not necessary to know the software details in order to proceed with the identification and design.

The step response of the horizontal system is shown in Figure 3.4.5. The step response of the vertical system with the same gain is similar. The step input was for an LVDT displacement of 2000 micrometres. The decay ratio was read off by measuring the height of consecutive peaks from the set point of 2000. The damped natural frequency was found by measuring the time between peaks. Equations 3-16 and 3-15 were then solved for the required system constants G_0 and τ for both the horizontal and vertical systems. The resulting system transfer functions are summarized in Table 3-1. This completes the system identification.

Table 3-1 The mirror system transfer functions.

System	Transfer function
Horizontal	$\frac{\theta(s)}{I(s)} = \frac{12.35}{s(s + 7.880)}$
Vertical	$\frac{\theta(s)}{I(s)} = \frac{10.80}{s(s + 9.487)}$

3.4.10 Control system design and simulation

The transfer functions are of second order double integrator systems. It is therefore expected that a lead compensators will be required to make the phase margins acceptable. The design process consisted of:

1. Determining the gains that would satisfy the required velocity constant.
2. Plotting Bode diagrams to see the amount of phase lead required to stabilize the systems.
3. Designing the lead compensators.
4. Converting the resulting compensators to their digital Z domain equivalents.
5. Simulating the system designs using Matlab Simulink.

The above five steps are straight forward and well documented in control systems books. The design methodology of Ogata (1997) for Bode Diagram design of lead compensators has been used. The parameters used for the design will be specified, but the details are omitted. A velocity constant K_v of 372 as stated in section 3.4.6 was used. A phase margin of 60 degrees was sought, since phase margin is approximately 100ξ , and a damping factor of 0.6 was wanted. The gain margin with this type of system is infinite. This means that the gain can be increased indefinitely without making the system unstable. The continuous time lead compensators were calculated as shown in Table 3-2.

Table 3-2 Mirror system compensators.

System	S Domain Compensator	Z domain compensator
Horizontal	$\frac{372(s + 13.46)}{(s + 54.1)}$	$\frac{357.7z - 348.2}{z - 0.8974}$
Vertical	$\frac{372(s + 13.86)}{(s + 45.10)}$	$\frac{360.9z - 351}{z - 0.9137}$

The Matlab “c2d” command was used to convert the S domain compensator to the equivalent Z domain compensator using a sampling time of 2 ms and the Tustin approximation.

The theoretical velocity constants for the resulting control systems can be calculated from the transfer functions for and Table 3-2. The results are 145 sec^{-1} and 130 sec^{-1} for the horizontal and vertical systems respectively. The design value of 372 has not been achieved due to the effects of the compensators. The acceleration constants are zero.

To try to increase the velocity constants by increasing the system gain was not an option, since it was found that compensator output is already driven beyond the maximum current outputs available. Therefore, these lower velocity constants had to be accepted.

Simulations of the systems were constructed using Matlab Simulink. The Simulink diagram for the horizontal system is shown in Figure 3.4.6. The output from the simulation is shown in Figure 3.4.7 . The simulation for the vertical system is very similar and therefore has not been shown. This completes the theoretical design.

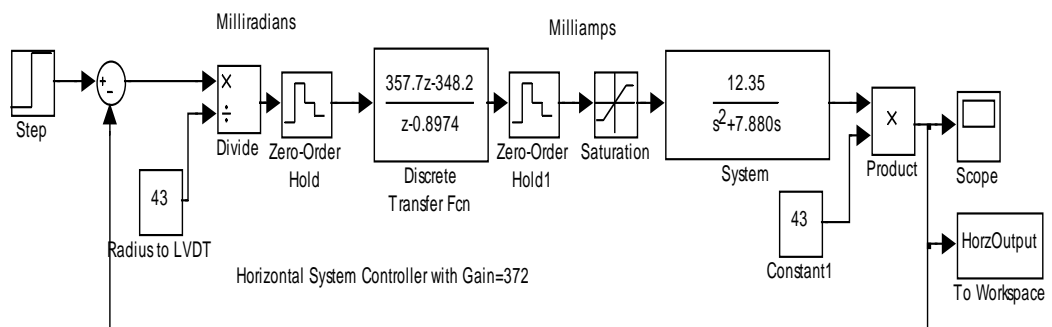


Figure 3.4.6 The horizontal system simulation block diagram

3.4.11 Performance measurements

The actual step response of the horizontal system is shown in Figure 3.4.7 for a step of 2000 micrometres in the LVDT position at time zero. The simulated output is shown on the same graph in dashed lines. When a first attempt was made, there was some small but significant oscillation around the steady state output at level 2000. It was believed that the oscillation was limit cycling caused by the effects of Coulomb friction. It is

known that such limit cycling can be eliminated by adding a dither signal to the controller's output. This idea is briefly mentioned by Franklin, Powell et al. (1998) page 440. The dither used here was a square wave with a frequency of 50Hz. The amplitude was experimented with until the limit cycling was reduced as much as possible.

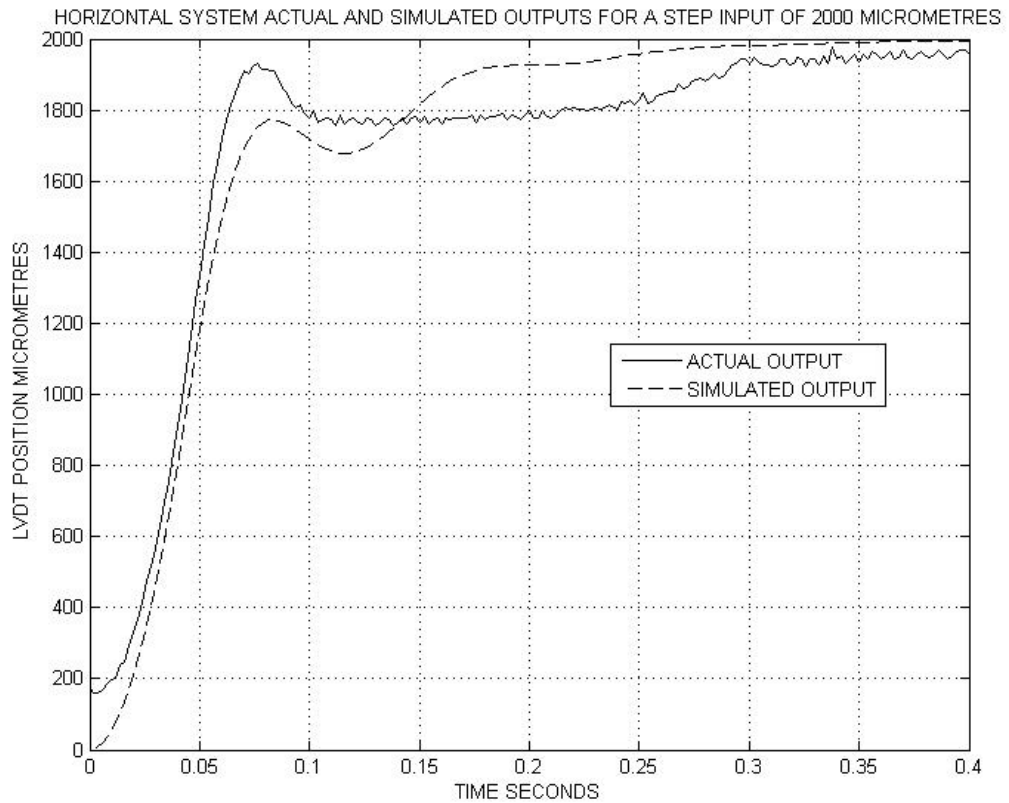


Figure 3.4.7 Horizontal system actual and simulation outputs

Furthermore, it was found that there was some 50Hz electronically generated noise in the LVDT measurement system. This was proven by measuring the output without any input to the motors. It is believed to be due to inadequate protection from power transformer magnetic fields. Its level was estimated to be 0.25% of full scale. Attempts were made to eliminate this before the use of the system with the optics.

The reader should not be concerned that the starting point for the LVDT measurements is not zero. The LVDTs are positioned so that they will cover the range of mirror movement required by the optics and the electronics adjusted accordingly. When at the bottom limit position the position output is not zero. The actual and simulated step responses for the vertical system are shown in Figure 3.4.8.

In both the horizontal and vertical step responses, the actual response curve is advanced in phase relative to that of the simulation. This suggests that the actual gains of the system are slightly higher than measured by the system identification. Furthermore, after the initial overshoot, the simulated response quickly rises to the final step value, whereas the actual response does not. This might be due to the effects of friction, but it was thought that friction effects would have been substantially reduced by adding dither.

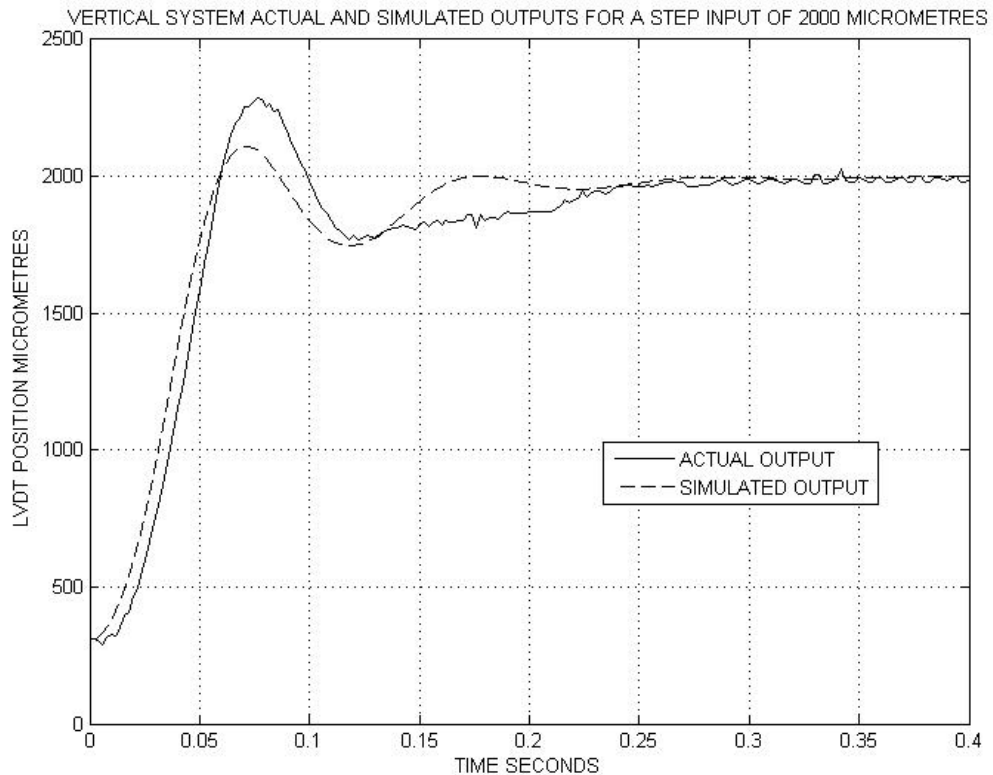


Figure 3.4.8 Vertical system step response

Another indication of Coulomb friction is that the horizontal system does not quite reach its final value. Perhaps the signal level of the dither should be increased. It will be noticed that there is some noise or oscillation in the actual outputs. This might be due to the dither or electronic noise.

The ramp response of both systems has also been measured. The ramp input corresponds to the mirror angular velocity required to track a saccadic eye movement. This was calculated at 0.212 radians/second in section 3.4.5. This angular velocity corresponds approximately to an LVDT velocity of 9 mm/sec. The actual responses and the input to the systems are shown in Figure 3.4.9 and Figure 3.4.10. Both graphs show the velocity error caused by a ramp input. The error is as much as a couple of tenths of a

mm, which is far more than was designed for. Another feature is that way the response

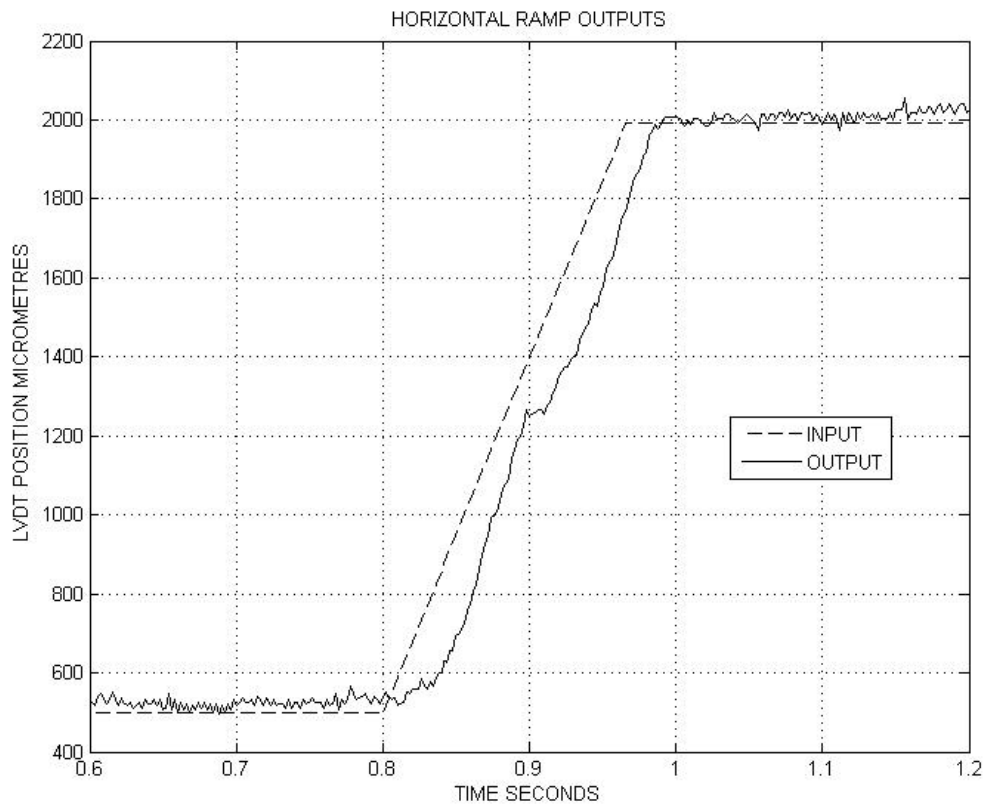


Figure 3.4.9 The horizontal system ramp response

shows a levelling off at about half way up.

The response of the system shows that the mirror can be moved faster than the ramp input, but then as the error is reduced the system's response stops. This behaviour is not understood. One explanation is that the phase lead of the compensator is derivative action. The derivative action will cause a large compensator output for a ramp input.

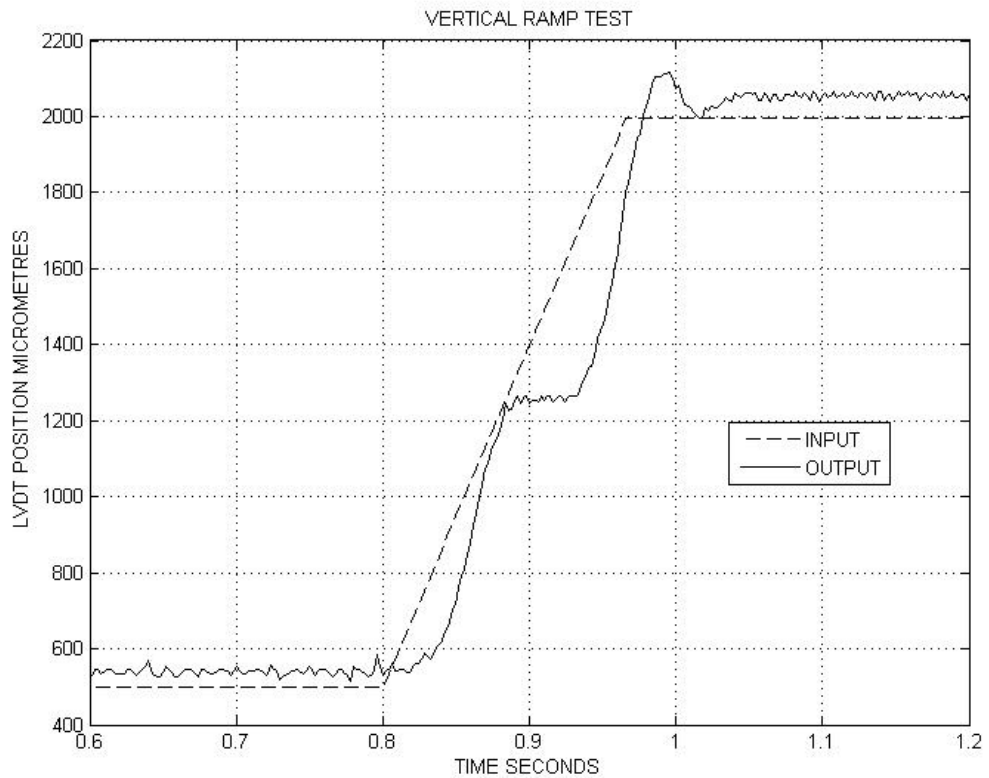


Figure 3.4.10 The vertical system ramp response

3.4.12 Conclusions

A two dimensional mirror system has been engineering from scratch and made to work. The precision required to work within the perceived requirements of the optical system appear very high and these goals have not been reached. Further design refinement could improve the control. There was not time for further refinements at this stage.

Consequently, the mirror system as is will be used for making the electro-optical measurements required to test the eye searching hypothesis of this investigation.

4 Outline of the embedded and computer software

4.1 Introduction

This chapter will briefly describe the software developed during the course of this investigation. The software is the *method* by which the experiment is implemented. All of the software developed for the optometer experimental tests described herein is included on the CD attached to this thesis. The location of specific folders on the attached CD will be referred to as:

CD:\folder\subfolder

Generally the software program used to implement a particular experiment will be found in one subfolder. The subfolder is specified under the corresponding section of the thesis.

All experiments described in this thesis are implemented in software, running on the embedded processor, which is an Atmel AT91SAM7A3 microcontroller. An AT91SAM7A3 is a 32 bit microcontroller which consists of a central ARM7 processor core with Atmel peripheral components. The processor was purchased as Atmel AT91SAM7A3 evaluation kit. The circuit board supplied with the kit was electronically interfaced to the peripheral devices of the optometer. Software modules for the various interfaces on the processor were developed from scratch for this project during the time of this degree.

The processor requires a collection of hardware dependent modules that are the interfaces to the optometer's electro-mechanical and electro-optical systems. These are briefly described in the section 4.3.

The real time nature of computer control systems and of concurrent multitasking make it necessary to use a Real Time Executive.(RTE) which is described in section 4.4.

Real-time data obtained from experimental tests has been sent back to the host computer via a serial link. The data was sent back using the XMODEM-CRC protocol, commonly used with modem file transfers. The file format used and conversion to the proprietary Matlab (.mat) format is described in section 4.6. Once in a Matlab file, the experimental variables names and values were read into Matlab for analysis and graphing.

4.2 Development tools

The public domain Yagarto IDE ARM development tools software was used to build the programs used for the optometer. The integrated development environment (IDE) is Eclipse CDT (C Development Tooling). Supplied with the IDE is a port of the GNU C compiler and other tools for the ARM processors. The development of programs using the GNU tools is very similar to development of programs on a computer running the UNIX operating system.

The JTAG electronic interface is widely used with microcontrollers and enables downloading of program and data to the processor's memory and program debugging. The processor is connected to a JTAG ICE (Joint Test Action Group In Circuit Emulator), and the emulator connected to the host computer via USB or serial port. An Atmel JTAG-ICE for the AT91 processors was used to program and debug the embedded processor used in this project. Atmel supply a free software programming tool for use with an Atmel AT91 JTAG ICE called the AT91-ISP (In System Programmer). This programming tool was used to download compiled programs to the embedded processor from the host computer.

The Eclipse IDE provides a debug mode in which source level debugging can be done. Source level debugging is possible in both assembly and C language with a maximum of 2 breakpoints. The Eclipse IDE uses the command line GDB debugger supplied with the GNU compiler and an ARM GDB Server. The ARM GDB server is a proprietary program developed by Segger Inc that enables the GDB debugger to communicate with the processor via the JTAG ICE. Communication between the GDB debugger and the GDB server is done by a network TCP port 2331. The GDB server requires a number of initialisation commands that are included in a script file called "DebugCutAndPastes.txt" included with each project. The contents of this file are cut and pasted into the appropriate windows of the IDE to setup debugging.

4.2.1 The files that make up a project

The experimental procedures described in this thesis each use a program compiled and downloaded to the embedded processor. The essential files that comprise each project are briefly described here.

Every program compiled for processor requires a C Run Time Startup (CRTS) file that is written in assembly language. This file contains the interrupt vector table and the corresponding low level interrupt handlers. It also contains code for copying program data burned into flash memory into RAM and finally calls the C function “main()”. Since the real time executive needs to determine which task runs when an interrupt occurs, there are two run time startup files. One is for programs that do not use the RTE, and is called “crts7a3.s”. The other is for programs that do use the RTE and is called “RTcrts7a3.s”. The appropriate file is included in each project on the attached CD. These start up files have been adapted for this project, from a few public domain sources, including the Atmel web site, examples supplied with the Yagarto IDE and the RTE. The CRTS is the only file in each project written in ARM7 assembler. The author has added the interrupt enabling and disabling functions for the ARM7 core processor to this file. All other files are written in the C programming language.

The CRTS file must be separately included and linked in each project as its contents must be the first to be placed in the processor’s memory. In other compiler systems, this CRTS is generally part of a library. However, this is not possible with the Yagarto development tools, since the GNU linker does not allow for a “VECTOR” or “STARTUP” segment that is the first to be placed in flash memory. The program code can only be placed in a TEXT segment. The code of the CRTS file must be the first to be placed in the text segment and consequently the CRTS object file has to be the first file on the linker command line.

Secondly every program compiled for the processor requires a linker command script which specifies where the code and data are to be placed in the processor’s flash and RAM memory. This file is called “lds7a3.lds” and is included with each project.

Thirdly, each program is compiled by the Eclipse IDE using a user supplied script called a “makefile”. The makefile is a script for the UNIX style “make” utility which specifies files are part of the overall project, the command used to process them, and

their dependencies on one another. The make files for each project including the library are included in the respective project's software folder.

Summarising each project included on the CD contains at least 5 files. These are:

1. The C Run Time Startup module. Either "crts7a3.s" or "RTcrts7a3.s".
2. The linker command script "lds7a3.lds",
3. The makefile script for compiling and linking the project.
4. The initialisation commands for debugging in the file "DebugCutAndPastes.txt",
5. The one or more C source files for the project.

4.3 The processor library

Software projects require functions from a large range of source files. Rather than including all the sources files in every project, it is more efficient to separately compile them and store them in a library file. All the files described in Table 4-1 are placed in the following folder:

CD:\Embedded\Library

All of the files in the library are compiled and then archived into a library file called "at91lib.a" stored in the same folder. Other projects are linked using this library.

A list of the processor specific modules is given in Table 4-1.

Table 4-1 Processor specific software modules.

Filename	Purpose and functionality
at91pio.c	Functions to enable or disable access to all programmable input/output pins on the processor. Required by all other modules.
bitmasks.c	Utility functions for generation of bitmasks from the start and end bit numbers. Used extensively in at91pio.c
at91efc.c	Functions for using embedded flash memory. Needed for setting the number of wait states when the processor reads flash memory.
at91pdc.c	Peripheral Direct Memory Access functions. These enable direct transfers from peripheral devices to the static memory. Used by the

	analogue to digital converters and serial port functions.
at91adc.c	Analog to Digital conversion functions.
at91dac.c	Functions for driving the Digital to Analog converter used to drive the 2D servo mirror. The DAC is connected to the processor via an SPI interface.
at91usart.c	Functions for driving the asynchronous serial port connected to the host computer.
at91aic.c	Interface to the processor's programmable interrupt controller
at91pmc.c	Power Management Controller and clock interface. Every program uses these functions to start system clock and the main phase lock loop clock. The main clock is set to run at 48 Mhz.
at91pwm.c	Pulse Width Modulation generation functions. Used to drive the carriage servo motor.
at91fp.c	Fixed point operations adapted to the ARM processor. Fixed point, not floating point arithmetic is used for all calculations.
xmodem.c rtsbuffer.c bufferoutput.c	An implementation of the XMODEM-CRC protocol for data transfers to the host computer. Used in conjunction with rtsbuffer.c and bufferoutput.c modules for buffering output data for transmission.
leadcomp.c	Digital implementation of a lead compensation network used in the all of the servo systems both for the mirror and the carriage drive.
photodiode.c	Functions for reading the photodiode outputs via the ADC.

4.4 The real time executive (RTE)

The pre-emptive real time kernel software developed by Barry (2009) was extensively used in this project. The software is freely available via the internet however the documentation is individually licensed. Such software is referred to as a “*real time executive*” (RTE), although is only a collection of functions that makes pre-emptive multitasking possible. Pre-emptive multitasking means that the currently executing task can have its execution suspended and the processor given to run another task. The task switching can only occur at uniform predetermined intervals, or when an interrupt occurs. It also makes intertask synchronization and communication possible via semaphores, critical sections and message queues.

4.5 The system tasks

Different projects require a different number of concurrent tasks. The one using the most tasks is the X-Y scanner project, whose tasks are described here. The program used to perform the XY scanning using the mirror system has three tasks. The code for this is found in:

CD:\Embedded\Mirror\XYScanner

The tasks created by this project are:

1. The main task having overall control of the process.
2. The mirror task used to performing feedback control on both the horizontal and vertical axes of the servo mirror system.
3. The photo reading task. This task reads photodiode readings and calculates the averages.

Each task consists of a loop or iteration that loops until the task exits or the program terminates. Using the time delay functions of the RTE, the code in each loop can be run at accurate time intervals. In the mirror control system, the time interval is the sampling period of 2 milliseconds. The period over which photodiode readings are averaged can be controlled in a similar manner. The tasks communicate via shared variables protected by semaphores used for critical sections.

4.6 Data transfer to the host computer

4.6.1 Introduction

Experiments require real time measured data be sent back to the host computer for graphing and analysis. This is done by having the programs save measurements to memory arrays whilst the real time measurements are in progress. Then after the measurements are complete, the data is sent to the host computer via the serial port. There are a number of issues to consider in sending data from the embedded processor to the host computer which will be considered next.

Firstly is the format in which the data is to be sent. In general data can be sent in binary form or as text. In binary form, each two or four byte integer is sent as is, whereas in

text form, the integer would be converted into ASCII characters in say decimal or hexadecimal and sent. Binary format is clearly much more compact and requires much less data to be sent. However, it is not directly readable and the order in which the bytes of an integer are placed in memory are generally processor dependent.

The order in which the bytes of an integer are placed in memory is called the “endianess” of the processor. Fortunately, the AT91SAM7A3 processor is little endian which is the same as Pentium processor used in the host computer. Little endian means that the low order byte or word of an integer is placed at the lower memory address.

Returning to the problem of embedded to host data transfer, a binary file format called RTS (Real Time Structures) has already been developed by the author. This file format stores records in sequential order. Each record consists of a number of variables of different data types, for example integer, floating point, character etc. The records are written to the file in the order which the results are obtained. The RTS format will be briefly described in section 4.6.2 and is used to send data from the embedded processor to the host computer over a serial communications link.

Once the format of data transfer has been decided, the flow control and reliability of data transfer must be addressed. Flow control means that the embedded system must not send data faster than the host computer can accept. Reliability means that should there be a transmission error, the erroneous data will be detected and the correct data resent. Both of these issues are handled by a point to point communications protocol. Since the XMODEM-CRC protocol is available on the Windows HyperTerminal program, it was decided to use it. Further details of XMODEM-CRC are given in section 4.6.3. This saves having to develop any custom program for Windows to receive data from a serial port. The details are further described in section 4.6.3.

4.6.2 Real Time Structure Files

Prior to the commencement of this thesis, the author invented or developed a binary file format called “Real Time Structures” (RTS) which stores many structures of binary data in a file. The specification of this format is given in Appendix 8.2. Each structure consists of a number of variables of different data type. When stored in the file, each variable of each structure is preceded by a tag byte, which uniquely identifies the type of binary data stored. The variable names of each of the structure elements are also

stored in the file's header section. The header section also contains other useful textual information about the file, such as its date and time of creation.

Instead of writing to a file stored on a disk drive, the data to be sent to the file can be written to a fixed size memory buffer that is filled and emptied. The functions of the file "rtsbuffer.c", in the above library perform the writing of data to a RTS memory buffer. The code for rtsbuffer.c was developed during the time of this thesis. The memory buffer can then be sent via the XMODEM-CRC protocol to the host computer.

The XMODEM-CRC protocol requires that a filename is specified when starting to receive a file. The filename given is the name of the RTS file to be received. When all the data saved by an experiment has been sent, the host computer has an RTS file that holds all the experimental data along with the names of each of the variables.

The author has developed a custom Windows command line program for direct conversion of the RTS file to a Matlab ".mat" file which can be directly loaded into Matlab. More details are given in section 4.6.4.

4.6.3 The Xmodem-CRC communications protocol

The XMODEM-CRC protocol was commonly used for file data transfers over a serial modem between computers separated by a phone line. The protocol details and code for its implementation on computer running MSDOS are given by Campbell (1987). The protocol packetizes the data into 128 byte packets with a 2 byte CRC (Cyclic Redundancy Checksum) at the end of each packet for transmission error checking. The code for sending files via XMODEM CRC has been ported to the processor used here in the file CD:\Embedded\Library\xmodem.c. The serial buffering required for sending 128 byte packets is implemented in the file CD:\Embedded\Library\bufferoutput.c.

4.6.4 Matlab conversion

The RTS files received by the host computer running Windows can be converted into Matlab files using the command line utility "rts2mat.exe". This utility was developed by the author before the time of this thesis. The code uses the proprietary Matlab libraries and the utility can only be run on computers which have Matlab installed. The code and executable are given in the folder: CD:\Windows\RealTimeStructureFiles\rts2mat.

4.7 Conclusions

An outline of the software that has developed and used to obtain the results described in this thesis has been given. The source code is supplied on the attached CD. To describe the interface and workings of each module or object would be a very long process and not directly relevant to the goals of this investigation.

The software tools used to develop the embedded code has also been described. All of these tools can be readily downloaded via the internet. The files needed to produce a program that can be downloaded to the embedded processor have been described and are included on the attached CD for each project.

Finally the method of transferring experimental results to the host computer files has been described. This method means that the values and names of result variables used in the embedded code can be read into Matlab from Matlab formatted files. In practice this has proven to be very quick, reliable and convenient.

5 The experimental evaluation of the optical system

5.1 Introduction

5.1.1 General

This chapter investigates the core hypotheses of this thesis, which are the following:

1. Can the image received on the retinal photodiodes be used to locate the pupil of the eye?
2. If so, can the image on the retinal photodiodes provide sufficient information to track eye motion?

The method used to implement objectives (1) and (2) must be conditional upon the retinal photodiodes fulfilling their primary purpose. The primary purpose is that it must be possible to make a Scheiner principle measurement of the refraction of the eye. This should be possible if radiation specularly reflected from the cornea has been adequately eliminated. The general idea behind how objectives (1) and (2) above could be achieved is briefly described in section 5.1.2. Whether such methods are practically possible is to be investigated.

It was proposed in chapter 2 that it should be possible to remove specularly reflected radiation by using crossed polarizers. This proposal must be tested as a prerequisite to pursuing objectives (1) and (2) above. The polarizers used to remove the corneal reflection need to be accurately crossed and the procedure for doing this is described in section 5.4. The results of performing a scan of the pupil plane with the polarizers crossed in the attempt to detect the location of the pupil will be described. If the polarization can be used to adequately remove the corneal reflection, then this is a significant research finding in itself since it could be applied to other optometer technologies.

The test of whether the corneal reflection has been adequately removed is whether the Scheiner principle can be used to make refractive measurement. Measurements of the overall refraction of the artificial eye will be attempted for five different locations of the

retina of the artificial eye. These measurements will be made with a known pupil location.

Assuming radiation reflected from the cornea has been removed, is there some feature of the radiation reflected via the pupil that enables the pupil's location to be found? This will be investigated by scanning the pupil plane using the servo mirror system. Then, by examining the plots showing the total radiant power received, some feature that shows the location of the pupil area will be looked for.

The artificial eye used for experimental measurements will be described in section 5.2.

5.1.2 The optical system reviewed

The optical principles of the optometer were explained in section 2.2. The Figure 2.2.1 showing the optics of the optometer has been reproduced here as Figure 5.1.1 since it will be referred to in this chapter. The lens pairs **L5/L4** and **L2/L1** relay the half moon images of both the IREDs to the pupil plane of the eye. The image at the pupil plane was termed the “*image of the sources*”. The position of the image of the sources at the pupil plane is determined by the angular rotation about of the X and Y axes of the two dimensional servo controlled mirror system.

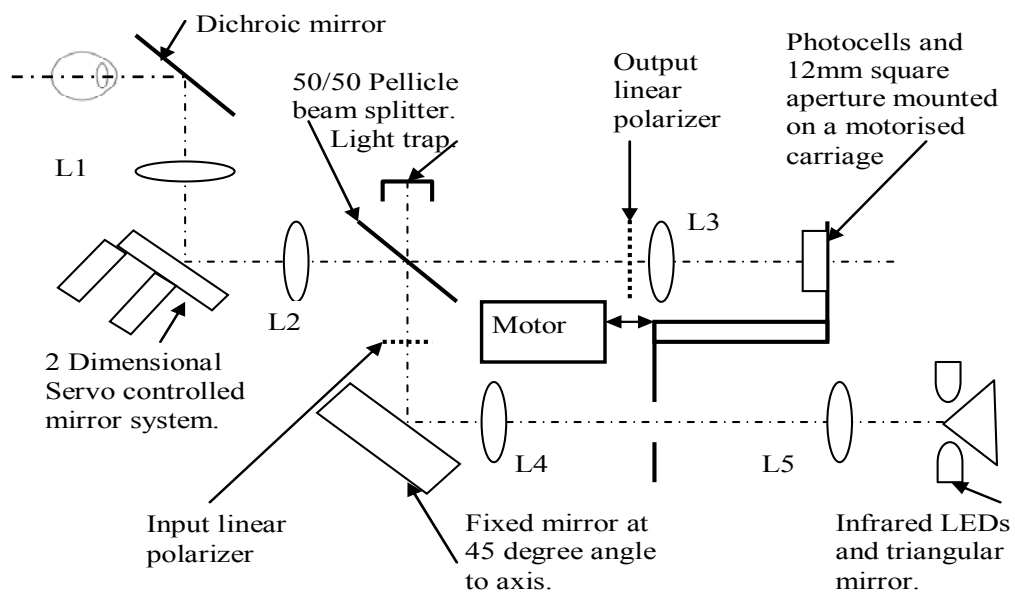


Figure 5.1.1 The optics of the experimental optometer

The X and Y axes in the pupil plane will be referred to as the *horizontal* and *vertical* axes respectively. The X and Y axes refer to image movement in the pupil plane not to the geometry of the mirror system as such. Mirror rotation about the mirror's X axis moves the image of the sources horizontally in the pupil plane. Mirror rotation about the mirror's Y axis moves the image of the sources vertically in the pupil plane. This terminology is used for simplicity, even though in reality a rotation about a horizontal axis at the centre of the mirror system results in a vertical motion of the image of the source at the pupil plane.

The half moon images of the IRED sources in the pupil plane are shown in Figure 5.1.2. The half moon images of the sources are shown in a lighter shade of gray than the entrance pupil of the eye. The IREDs are rotated at 45 degrees to the horizontal axis of the instrument and this is why the dividing line between the half moon images of each IRED is shown at 45 degrees in Figure 5.1.2.

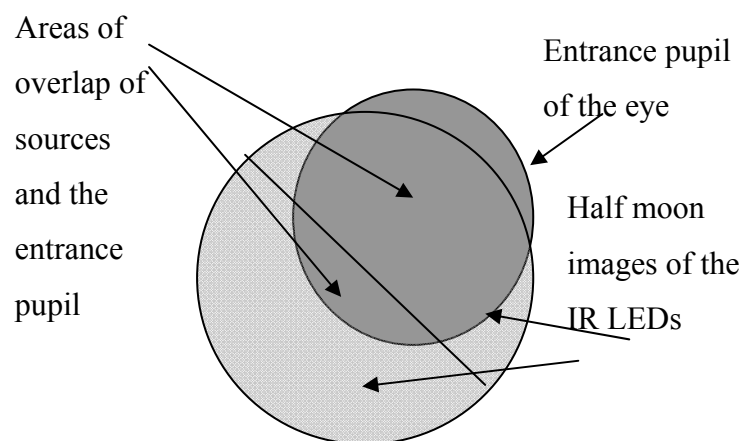


Figure 5.1.2 Images of the sources overlapping the pupil of the eye

It will be seen that if the half moon images of the IREDs have some overlap with the pupil of the eye, then the *radiant flux entering the pupil from each IRED will differ depending on the area of the overlap*. The radiant flux entering the pupil will be reflected from the retina and a small percentage of it be returned to the output optical path of the instrument and therefore to the photodiodes.

When there is no overlap of the image of the sources and the pupil, there will be some diffuse reflection of the incoming radiant flux from the iris and sclera surrounding the

pupil. The first question is will there be a measureable change in the total output of the photodiodes when the image of the sources overlaps or falls within the area of the pupil? This question will be answered experimentally using an artificial eye, where the iris is cardboard.

The second question is can the output of the photodiodes be used to track pupil lateral motion? There are few possibilities for such a control system, but they all depend on the answers to the first question above. Theorising about control systems should wait until it is known what changes occur in the photodiode outputs, when the image of the sources overlaps the pupil of the eye.

5.1.3 Infrared flux measurements

Before any experimental measurements can be described, the quantities measured must be defined. The arrangement of the four retinal photodiodes is shown in Figure 2.2.2 and reproduced in Figure 5.5.1. The photodiodes will receive infrared flux reflected from the pupil plane of the eye and from the retina of the eye.

The infrared flux is produced by two IREDs mounted at 45 degrees to the horizontal. The IREDs are mounted on either side of a triangular prism mirror as shown in Figure 5.1.1. The 45 degree inclination of the IREDs and prism mirror is not shown Figure 5.1.1 since it is out of the plane of the paper. The infrared flux reflected from each IRED is separately measureable on each photodiode. Since there are four photodiodes, there are 8 separate channels of data. The upper IRED will be referred to as the *top* IRED and the lower IRED as the *bottom* IRED. The radiant flux in watts/metre² falling on the photosensitive area of a photodiode generates a output voltage proportional to the value of the radiant flux and the fixed photosensitive area of the diode. The outputs of the four photodiodes can be *summed* for each IRED. Therefore the total outputs from the photodiodes for each of the top and bottom IREDs will be referred to as *the top and bottom radiant fluxes*, even though the actual outputs of the photodiodes are voltages. The individual voltage outputs of each photodiode will be of interest in determining the position of the retinal image, but should not be relevant to locating the pupil.

The Analogue to Digital Converters (ADC's) of the processor have a maximum output of 10 bits, which is 1024. Consequently, the maximum output for the sum of four

photodiodes is 4096. The measured output from the photodiodes was converted into a percentage of the maximum possible (normalized) by the equations 5-1 and 5-2.

$$\text{Top Flux} = ((\text{Sum of photodiode outputs for the top IRED})/4096)*100 \quad \text{5-1}$$

percent

$$\text{Bottom Flux} = ((\text{Sum of photodiode outputs for the bottom IRED})/4096)*100 \quad \text{5-2}$$

percent

In the following sections, experiments will be described that measure these quantities.

Experimental measurements are based on knowing where the image of the IREDs appears in the pupil plane. Before the experimental work can be described, the mirror positioning in relation the pupil plane image of the sources must be specified.

5.1.4 Pupil plane positioning of the image of the IREDs

The position of the image of the IREDs on the pupil plane is completely determined by the angular positions of the horizontal and vertical axes of the servo mirror. This position is measured by the LVDTs described in chapter 3. Position in the pupil plane is determined by mirror position and the focal length of lens **L1** shown in Figure 5.1.1. The zero position of the horizontal and vertical axes in the pupil plane does not matter since it is an arbitrary reference point. Consequently, pupil plane position will be calculated in millimetres from equation 3-2 as shown in equations 5-3 and 5-4.

$$X_{pp} = X_{LVDT} * 9.302/1000 \quad \text{5-3}$$

$$Y_{pp} = Y_{LVDT} * 6.896/1000 \quad \text{5-4}$$

Where X represents horizontal position and Y represents vertical position. The subscript _{pp} refers to pupil plane position and the subscript _{LVDT} refers to LVDT position in micrometres. The constants in the equations 5-3 and 5-4 are determined by the radii from the centre of rotation to the LVDT axes of the mirror and the 200 mm focal length of lens **L1**.

5.1.5 The X-Y scanning program

Experiments reported in this chapter require the top and bottom flux measurements as calculated by equations 5-1 and 5-2 for many points in a region of the pupil plane.

These measurements were obtained by using the X Y Scanner program whose code is given in the folder:

CD:\Embedded\Mirror\XYScanner

The program moves the mirror (X,Y) position to each of the points in a uniformly spaced rectangular grid. At each point of the grid, the total flux received by the photodiodes was measured. The measurement includes the total flux received from the top and bottom IREDs. The spacing of the grid points horizontally and vertical does not need to be the same. The horizontal and vertical spacing between points was chosen from 0.5 to 0.7 mm, so that a grid of 400 points would be sufficient to cover the area of pupil plane of interest. The limitation of 400 points was due to the limited memory of the microcontroller.

The results from an XY scan were sent to the host computer via Windows HyperTerminal and saved in an RTS file as described in section 4.6. The RTS file was then converted into a Mat formatted file which could be read into Matlab. The Matlab three dimensional plotting functions showing contours and three dimensional surfaces were used to display the results. Some of these graphs have been included into the following sections.

5.2 The artificial eye

5.2.1 Physical construction

An artificial eye is needed to test the operation of the optometer and the theory proposed herein. A schematic diagram of the artificial eye used is shown in Figure 5.2.1. One 20 dioptre plano-convex, lens is placed against a piece of cardboard containing a hole which forms the pupil. The lens and cardboard pupil are mounted inside a plastic tube of 25 mm internal diameter, not shown in Figure 5.2.1. The retina of the artificial eye consists of a cardboard fastened to a backing plate. The plate is mounted so that the position of the retina can be adjusted relative to the lens.

The artificial eye assembly was mounted on the chin and head rest frame used to position the patient's head. The chin rest assembly was moved until the pupil of the artificial eye was approximately centred on the optical axis of the optometer. This position remained fixed for all the following experiments.

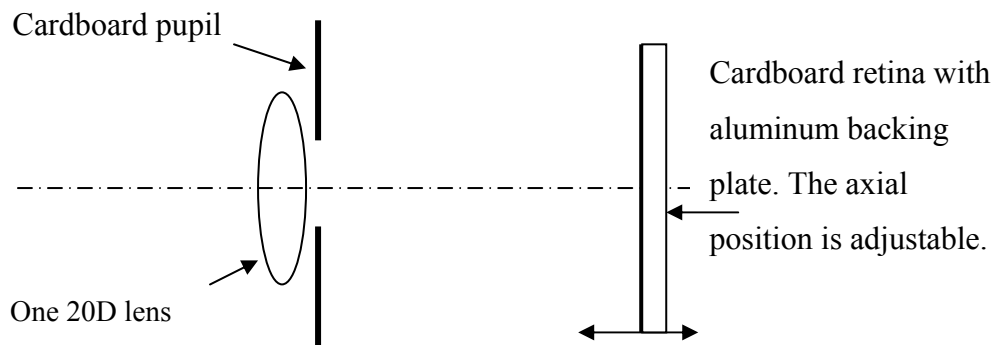


Figure 5.2.1 A schematic diagram of the artificial eye

5.2.2 Radiant flux transmission

It is the radiant flux reflected from the matt (as opposed to white and smooth) surfaced cardboard retina that is to be transmitted back through the pupil and lens of the artificial eye and received by the photodiodes. The flux transmitted back through the pupil depends upon the solid angle subtended by the cardboard pupil at the retina. The solid angle can be calculated from the pupil diameter and the distance of the retina from the pupil plane. The total radiant flux emitted back from the artificial eye also depends on the reflectance of the matt cardboard for infrared radiation. However, only the solid angle subtended by the pupil at the retina was considered in the design of the artificial eye at this stage.

The design was based on an equivalent *exit pupil* size of a human eye. The exit pupil is used, since it is the image of the actual pupil refracted by the crystalline lens of the human eye. Therefore the exit pupil is the size of the pupil as seen from the retina. According to diagrams shown on pages 23 and 24 of Atchison and Smith (2000) the exit pupil is very close to the actual diameter of the iris and situated 3.67 mm posterior of the apex of the cornea. From the information provided on page 24 of the book by Atchison and Smith (2000), a 4 mm diameter of the iris is typical figure for the midrange of illumination. Consequently, an exit pupil of diameter 4 mm was chosen. Using the representative dimensions of the human eye on page 9 of Atchison and Smith (2000), the iris is located 19.5 mm from the retina. Therefore the solid angle subtended by a 4 mm exit pupil at the retina is:

$$\text{Solid Angle} = \text{Area}/\text{Radius}^2 = 0.033 \text{ Steradians}$$

The pupil of the artificial eye should have a radius that will subtend approximately the same solid angle, in order to provide similar levels of reflected radiant flux. This statement does not take into account the other losses in radiant power that occur in the human eye. These include reflections from the surfaces of the lens and cornea and losses in transmission through the ocular media. Even in the artificial eye, there will be a reflection from the back surface of the 20 D lens. However, having the pupil subtend the same solid angle is a reasonable starting point.

Unlike the human eye, the refraction of the artificial eye is changed by moving its retina. Therefore the solid angle subtended by the pupil will vary as the retinal position changes. For the purposes of this thesis, the overall refraction of the artificial eye was varied from 0 to +4 dioptres. The overall refraction of the artificial eye in dioptres is taken as the inverse of this distance (in metres) from the vertex of the 20 D lens to an object point that is conjugate to the retina. The corresponding retinal distances were calculated using the thin lens equation. The distance from the vertex of the 20 D lens to the back of the cardboard pupil is 6.5 mm. The calculated retinal distances from the back of the pupil are shown in Table 5-1.

Table 5-1 Retinal distances for a range of refractions of the artificial eye.

Overall refraction (D)	Distance from pupil to retina (mm)
0	43.5
1	46.1
2	49.0
3	52.3
4	56.0

The distances shown in Table 5-1 will be used in section 5.5 for assessing the optometer's measurement of refraction. The pupil diameter of the artificial eye for refraction measurement was calculated using the maximum retinal distance of 56 mm. Given a required solid angle of 0.033 steradian, this requires a pupil diameter of 11.47 mm. A pupil diameter of 12 mm was used.

This pupil diameter is well outside the actual range of pupil sizes of the human eye. To make the pupil diameter of the artificial eye comparable with that of the human eye, the refractive power of the lens should have been close to the overall refractive power of the human eye, which is about 60 D. Unfortunately, the radiant power issue was not considered when the lens of the artificial eye was purchased.

5.3 Locating the pupil of the artificial eye

5.3.1 The use of photodiodes behind the pupil

The mirror system (X,Y) coordinates of the centre of the pupil of the artificial eye need to be known. This was done by mounting two adjacent photodiodes and a pre-amplification system behind a 5 mm diameter cardboard pupil. The outputs of the photodiodes preamplifiers were connected into two of the four channels of the retinal photodiodes. The retinal photodiode preamplifiers were disconnected. The summed

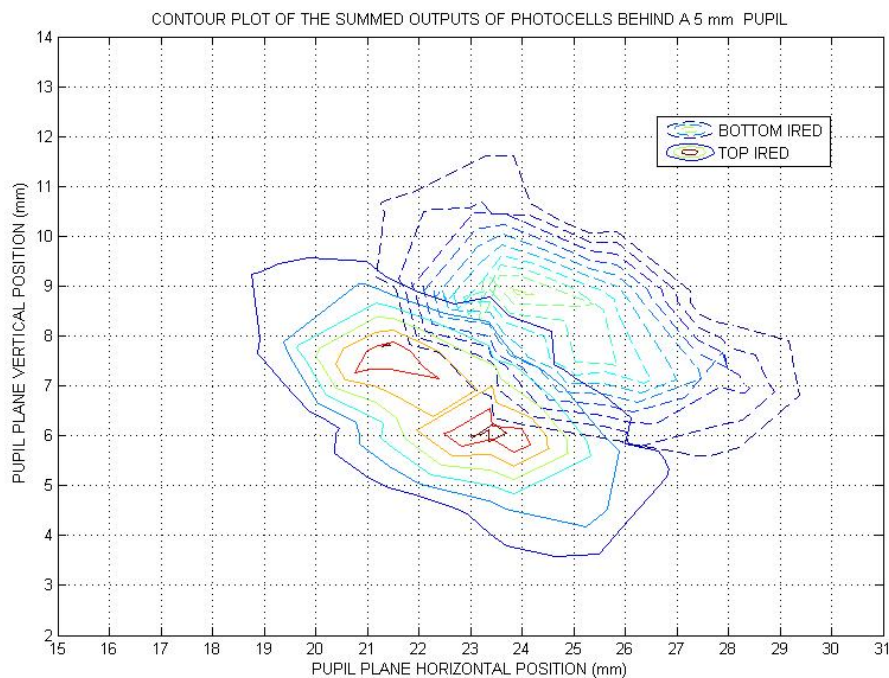


Figure 5.3.1 Contour plot of the summed outputs of photodiodes behind a 5 mm pupil.

outputs of the two photodiodes for the top and bottom IREDs was measured over a grid of mirror positions using the X-Y scanning program of section 5.1.5.

The colour contour plot shown in Figure 5.3.1 shows the measurement obtained from the scan. The pupil plane vertical coordinate increases as the image of the sources

moves downwards. The upper dashed group of contours shows the contours of constant value for the photodiode output received from the bottom IRED. The lower non-dashed contours show the summed output received from the top IRED. The contour enclosing the smallest area encloses the region of maximum output. The centre between the two maximum output regions was visually estimated to be at the coordinates (23.5,7.5) from the Figure 5.3.1.

This pupil plane coordinate can be converted into a mirror system LVDT coordinates. These coordinate values were used in all other experiments where the images of the sources are to be centred on the pupil. Although the pupil diameter was changed to 12 mm, the location of the artificial eye was not changed in all subsequent experiments.

The optometers described in the literature review used the corneal reflection of the human eye to locate the pupil. The corneal reflection of the artificial eye is the reflection from the surface of the 20 D lens. If the retina of the artificial eye was replaced by a black cone to absorb all received radiation, all that should be reflected is radiation from the lens surface.

However, the lenses **L1** and **L2** are also common to the input and output path of the optometer. Any reflection from these will appear in the output as well. Even though lenses **L1** and **L2** were purchased as optically coated to reduce unwanted reflections in the near IR region, there will be still be some energy reflected. The actual amount of reflected radiant flux will depend on how much is removed by the crossed polarizers.

5.4 Removing unwanted reflections

5.4.1 Sources of unwanted reflection

There are three lens surfaces that will create unwanted reflections. These are the surfaces of lenses **L1**, **L2** and the lens of the artificial eye. To see the effects of these reflections, the retina of the artificial eye was replaced with a cone of black paper. The black cone should absorb any radiation that enters through the pupil. The output polarizer shown in Figure 5.1.1 was removed. This was done so that none of the specularly reflected radiation would be removed.

The carriage housing the photodiodes was positioned about 200 mm from lens **L3**. At this position the retinal photodiodes are at optical infinity to the artificial eye. The

carriage could have been at other locations as well. An X-Y scan of the pupil plane was made. The outputs for the 4 retinal photodiodes was summed for both the top IRED and the bottom IRED. A mesh plot of the total output received from the top IRED is shown Figure 5.4.1. The results for the bottom IRED as similar except the peaks occurs at a slightly different positions

It will be seen that a peak output of around 80% of the maximum possible output of the amplification system was obtained. The question is how well can polarization remove these unwanted reflections? It is hoped this will be achieved by adjustment of the output polarizer relative to the input polarizer, described next.

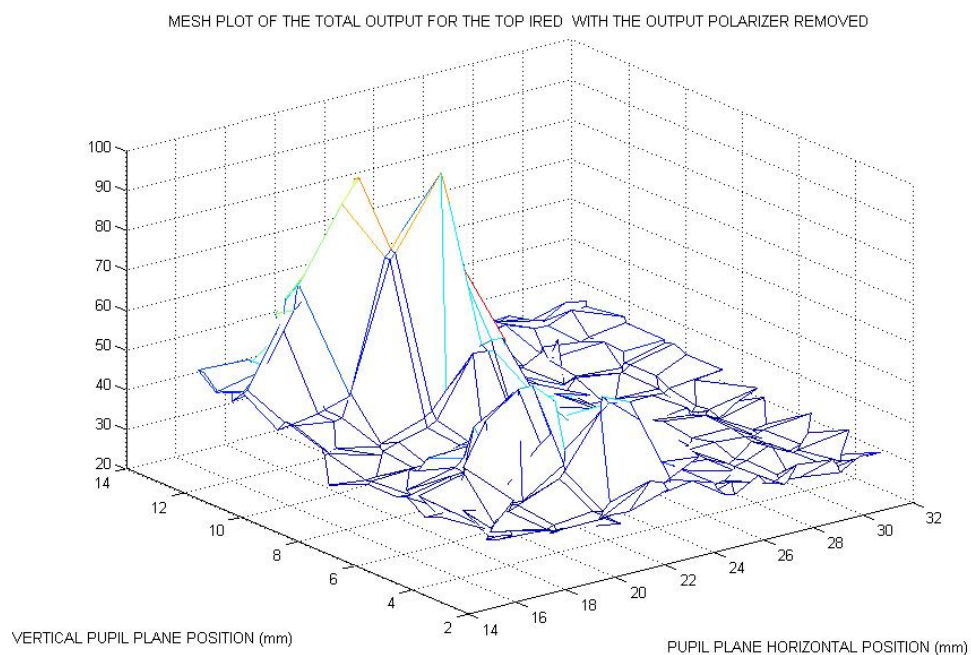


Figure 5.4.1 Mesh plot of the total output for the top IRED with the output polarizer removed

5.4.2 Adjustment of the crossed polarizers

The input polarizer shown in Figure 5.1.1 has a fixed position. The output polarizer should be adjusted to minimize the transmitted radiant flux. The mirror was positioned at a location that will maximize the specular reflection. From Figure 5.4.1 the pupil plane position for a large specular reflection is about (22,12).

The output polarizer was replaced and orientated crossed with the input polarizer when the two polarizers were side by side. Using an oscilloscope to visually observe the output of the photodiode amplifiers, the angular position of the output polarizer was

rotated until a minimum output was obtained. This position was found to be at approximately 90 degrees to the original orientation. A second scan of the pupil plane was made and the results for the top IRED are shown in Figure 5.4.2.

The specular reflections have not been entirely removed but substantially reduced from 80 % to 18%. This is a reduction of 77.5 %. It will be noticed that the pupil plane position of the maximum output is distant from the position of the pupil at (23.5,7.5) found earlier.

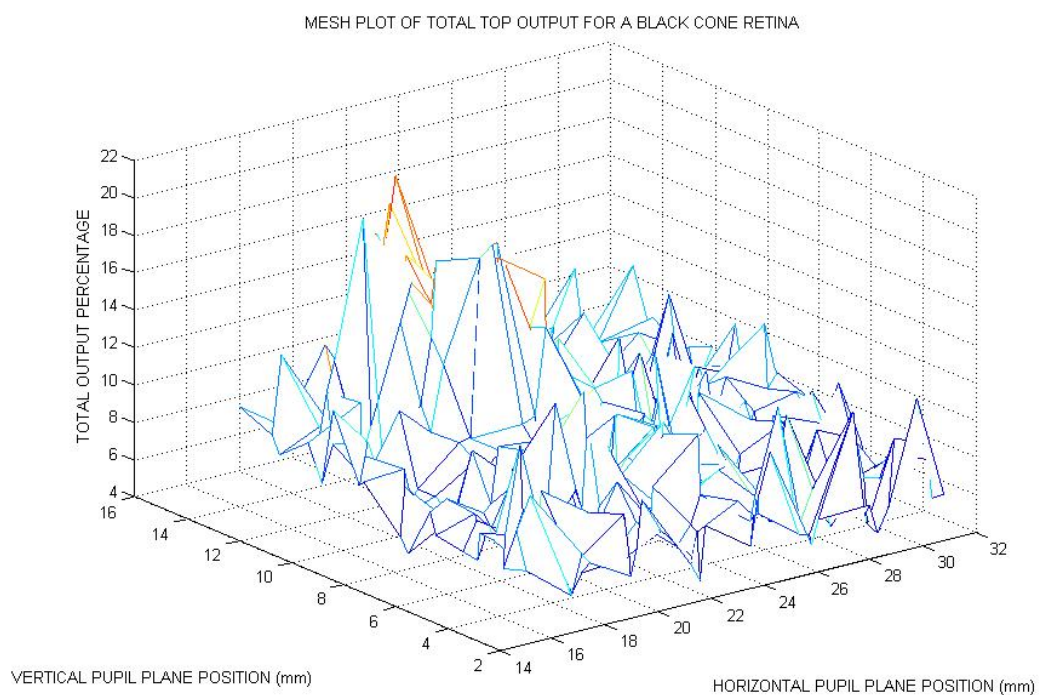


Figure 5.4.2. Mesh plot of the total output for the top IRED with the output polarizer optimally adjusted.

Why did crossed polarizers not remove the specular reflections as well as expected? One possibility is that components of the reflections seen in Figure 5.4.1 and Figure 5.4.2 are due to reflections from the optometer lenses **L1** and **L2**. Unfortunately, these lenses are common to the input and output path of the instrument. Even though they have been optically coated to remove reflections of near IR radiation, there still will be some reflection.

These results raise two questions.

1. Is the reduction in specularly reflected IR sufficient for Scheiner principle refractive measurements to be made?
2. If so, can the location of the pupil be detected with the polarizers in place and crossed so as to minimise the throughput of radiant flux?

These questions will now be answered in order.

5.5 Scheiner principle refractive measurement test

5.5.1 Introduction

Given that the infrared polarizers do not totally remove the reflection from surfaces of the lenses of the artificial eye, is it still possible to measure the refraction of the artificial eye? This question will be answered by attempting to measure the refraction of the artificial eye using the Scheiner principle. The method of making this measurement using the photodiode outputs will be described in the next section.

The overall refraction of the artificial eye can be changed by moving the cardboard retina relative to the lens. The axial movement of the retina is shown in Figure 5.2.1. If changing the position of retina of the artificial eye changes the distribution of radiant power on the photodiodes, then an image from the retina is being received. If not, then the reflections from the lens surfaces cause unacceptable error in refraction measurement. This means that the use of polarizers and dielectric mirrors if not sufficient adequately to remove the specular reflections from the cornea of the eye.

5.5.2 Using the photodiode outputs for Scheiner principle refractive measurement

The Scheiner principle was explained in section 1.3.2 and its use in optometers. It will be briefly reviewed before describing the experimental procedures used to apply it. It is applied by detecting the movement of the retinal image of an aperture, as the source of infrared is moved to and fro across the pupil. The movement of the infrared source is achieved by having two separate IREDs side by side that are alternately powered. These are the top and bottom IREDs mounted on either side of the prism mirror in Figure 5.1.1. The 12 mm square aperture and the photodiodes are fastened to a moveable carriage so that they are both at the same optical distance from the eye. Consequently,

when the aperture is focused on the retina so will the reflected image of the aperture that arrives at the photodiodes.

The Scheiner principle implies that when the aperture is focused on the retina, there should be no movement of the image of the 12 mm aperture, as the infrared sources alternately powered. Since the image of the reflected image of aperture on the retina appears at the photodiodes, the Scheiner principle is applied by measuring the difference in the image position of the aperture produced separately by the top and bottom IREDs.

When the retinal image is in focus, the difference in aperture image position for both of the IREDs should be zero. When the image is not in focus, the defocused images of the 12 mm aperture from both IREDs will be at different positions. How image position on the photodiodes is measured will be considered next.

The infrared detecting photodiodes are arranged in a cross as shown in Figure 5.5.1. This has been copied from Figure 2.2.2 of chapter 2 for the reader's convenience. The pair of horizontally mounted diodes are intended to measure the horizontal position of the received image. The pair of vertically mounted diodes are intended to measure the vertical position of the received image. The position measurement is made as follows.

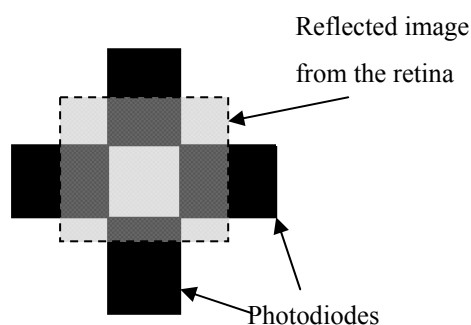


Figure 5.5.1 The arrangement of the photodiodes to detect image movement.

Unfortunately the actual area of the photo sensitive region of the photodiodes is not specified the manufacturer's data sheet. (Liteon LTR536AB). Only an offset of the centre of the photosensitive area from the base of the diode is given. As the received image changes position on the radiant sensitive area, the output of each diode will

change accordingly. Let the amplified electrical voltages of the diodes be V_{right} , V_{left} , V_{upper} , V_{lower} for the horizontal right and left hand diodes and the vertical upper and lower diodes respectively. Let the point of intersection of the horizontal and vertical centre lines of the diodes be called the *centre point*.

Dimensionless measures of the position of a sharp image with respect to the centre point are the ratio shown in equations 5-5 and 5-6. The difference of voltages is proportional to image position. Dividing by the sum makes the ratio independent of the total radiant flux falling on the diodes.

$$HorizontalPositionRatio = \frac{(V_{right} - V_{left})}{(V_{right} + V_{left})} \quad 5-5$$

$$VerticalPositionRatio = \frac{(V_{upper} - V_{lower})}{(V_{upper} + V_{lower})} \quad 5-6$$

These ratios will be zero only when the differences are zero, meaning that the image is centrally located on the four diodes. The ratios can be positive or negative depending on the image position relative to the diodes.

The horizontal and vertical position ratios will be calculated for the outputs received from both the top and bottom IREDs. The results will be subtracted to obtain the *position ratio difference* (PRD). Using the subscripts ‘t’ for top IRED and ‘b’ for bottom IRED, and replacing the words “right”, “left”, “upper” and “lower” with the subscripts ‘r’, ‘x’, ‘u’, ‘l’, the position ratio differences are defined by equations 5-7 and 5-8.

$$HorizontalPRD = \frac{(V_{rt} - V_{xt})}{(V_{rt} + V_{xt})} - \frac{(V_{rb} - V_{xb})}{(V_{rb} + V_{xb})} \quad 5-7$$

$$VerticalPRD = \frac{(V_{ut} - V_{lt})}{(V_{ut} + V_{lt})} - \frac{(V_{ub} - V_{lb})}{(V_{ub} + V_{lb})} \quad 5-8$$

Should any of the quantities in these equations be zero the corresponding ratio would go to one. Any changes in the PRD due to changes in the other variables would be lost. Furthermore, subtraction of small quantities can be inaccurate, particularly when the number of bits used for representation is limited. Consequently, simply subtracting the

ratios is not the best method of performing the calculation. The problem can be resolved by subtraction using a common denominator and some algebraic simplifications. The rearranged equations are shown in equations 5-9 and 5-10.

$$\text{HorizontalPRD} = 2 \frac{(V_{rt} * V_{xb} - V_{xt} * V_{rb})}{(V_{rt} + V_{xt}) * (V_{rb} + V_{xb})} \quad \text{5-9}$$

$$\text{VerticalPRD} = 2 \frac{(V_{ut} * V_{lb} - V_{lt} * V_{ub})}{(V_{ut} + V_{lt}) * (V_{ub} + V_{lb})} \quad \text{5-10}$$

The concept of a precise position is only valid when the image is sharply focused. If the image boundaries are blurred and the image is in fact a distribution of radiant flux, then the meaning of a millimetre distance is not clear, but the voltage ratios are still meaningful. This is because the ratio still indicates the relative distribution of radiant flux over the diodes.

The position ratio differences shown in equations 5-9 and 5-10 should be zero when the aperture and photodiodes are conjugate to the retina. However this depends on a few conditions:

1. The aperture is uniformly irradiated by the photodiodes. If not, there will be differences in position ratio due to distribution of radiant flux even when the image is in focus.
2. The reflected image is sufficient to give a reading on all the photodiodes. Zero readings on some photodiodes will invalidate the relation between image position and position ratio as measured.

Ideally there should be one carriage position that results in a PRD of zero. The position of the carriage to produce this zero value will correspond to overall refraction of the eye measured. Let the photodiode distance from lens L3 be X_3 when the PRD is zero. The overall refraction of the eye can then be calculated from equation 2-2. This equation is repeated here as equation 5-11 for the reader's convenience:

$$D_e = \frac{f_2^2}{f_3 f_1^2} \left(1 - \frac{X_3}{f_3} \right) \quad \text{5-11}$$

To determine the distance X_3 , the PRDs must be calculated over a range carriage positions. At each carriage position the PRDs are calculated and plotted. The value of the carriage position at which the PRDs are zero is X_3 in equation 5-11.

The following was done to perform this measurement in practice. Readings were taken from the all of the photodiodes for a set of carriage positions. The carriage was moved manually in 12 to 15 mm increments and a reading taken. The results were saved and read into Matlab. The calculations of PRDs were then performed and plotted in Matlab. The program run by the micro controller to make the measurements in this section can be found on the attached CD at:

CD:\Embedded\Mirror\Scheiner

Changes in the carriage position were accurately measured by a shaft encoder attached to the carriage belt sprocket opposite the motor. The raw results were at non uniform carriage positions. To obtain a set of readings at precisely 12 mm intervals, the photodiode readings read into Matlab and were interpolated using the Matlab “**interp1()**” function. This function performs interpolation with one dimensional data.

The reason for wanting photodiode outputs at repeatable and accurate carriage positions is so that one set of readings can be subtracted from another set. This will be useful, since it enables the readings taken for specular reflections only, to be subtracted from those obtained for refractive measurement. A set of readings was taken with the retina of the artificial eye replaced by a black cone. The photodiode readings will contain the results that show the reflections from lens surfaces only. The data was saved into a file to be used in later calculations.

An initial run showed that a number of photodiodes had zero values. For example the reading for the horizontal right photodiode would change as the carriage position changes but the reading from the horizontal left cell remained zero. These zero values will reduce the accuracy of the results.

5.5.3 Photodiode position ratio difference measurements

To test how well the PRD measures the refraction of the artificial eye, the eye was adjusted for 5 different overall refractions. This was done by adjusting the distance of

the cardboard retina from the lens. These refractions and distances are shown in Table 5-1. For each level of overall refraction, there will be a corresponding distance X_3 which will make the photodiodes conjugate to the retina of the artificial eye. These distances can be calculated by rearranging equation 5-11 to solve for X_3 in terms of D_e . The focal lengths of all of the lenses are 200 mm, and therefore focal lengths f_1 and f_2 cancel, giving the result is shown in equation 5-12.

$$X_3 = f_3(1 - f_3 D_e) \quad 5-12$$

Using this equation, the distances X_3 corresponding to overall refractions of the artificial eye between 0 and 4 dioptres were calculated and are shown in Table 5-2.

Table 5-2 Overall refractions, retinal and corresponding photodiode distances.

Overall refraction (D)	Retina distance (mm)	Theoretical photodiode distance from lens L3 (X_3) (mm)
0	43.5	200
1	46.1	160
2	49.0	120
3	52.3	80
4	56.0	40

At each of the retinal distances shown in Table 5-2, the PRDs were calculated for the carriage positions varying between 40 to about 370 mm at 12 mm increments. The results for the vertical photodiodes are shown in Figure 5.5.2. The results for the horizontal photodiodes are shown in Figure 5.5.3.

Are these curves being distorted due to the presence of specular reflections from lenses? This hypothesis was tested by obtaining a set of photodiode readings when the retina of the artificial eye was replaced by a black cone. These readings were subtracted from the results taken with the retina present. The new PRDs versus carriage position were plotted. The plot of vertical position ratio differences in this case is shown in Figure 5.5.4. The only difference noticeable was for large distances of the photodiodes from the lens **L3**. There was no noticeable difference in the separation of the curves for different retinal distances. This measurement completes the experimental assessment of the Scheiner principle measurements.

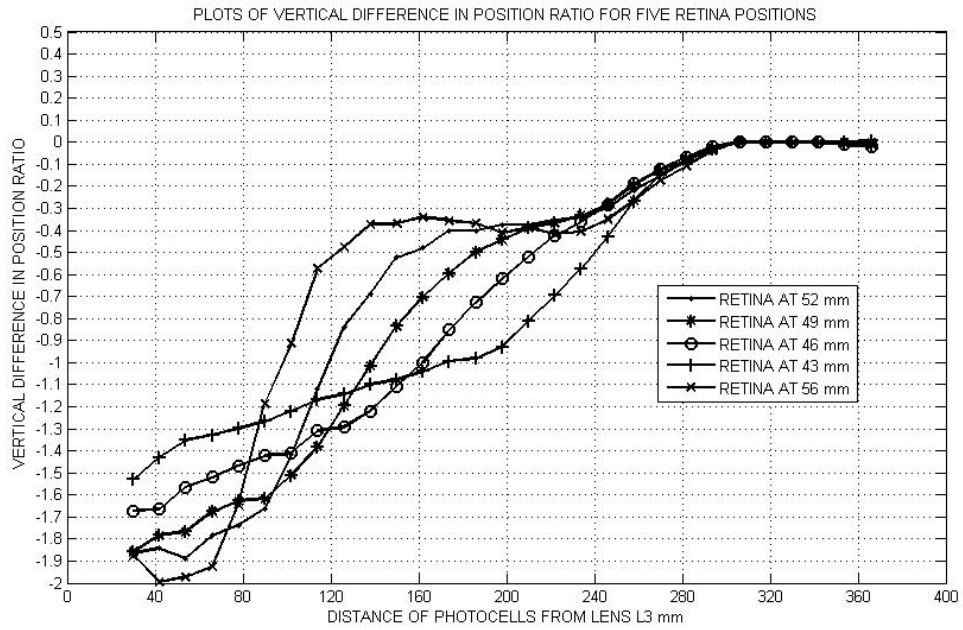


Figure 5.5.2 Plots of vertical difference in position ratio for five retina positions.

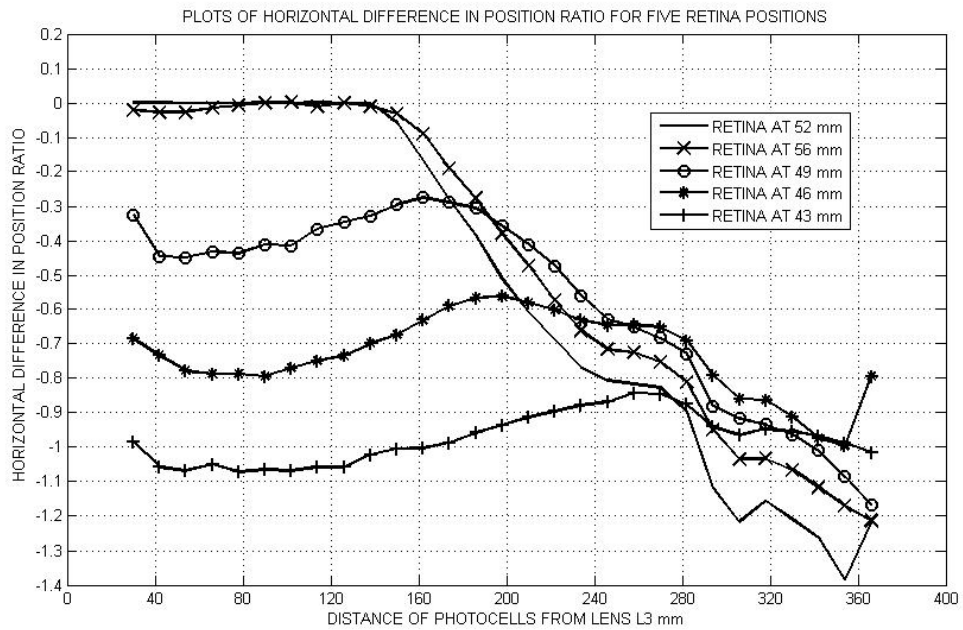


Figure 5.5.3 Plots of the horizontal difference in position ratio for five retina positions.

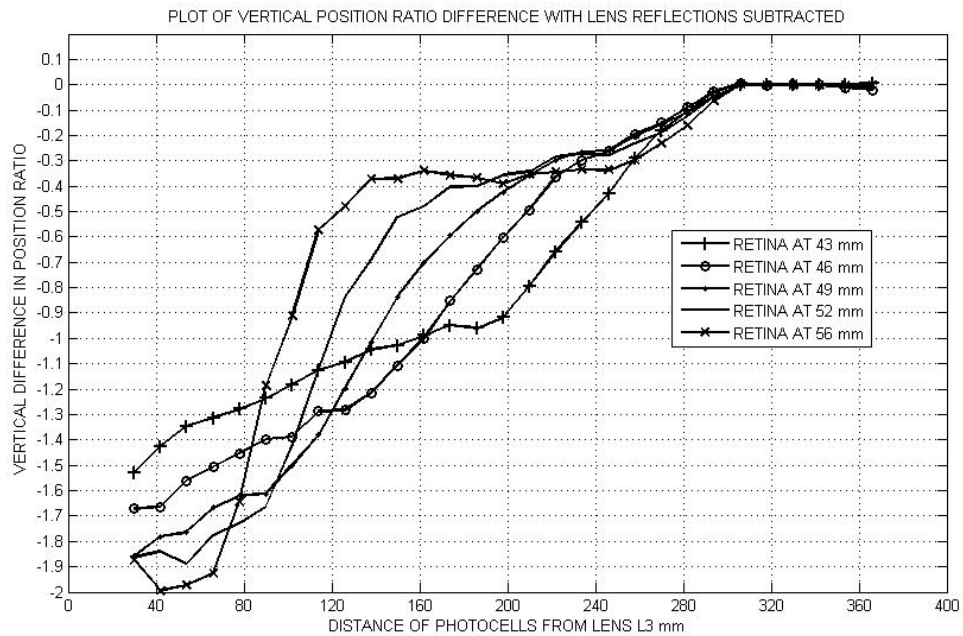


Figure 5.5.4 Plots of the vertical position ratio difference with lens reflections subtracted.

5.5.4 Discussion and conclusions

The second question of section 5.1.1 was is it possible to measure refraction using the Scheiner principle despite the presence of some radiation due to specular reflections? What has been found is that radiation due to specular reflection did not change the results of the Scheiner principle measurement to any noticeable degree. However the Scheiner principle measurements using position ratio differences did not give a correct measurement of the refraction of the artificial eye. There were only shifts in the curves of PRD versus carriage position for each overall level of refraction of the eye.

It is believed this failure to measure refraction is due to two main reasons:

1. The photodiode readings had many zero values. This shows that the image received on the photodiodes did not adequately overlap the radiant sensitive areas. Unfortunately the information on the photodiodes used for the retinal photodiodes does not clearly specify where the radiant sensitive areas are. This needs to be investigated further. The zero values would invalidate/corrupt the measurements of position ratio.
2. The vertical PRD curves show a general increase over the range of carriage positions. Theoretically the PRD curves should reach a minimum or maximum value at which the carriage position corresponds to the refraction of the eye. It is

possible that both the images from the top and bottom IREDs are shifting vertically as the carriage position changes. It is also possible that the image position of the aperture on the photodiodes would be determined by the position of the servo mirror. Unfortunately the requirements of having the image of the IREDs centred on the pupil and having the retinal image centred on the photodiodes could require two different positions of the servo mirror. This is a fundamental failing in the optical design, which possibly requires two servo mirror systems.

5.6 Locating the pupil using the retinal reflection

5.6.1 Introduction

The first question raised at the end of section 5.1.1 is whether it is possible to locate the pupil using radiant flux reflected from the retinal image. It has already been seen in section 5.4.2 that there will be some specular reflection, yet is it relatively small. Since the degree of specular reflection did not affect the Scheiner principle measurements, it should be possible to distinguish the radiant flux reflected from the retina as opposed to the much smaller reflection from the lens surface of the artificial eye.

To find out, an X-Y scan was done of the artificial eye using the 12 mm pupil diameter used for the Scheiner principle measurements.

5.6.2 XY Scan of the artificial eye

The carriage was set to 200 mm from lens **L3** and the retina of the artificial eye adjusted for zero dioptres overall refraction. Using the X-Y scanning program referenced in section 5.1.5, a scan of the total output of the photodiodes for the top and bottom IREDs was made. The resulting contour and mesh plots are shown in Figure 5.6.1, Figure 5.6.2, Figure 5.6.3 and Figure 5.6.4.

5.6.3 Discussion and conclusions

In discussing these figures, it is important to know the (X,Y) location of the pupil centre on the pupil plane. In section 5.3 the pupil centre was estimated to be at (23.5,7.5). This location is close to the centre of the contour plot Figure 5.6.1. This centre is

approximately 6 mm from the curved contour lines at the periphery of the Figure 5.6.1. Therefore it is believed that these curved contours mark the boundaries of the pupil. The corresponding mesh plot Figure 5.6.2 shows a slow increase in output from the peripheral areas to the location (23.5,7.5). This is consistent with the overlap of the image of the sources and the pupil increasing, as the image of the sources move over the pupil region. The image of the sources at the pupil plane would have the same diameter as one IRED which is about 5 mm. Once this 5 mm diameter region of the image of the sources is within the pupil area, there will not be any further increase in radiant flux entering the artificial eye.

Now consider the plots of the total output of the photodiodes for the bottom IRED, shown in Figure 5.6.3 and Figure 5.6.4. The curved boundaries of the pupil periphery are less marked in Figure 5.6.3 than they are in Figure 5.6.1. Nonetheless, the yellow and red centrally located contours of Figure 5.6.3 show a region of higher output in central region around the point (23.5,7.5). The same region of higher output is shown in the corresponding mesh plot of Figure 5.6.4.

On the upper region of all the plots between the X locations 20-24 mm and Y locations 10-12 mm there is smaller but relatively large output peaks. These are believed to be due to specular surface reflections (corresponding to corneal images) of the 20 D lens of the artificial eye. These large output areas are distant from the pupil centre at (23.5,7.5) in Y location by 2.5 to 4.5 mm. It is concluded that the location of the maximum corneal reflection does not necessarily coincide with the centre of the pupil. If the radius of the lens surface was smaller, the location of the pupil centre and the corneal reflection would be closer. This is the case in the human eye with a corneal radius of approximately 7.8 mm. The plastic planar convex 20 D lens of the artificial eye was estimated to have an surface radius of 75 mm assuming the plastic has a refractive index of 1.5.

Concluding, it has been seen that the pupil boundaries and pupil region are associated with an increase in output from the retinal photodiodes. Despite the use of crossed polarizers, there is still significant specular reflection. In this case the centre location of the pupil is not correctly detected by the point of maximum output. However it *could be estimated from finding the centre of the pupil from the curvature of the boundary contours.*

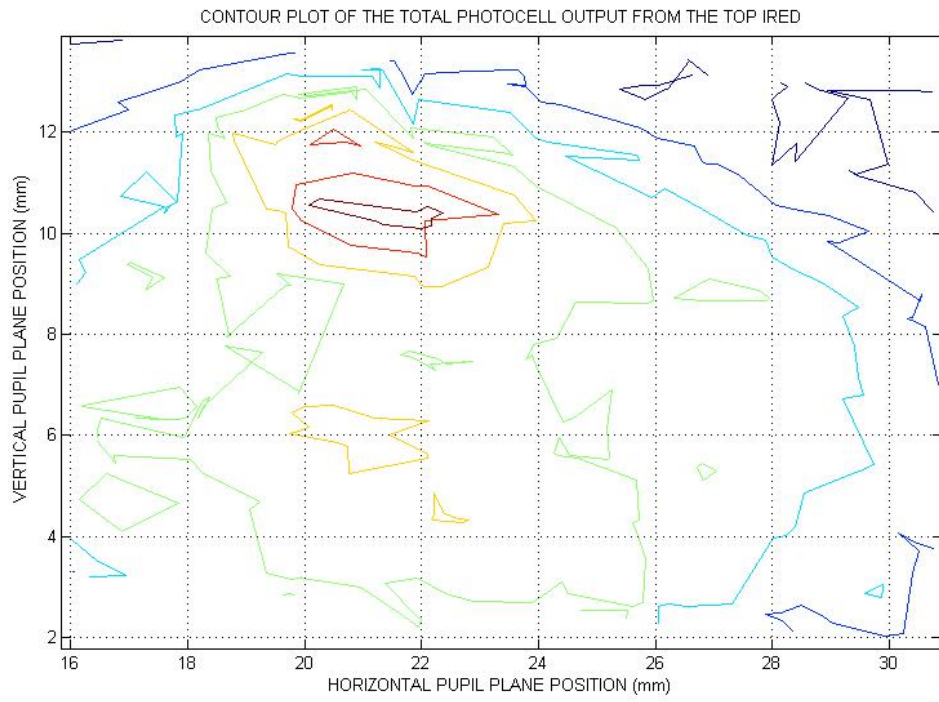


Figure 5.6.1 Contour plot of the total photodiode output from the top IRED.

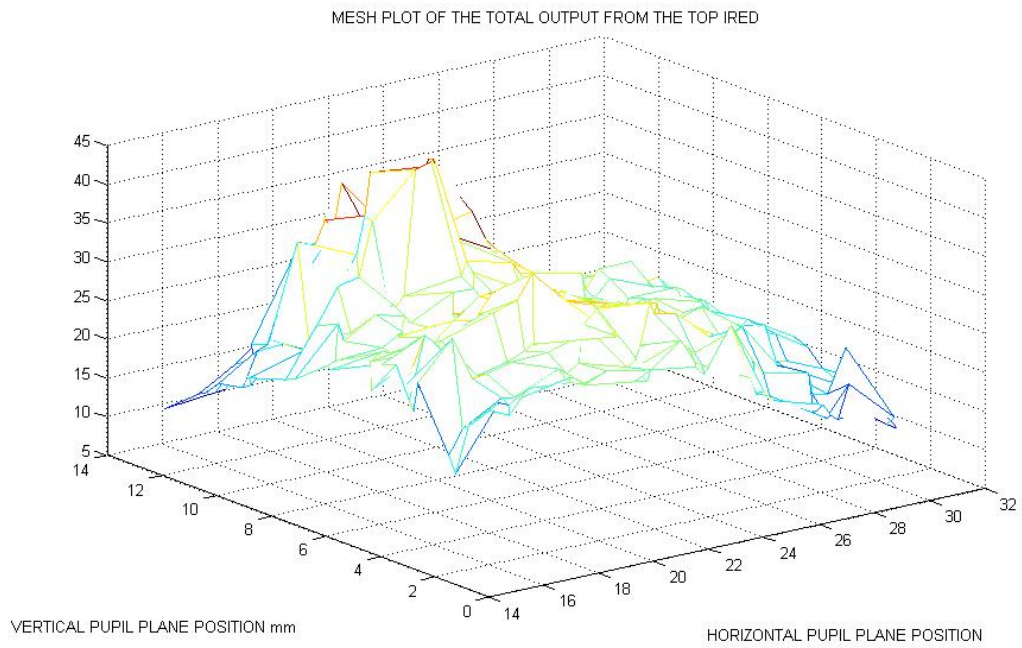


Figure 5.6.2 Mesh plot of the total photodiode output from the top IRED.

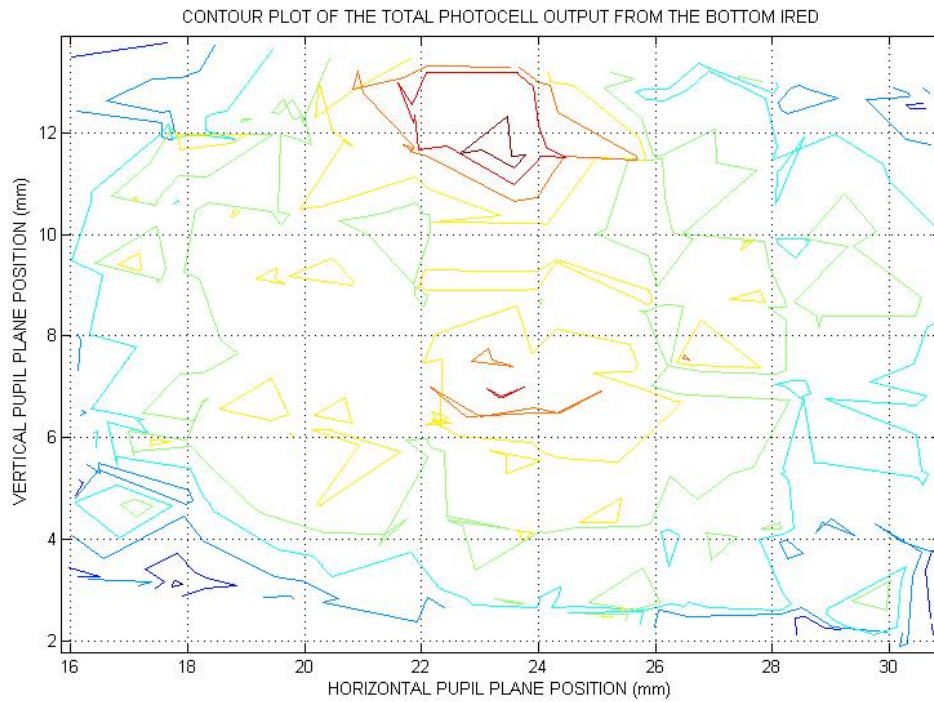


Figure 5.6.3 Contour plot of the total photodiode output from the bottom IRED.

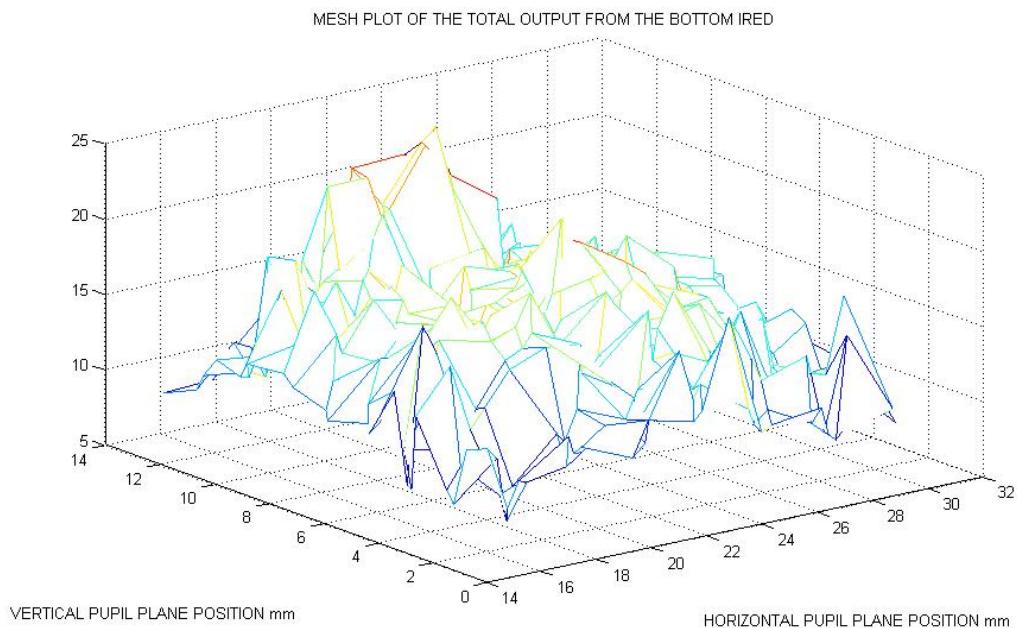


Figure 5.6.4 Mesh plot of the total photodiode output from the bottom IRED.

5.7 Conclusions

This chapter attempts to evaluate of the proposals made in chapter 2. The first idea was to scan for the increased radiant output from the retina to locate where the pupil of the eye is. A related idea was to eliminate the specular reflection from the cornea to make

the first one possible. It was intended to remove the specular reflection by using linear polarizers and dielectric mirrors.

It has been found that the use of crossed linear polarizers and dielectric mirrors do not totally eliminate specular reflections from spherical surfaces but do substantially reduce them in the order of 77.5%. Secondly, it was found that the location of the corneal reflection did not coincide with the pupil centre.

The output measured due to specular corneal reflections did not affect the measurements of retinal image position using position ratio differences. It was possible to independently measure the photodiode outputs due to the specular reflections and subtract them from other readings where a retina is present. This could be a method of dealing with the corneal reflection when measuring human eyes. Such a method would not have been available to the early optometers that used analogue electronic systems.

The refraction measurements were not successful in predicting the overall refraction of the artificial eye. It is believed that this was mainly due to a mismatch in the size of the reflected image and the position of the photo sensitive areas of the photodiodes. This resulted in many zero outputs from photodiodes which would have upset the position ratio measurements.

Secondly there was an unexplained general shift in position ratio difference as the carriage was moved from one end to the other. This could have been due to movement of the retinal images with carriage position due to mirror position. This needs to be further investigated theoretically using ray tracing techniques.

Regarding the location of the pupil using the radiant flux reflected from the retina, it was found that the pupil boundaries could be detected from contour plots. If time had permitted, an automatic method of using these contours to locate the centre of the pupil could have been developed. Similarly, if time had permitted, it could have been possible to develop a means of tracking pupil motion using the pupil boundaries.

Finally, the optical design of the artificial eye was inadequate. If pupil sizes of the same size as the human eye are to be used, then the power of the lens needs to be of the same

order as the total power of the human eye. This varies from 59.9 to 67.67 D from for a theoretical eye according to Smith and Atchison (1997) pages 784 and 785.

6 Conclusions and future work

6.1 Introduction

This chapter will summarise the main conclusions that have come out the work of this investigation. The sections correspond to previous chapters of this thesis. Possible future work will be suggested.

The review of the methods of patient eye alignment used by optometers found that using the image reflected from the retina has not been used for patient eye alignment. Investigating the possibility of doing this has been partially explored in this study.

It was found that several optometer systems do use the radiant flux reflected from the cornea of the human eye for alignment purposes. This investigation has attempted to remove the specular reflection from the cornea, firstly so that it does not need to be blocked and secondly, so that it does not obscure the radiant flux reflected from the retina.

6.2 The optical system

There are three features of the optical design of the optometer which make it different from other Scheiner principle optometers. These are:

1. The use of linear polarizers and dielectric mirrors to attempt to eliminate the need to block the specular reflection from the cornea of the eye.
2. The absence of a stop to block radiant flux reflected from the cornea from reaching the photodiodes.
3. The system does not attempt to use the corneal reflection for optical alignment.

This investigation has shown that the proposed system of polarizers and dielectric mirror does not entirely eliminate specular reflections, but substantially reduces them. A measured figure of 77.5 percent reduction was obtained. Why a greater reduction of the

specular reflection from the surface of the lens of the artificial eye has not been possible, is not understood. Theoretically a better reduction should have been obtained.

It was found with that the pupil plane location for the maximum corneal reflection did not coincide with the pupil location. However, the radius of curvature of the pupil of the human eye is approximately 10.4 % of the radius of curvature of the artificial eye tested. Therefore in the case of the human eye, it is likely that the maximum corneal reflection and the centre of the pupil will be much closer than the few millimetres difference found here.

The lens power of the artificial eye needs to be substantially increased and the pupil size reduced, so the pupil sizes of the human eye can be used with the artificial eye.

Whether a corneal stop is still needed for refraction measurement with a human cornea is still to be tested.

The results of measurement of retinal image position by the photodiodes, suggested that the retinal image at the photodiodes moves perpendicular to the axis of the carriage. Therefore the retinal images from the two IREDs cannot always be centred on the photodiodes. The relationship between servo mirror position and retinal image position at the photodiodes needs to be further investigated with ray tracing techniques. It might be that having a single two dimensional servo mirror system is not adequate to ensure that retinal image position remains centred on the axis of carriage movement.

An improvement that could be made in the optical system design would be to use the system of Crane and Steele (1978) to reduce the size of the IREDs image at the pupil plane of the eye. Crane and Steele (1978) used lenses to image the IREDs onto the prism mirror, thereby reducing their size. This would enable the instrument to work with smaller pupil sizes. In the case of the experimental optometer, it would also nearly double the radiant flux delivered to the eye. This is because with current arrangement, nearly half of the radiant flux of the IREDs is lost, as they appear as half moons at the pupil plane of the eye.

6.3 The electronic and electro-mechanical systems

The development of the servo mirror system revealed a problem with the electro-mechanical method of moving the pupil plane image of the IRED sources. The position of the pupil plane image of the IREDs is *very* sensitive to the angular position of the mirror. This is because the position of the image on the pupil plane is the product of the angular position of the mirror and the focal length of lens **L1**. This sensitivity placed extreme demands on the precision of mirror position to obtain precision in the pupil plane positioning. The current system is barely adequate, but has been used to obtain the results of this thesis. Whether it is adequate with smaller pupil sizes remains to be seen.

6.4 Detection of the pupil

The hypothesis of section 1.5 was that the radiant power received by the photodiodes will be maximised when the optical axes of the optometer is aligned to the patient's eye. This hypothesis has been found that this is not correct. What actually occurs is:

1. The peak radiant flux received is still due to the corneal reflection.
2. There is a smaller but measurable increase in flux as the boundaries of the pupil area are traversed by the optical axis of the optometer.
3. In the case of an artificial eye with a lens surface radius of 75 mm, the corneal reflection does not coincide with the centre of the pupil. Therefore the detection of the radiant flux peak is not a valid method of locating the centre of the pupil for an artificial eye with a lens that has a large radius relative to the human eye.

The boundaries of a pupil of 12 mm diameter could be detected by the contours of constant radiant flux received by the retinal photodiodes. This was a finding of major significance. Firstly, it means there was an increase in the radiant flux reflected from the artificial eye when the image of the IREDs overlapped the pupil. Secondly, it provides the basis upon which a method of automatic pupil location could be developed. Such a system would detect the change in photodiode outputs at the pupil boundaries, and use the boundary locations to calculate the location of the pupil centre.

6.5 Refractive measurement using the Scheiner principle

The method of detecting retinal image position using the photodiodes did not work sufficiently to make Scheiner principle measurement of refraction work. However the curves of difference in position ratio showed clear changes as the overall refraction of the artificial eye was changed. Never the less there was no one feature of the position ratio measurements that corresponded to the refraction of the artificial eye. The reason for this is not fully understood, but is believed to be caused by the area of the retinal image not completely overlapping the photo sensitive areas of the photo diodes. Also, as mentioned in section 6.2, there appears to be general lateral shift in the centre of the retinal images as the carriage is moved.

The radiant power received from the specular reflection from the lens surface of the artificial eye did not make any noticeable difference to the position ratio measurements used for refraction measurement. The photodiode outputs due to specular reflections alone, was measured at all the carriage positions used for refractive measurement. Since the photodiode outputs due to specular reflections will be approximately constant, they could be saved in the program code memory. Then when subsequent refractive measurements are made, the values of photodiode output for specular reflections subtracted. The ability of the computer system to store these constant values would save having to totally eliminate the specular reflections optically.

The four photodiodes used in the experimental optometer were not designed for detecting image position. The method of having an image overlap separate photosensitive areas to detect its position, has now be superseded by lateral effect photo detectors. The 2 dimensional *lateral effect* Position Sensitive Detector (PSD) has one photosensitive area and four outputs. The electronic circuitry used for image position is still the same as used for separate photodiodes. However, the advantage of the lateral effect PSD is that the image does not need to overlap four separate regions in order to have its position determined. The current four photodiodes used in the experimental optometer will be replaced by a lateral effect PSD.

It is believed that this replacement will partially resolve the failure of the system to measure refraction using the Scheiner principle. As previously explained, the other issue is whether the mirror system is causing a general lateral shift in retinal image position at the photodetectors.

6.6 Conclusions

The thesis will be concluded by considering which objectives of section 1.5 have been achieved. The first objective was to test whether an optometer system can be developed that can use the radiant power received from the retinal photodetectors to align the optometer's axis to the patient's eye.

This question has been partially answered; it has been shown that the pupil can be located by the radiant power received from the reflection from the retina. However, an automatic method of locating the pupil was not developed. Neither has it been shown that the refraction of the eye can be measured with such a system.

The second objective was to test whether an optometer system that uses retinal reflection for alignment, can maintain its alignment when the pupil is moving. This question has not been answered yet. It remains a question for future research.

Finally, the third objective of whether such an alignment and tracking system can continuously measure the refraction of the eye, has not been answered. It also remains as future research.

6.7 Future work

The proposed future work has already been described in its appropriate context in the preceding sections. To summarise:

1. The design of the artificial eye needs to be revised with front lens that has the same curvature as the human cornea of about 7.8 mm radius and a substantially higher refractive power. The higher power will enable pupil sizes comparable with that of the human eye to be used.
2. The relationship between mirror position and the position of the retinal image position at the plane of the photodetectors needs to be investigated using ray tracing techniques.
3. The four individual photo diodes should be replaced by on lateral effect position sensitive detector.
4. The position resolution of the servo mirror system should be increased and the small friction oscillations removed.

7 References

- Allen, P. M., H. Radhakrishnan, et al. (2003). "Repeatability and Validity of the PowerRefractor and the Nidek AR600-A in an Adult Population with Healthy Eyes." Optometry and Vision Science **80**(3): 245-251.
- Atchison, D. A. and G. Smith (2000). Optics of the Human Eye, Butterworth, Heinemann.
- Barry, R. (2009). Using the FreeRTOS real time kernel.
- Behrens, F. and L. R. Weiss (1991). "An algorithm separating saccadic from nonsaccadic eye movements automatically by use of the acceleration signal." Vision Research **32**(5): 889-893.
- Campbell, F. W. and J. G. Robson (1959). "High Speed Infrared Optometer." Journal of the Optical Society of America **49**(3): 268-272.
- Campbell, J. (1987). C programmer's guide to serial communications, Howard W. Sams & Company.
- Charman, W. N. and G. Heron (1975). "A Simple Infra-Red optometer for accommodation studies." British Journal of Physiological Optics **30**(1): 1-12.
- Cornsweet, T. (1970). "Servo Controlled Infrared Optometer." Journal of the Optical Society of America **60**(4): 548-553.
- Cornsweet, T. N. and H. D. Crane (1973). "Accurate two dimensional eye tracker using first and fourth Purkinje images." Journal of the Optical Society of America **63**(8): 921-928.
- Crane, H. and C. Steele (1978). "Accurate three-dimensional eyetracker." Applied Optics **17**(5): 691-705.
- Davies, L. N., E. A. H. Mallen, et al. (2003). "Clinical Evaluation of the Shin-Nippon NVision K 5001/Gran Seiko WS-5100K Autorefractor." Optometry and Vision Science **80**(4): 320-324.
- Edmund, R. M. (2008). Optics and instruments catalog. Singapore, Edmund Optics.
- Elkington, A. and H. Frank (1991). Clinical Optics. London, Blackwell Scientific Publications.
- Franklin, G. F., D. J. Powell, et al. (1998). Digital Control of Dynamic Systems, Addison Wesley Longman Inc.

- Gekeler, F., F. P. Schaeffel, et al. (1997). "Measurement of Astigmatism by Automated infrared photoretinoscopy." Optometry and Vision Science **74**(7): 472-482.
- Golten, J. and A. Verwer (1991). Control System Design and Simulation, McGraw Hill.
- Heron, G., B. Winn, et al. (1989). "Twin Channel Infrared Optometer for Recording Binocular Accommodation." Optometry and Vision Science **66**(2): 123-129.
- Hunt, O. A., J. S. Wolffsohn, et al. (2003). "Evaluation of the measurement of refractive error by the Power Refractor: a remote, continuous and binocular measurement system of oculomotor function." British Journal of Ophthalmology **87**: 1504-1508.
- Jenkins, F. A. and H. E. White (1981). Fundamentals of Optics, McGraw-Hill Inc.
- Kruger, P. B. (1979). "Infrared Recording Retinoscope for Monitoring Accommodation." American Journal of Optometry and Physiological Optics **56**(2): 116-123.
- Lim, K. W., N. C. Cheung, et al. (1994). Proportional control of a solenoid actuator. Industrial Electronics, Control and Instrumentation, 20th Intl. Conference, Bologna, Italy.
- Mallen, E. A. H., J. S. Wolffsohn, et al. (2001). "Clinical evaluation of the Shin-Nippon autorefractor SRW 5000 autorefractor in adults." Ophthalmic and Physiological Optics **21**(2): 101-107.
- Ogata, K. (1997). Modern Control Engineering.
- Okuyama, F. and T. Tokoro (1989). "Eye-tracking infra-red optometer." Ophthalmic and Physiological Optics **10**(July): 291-299.
- Pfabisen, K. R. and T. Millbocker (1989). Eye fundus tracker/stablizer. U. S. Patent. USA, Eye Research Institute fo Retina Foundation.
- Pugh, J. R. and B. Winn (1988). "Modification of the Canon AutoRef R1 for use as a continuously recording infra-red optometer." Ophthalmological and Physiological optics **8**(October): 460-464.
- Renn, J. and Y. Chou (2004). "Sensorless plunger position control for a switching solenoid." JSME International journal **47**(2): 637-645.
- Roger, W. H. and M. H. Edwards (2001). "Interfacing the Shin-Nippon autorefractor SRW-5000 with a personal computer." Ophthalmic and Physiological Optics **21**(2): 114-116.
- Roorda, A., W. R. Bobier, et al. (1997). "An infrared eccentric photo-optometer." Vision Research **38**: 1913-1924.

- Scerra, C. (2001). "Tracking, scanning features help improve laser vision correction procedures : Excimer laser system is able to track all saccadic eye movements." Ophthalmology Times **V27i7**: 18.
- Schimitzek, T. and W. Wesemann (2002). "Clinical evaluation of refraction using a handheld wavefront autorefractor in young and adult patients." Journal of Cataract and Refractive Surgery **28**(9): 1655-1666.
- Smith, G. and D. A. Atchison (1997). The eye and visual optical instruments, Cambridge University Press.
- Straube, A. and H. Deubel (1995). "Rapid gain adaptation affects the dynamics of saccadic eye movements in humans." Vision Research **35**(23/24): 3451-3458.
- Takeda, T., Y. Fukui, et al. (1988). "Three Dimensional Optometer." Applied Optics **27**(12): 2595-2602.
- Taylor, D. G. (2003). Development of an infrared optometer. Electrical Engineering, AUT University. **PG Diploma**: 127.
- Wolffsohn, J. S., B. Gilmartin, et al. (2001). "Continuous recording of accommodation and pupil size using the Shin-Nippon SRW-5000 autorefractor." Ophthalmic and Physiological Optics **21**(2): 108-113.
- Yancey, D. R. (1997). Device and method for evaluation of refraction of the eye. U. S. Patent. USA.
- Yancey, D. R., L. Schupak, et al. (2006). Complete autorefractor system in an ultra compact package. U. S. Patent. USA.

8 Appendices

8.1 Appendix 1. Calculation of the size of the corneal reflection of the aperture.

If the beam splitters and mirrors are taken away and the lenses and aperture of the optometer system made linear, then the optical arrangement would be as shown in Figure 8.1.1. The system depends on the telescopic relay formed by lenses **L4** and **L2**.

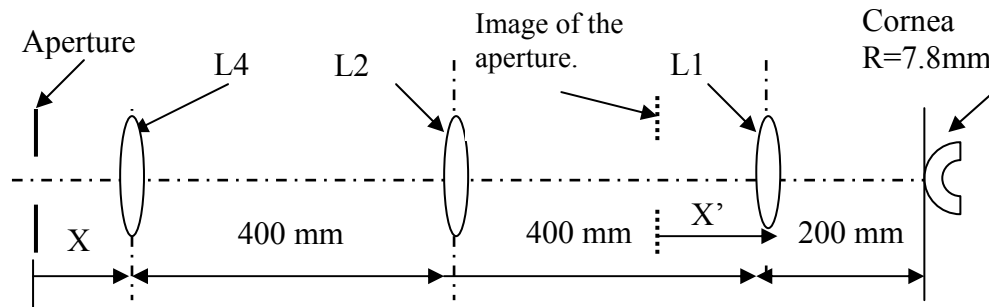


Figure 8.1.1 The lens system between the aperture and the cornea.

Let Y be the distance of the image of the aperture from centre of lens **L2** and let f_4 and f_2 be focal lengths of lenses **L4** and **L2**, then Y can be found from equation 8-1. (Crane and Steele (1978))

$$Y = f_2 \left(1 + \frac{f_2}{f_4} \right) - \left(\frac{f_2}{f_4} \right)^2 X \quad 8-1$$

Since $f = f_2 = f_4$, then the equation is simplified to equation 8-2.

$$Y = 2f - X \quad 8-2$$

Lenses **L1** and **L2** are separated by twice their focal length $2*f$, and since $X' = (2*f - Y)$, then $X' = X$ in Figure 8.1.1. Let Z be the image distance of the image of the aperture at X' from the centre of lens **L1**. Then using the thin lens equation, the optical sign convention of Smith and Atchison (1997) on page 28 and that $f = 0.2$ metre, then Z is as shown in equation 8-3.

$$Z = \frac{X}{(5X - 1)}$$

8-3

The transverse magnification of the image due to lens **L1** is the ratio (Z/X). Now calculate the position and magnification of this image as it is reflected by the convex surface of the cornea. The mirror equation from Smith and Atchison (1997) on page 91 is:

$$\frac{1}{l'} + \frac{1}{l} = \frac{2}{r}$$

8-4

Where r is the radius of curvature of the mirror surface. For the cornea, the radius will be taken as 7.8 mm from Atchison and Smith (2000). The object and image distances are l and l' . The object and images distances are shown in equation 8-5.

$$l = -(f - Z) = \frac{1}{5(5X - 1)} \quad l' = \frac{lr}{(2l - r)}$$

8-5

The image magnification due to the reflection can be calculated as shown in equation 8-6.

$$M_c = \frac{-l'}{l} = \frac{r}{\left(\frac{2}{5(5X - 1)} - r\right)}$$

8-6

Combining this magnification with the transverse magnification due to lens **L1** gives the overall transverse magnification of the aperture shown in equation 8-7.

$$M_{total} = M_1 * M_c = \frac{1}{(5X - 1)} * \frac{r}{\left(\frac{2}{5(5X - 1)} - r\right)} = \frac{r}{\left(\frac{2}{5} - \left(\frac{r}{5X - 1}\right)\right)}$$

8-7

As X approaches f ($=0.2$ metre) the magnification approaches zero. When X is zero the magnification will be maximum. Inserting $r=7.8$ mm and $X=0$ in equation 8-7 gives a magnification of 0.0191. *Since the aperture is a 12mm square, the maximum possible size of the corneal reflection is 0.23 mm square.* This image will be located at l' calculated from equation 8-5 as +3.82 mm posterior of the corneal apex. Finally when $X=0.4$ which is when the aperture is close to lens **L5**, the image size is 0.237 mm and the position is 3.86 mm posterior of the corneal apex. In each case the position of the corneal image is very close to the entrance and exit pupils of the eye. According to Atchison and Smith (2000), the entrance and exit pupils are located at 3.60 and 3.67 mm posterior of the corneal apex respectively, for a Gullstrand number schematic eye.

8.2 The Real Time Structures File Format Specification

Version 1.0 23 February 2006

Version 1.1 7 March 2006. The total number of structures is the first variable in the binary section.

8.2.1 The problem

A method of recording structures of variables in a file is needed that:

1. Contains the name and type of variables in each structure.
2. Contains the date when the file was created.
3. Contains a brief description of what the data is about.

8.2.2 The solution

Store the information about the date, the name and type of variables and description in an ASCII header, followed by variable length data field. It is expected that RTS files will have the file name extension “.rts” The idea is that each variable type used for data can be identified by a number. Since it is intended to be able to convert the files generated into Matlab files, use the Matlab types for variable types as below:

8.2.3 RTS file data types.

<i>Value</i>	<i>Symbol</i>	<i>Data type</i>
1	Int8	8 bit signed
2	uInt8	8 bit unsigned
3	Int16	16 bit signed
4	uInt16	16 bit unsigned
5	Int32	32 bit signed
6	uInt32	32 bit unsigned
7	Float	IEEE 754 single format
	Double	IEEE 754 double format.

8.2.4 The RTS header section

The header will consist of newline terminated lines each starting with a % character to identify the header lines. The first line must be:

```
%Real Time Structures
```

This identifies the type of file. The next line must be the date of recording as produced by the ctime() function in C. The line will contain 27 bytes followed by a newline as follows:

```
%Mon Feb 23 11:15:53 2006\n
```

The following lines contain the specification for each of the variables in the recorded structures. Each entry consists of a number from 1 to 9 specifying the type of the variable followed by a space then the variable name and terminated by a new line. eg:

```
%7 UpperPhotodiodeReading\n
```

```
%8 LowerPhotodiodeReading\n
```

The variable names are taken to be elements of the structure and the order in which they are written to the file. Binary structures will be read in this order.

A variable entries are terminated by any line that does not have an ASCII numerical digit as the first character after the %.

Any of the following lines that start with a % sign are taken as documenting comments for the file. The header section must terminate with a line:

```
%Header End\n
```

If this line is not found, no further reading takes place.

8.2.5 The RTS data section

Each of the structures are recorded as group of variables written in the order specified in the header. Each variable consists of a data type tag byte followed by the variables data:

Data type tag. A binary byte that contains the data type number between 1 and 9.	The variables data value. The length depends on the preceding tag. (1,2,4,8 bytes)
---	---

For example, the C structure:

```
typedef struct
{
    UInt16    SampleNumber;
    float     PhotoReading;
    double    Position;
}
```

Would be stored as follows:

<i>Type</i>	<i>Data</i>
-------------	-------------

<i>Type</i>	<i>Data</i>
4	SampleNumber (2 bytes)
7	PhotoReading (4 bytes)
9	Position (8 bytes).

The reading program can check that the read type for each variable of the structure matches the expected type as specified in the header. The next structure follows immediately after the preceding one. There is an overhead of 1 byte per variable of each structure recorded. However this enables tight data type checking when the file is read.

8.2.6 The total number of structures variable

The first variable in the data section is a 32 bit integer that contains the total number of structures written to the file. Its type is 6 (unsigned 32 bit integer). After it follow the actual structures. It is written when the RTS file is first created and when it is closed after all the structures have been written. It is written with the type byte first, followed by the 32bit integer value of the number of structures that follow.

End of specification.